Review

Cu(I) hybrid inorganic–organic materials with intriguing stimuli responsive and optoelectronic properties

Q1 Elena Cariati [a,b,*], Elena Lucenti [b,c], Chiara Botta [d], Umberto Giovanella [d], Daniele Marinotto [c], Stefania Righetto [a]

[a] Dipartimento di Chimica dell'Università degli Studi di Milano, via Golgi 19, 20133 Milano, Italy
[b] UdR INSTM di Milano, Via Golgi 19, 20133 Milano, Italy
[c] ISTM-CNR, Via Golgi 19, 20133 Milano, Italy
[d] ISMAC-CNR, Via Bassini 15, 20133 Milano, Italy

Contents

ARTICLE INFO

ABSTRACT

The continuous search for hybrid inorganic–organic compounds to be used in a variety of applications points obviously to the abundant, cheap, and environmental friendly copper. Cu(I) complexes exhibit a high structural diversity and are emissive with several classes of ligands with properties varying markedly with structure and environment. Solid state materials that display reversible stimuli-responsive emission

Abbreviations: CC, cluster centered; CE, current efficiency (or luminous efficiency); CIE, chromaticity coordinates; CRI, colour rendering index; CT, charge transfer; DF, delayed fluorescence; DFT, density functional theory; EBL, exciton bloking layer; EL, electroluminescence; EQE, external quantum efficiency; E_T, triplet energy; ETL, electron transporting/injecting layer; HE, high energy; HLS, harmonic light scattering; HOMO, highest occupied molecular orbital; HTL, hole transporting/injecting layer; ILCT, intraligand charge transfer; L, luminance; LE, low energy; LEC, light-emitting electrochemical cell; LMT, luminescent molecular thermometer; LUMO, lowest unoccupied molecular orbital; MC, metal centered; MLCT, metal to ligand charge-transfer; MMCT, metal to metal charge transfer; MOF, metal–organic framework; NLO, non linear optics; NMR, nuclear magnetic resonance; OLED, organic light-emitting diodes; PE, power efficiency; PL, photoluminescence; PLQY, photoluminescence quantum yield; PXRD, powder X-ray diffraction; RISC, reverse inter system crossing; r.t., room temperature; SHG, second harmonic generation; TADF, thermally activated delayed fluorescence; TDDFT, time-dependent density functional theory; T_g, glass transition temperature; VOC, volatile organic compound; V_{ON}, voltage onset; ΔE_{ST}, singlet–triplet energy splitting; λ_{EL}, electroluminescence spectrum peak.

Q2 * Corresponding author at: Dipartimento di Chimica dell'Università degli Studi di Milano, via Golgi 19, 20133 Milano, Italy. Tel.: +39 0250314370.
E-mail address: elena.cariati@unimi.it (E. Cariati).

are attracting considerable attention because of their basic science interest and potential applications in sensors, displays, and memory fields.

While the photochemical and photophysical properties of Cu(I) complexes and clusters have been extensively studied, their optoelectronic characterization in view of second order non linear optical and electroluminescent applications has been performed more recently. However, the excellent results so far obtained in studies concerning OLED devices based on some highly stable Cu(I) complexes have proved the great potentiality of these materials in low cost flat panel displays and solid state lighting technologies. This review gathers the literature concerning stimuli responsive, electroluminescent and second order non linear optical studies on Cu(I) compounds published up to late 2014.

1. Introduction

Q3

The search for new materials with appreciable optoelectronic properties has produced a wide variety of new chromophores. Among them, coordination complexes represent an emerging and growing class of materials. Compared to organic molecules, they offer a larger selection of molecular structures, the possibility of high environmental stability, and a diversity of electronic properties by virtue of the coordinated metal center.

In this regard, the development of new systems based on Cu(I) is strongly motivated by the low toxicity, low cost and availability of copper compared to the noble metals and rare earths. These obvious advantages make Cu(I) compounds as excellent candidates for optoelectronic materials with a potential toward mass production and broad application. One of the most interesting peculiarity of Cu(I) derivatives is the number of different structural formats obtainable by simply varying reaction conditions [1]. Many of them provide a tunable phosphorescent emission at room temperature and a long luminescence lifetime of several microseconds that can be also affected by external stimuli such as temperature and pressure. All these properties make these compounds particularly appealing for the synthesis of materials exhibiting original behaviors.

While photochemical and photophysical Cu(I) complexes and clusters have been extensively studied since the early 70s, their optoelectronic characterization in view of second order Non Linear Optical (NLO) application has been performed only in the last two decades and it is still in its infancy with respect to that of other transition metal compounds. In addition, despite the variety of highly emissive Cu based compounds reported in the literature, a much fewer number of reports, mainly dated in the last decade, presents the fabrication and characterization of Organic Light-Emitting Diodes (OLEDs). This is because Cu based complexes are often unstable toward vacuum sublimation and solution processing. Only thanks to the latest development of highly stable complexes, devices with performance reaching those of Ir based ones have been obtained.

Recently, some reviews have appeared in which Cu(I) compounds' stimuli responsive photoluminescence (PL) [2–4], electroluminescence (EL) [5–8] or second order NLO [9,10] properties are treated separately among those of other transition metals. Motivated by our research interest, here we report the first survey which gathers and covers all these multidisciplinary aspects of Cu(I) materials only. Studies on the external stimuli triggered luminescence, in particular thermochromism, vapochromism, and mechanochromism displayed by solid polynuclear Cu derivatives, will be presented at first. On this regard, a restriction to the scope of this article is that in the vapochromic section only luminescence triggered by vapor and not by immersion in solvents will be enclosed. We will then cover the two main classes of light-emitting devices, OLEDs and Light-emitting electrochemical cells (LECs) with active layers based on Cu(I) complexes. The OLED literature will be presented by gathering the devices according to their fabrication techniques, first the vacuum evaporation ones (complex sublimation and *in situ* co-evaporation) and later the solution processing one. At the beginning of the section, the main parameters of all the devices will be summarized in a Table for an easy comparison.

The NLO section will cover the experimental results organized in different paragraphs according to the detection technique employed (*i.e.* solution Harmonic Light Scattering (HLS), solid state Kurtz–Perry, thin film poling, single crystal Second Harmonic Generation (SHG)).

2. Stimuli responsive Cu(I) materials

The possibility to control or tune the PL properties of materials is particularly attractive for practical applications like sensing, detection, memories and display devices. The modification of luminescence color in response to an external stimulus (*e.g.* light, pH values, temperature, mechanical force or electric and magnetic fields) is one strategy to achieve this goal. There are various stimuli-responsive materials which show modification of the luminescence color in response to mechanical (mechanochromism), chemical or thermal (thermochromism) stimuli according to different mechanisms. In this context, d^{10} polynuclear metal clusters with metallophilic properties seem particularly intriguing since metal$\cdots$metal interactions can respond to various environmental stimuli, and slight alterations to them result in marked changes in their photophysical properties.

Cuprophilic interaction, the attractive force between closed-shell d^{10} copper(I) atoms, requires Cu$\cdots$Cu distances shorter than the orbital interaction radius (the van der Waals radius of Cu is 1.4 Å [11] recently re-evaluated to be 1.92 Å [12,13]). It was however pointed out that short Cu$\cdots$Cu separation does not automatically imply the establishment of metal—metal bonds and the effect of the bridging ligands has to be taken into account [14–16]. It is this cuprophilic interaction that constitutes the most distinguishing photophysical feature of the polynuclear copper(I) complexes, relatively to their mononuclear analogs and which, in many cases, is responsible for the environmental effect on the luminescent behavior of polynuclear cuprous compounds [17].

Examples of Cu(I) stimuli responsive materials date back to the pioneering works of Hardt, Vogler and Ford. The term "luminescence thermochromism" was coined by Hardt and co-workers [18] referring to the effect of the temperature on the emissive behavior of [CuI(py-x)]$_4$ displaying at 77 K in the solid a blue emission and a yellow one at room temperature. This behavior has been attributed to changes in

the relative intensities of two emissions: a HE (at about 450 nm), displayed in systems with π-unsaturated ligands, attributed to a [3]XLCT excited state and a LE (at about 600 nm), found in cluster with Cu···Cu distances less than 2.8 Å, indicated as "cluster centered" ([3]CC).

The "luminescence rigidochromism" involves changes in the emission based on the rigidity of the local environment. It was first observed in [Culpy]$_4$ by Vogler [19] and further investigated by Ford [20]. The compound displays at room-temperature in benzene solution, a [3]CC emission at λ_{max} = 695 nm, red shifted with respect to that of the solid, and an intermediate 610 nm emission in polymethacrylate resin. When hydrostatic pressure was used to freeze the room-temperature benzene solution, the color of emission was found to shift from red to yellow (λ_{max} = 575 nm). Such sensitivity to the medium rigidity was attributed to the distortion of the [3]CC excited state relative to the ground state.

Exploiting the sensitivity of Cu(I) halide adducts to the environment, Ford reported also the first observation of "luminescence vapochromism" from two Cu(I) solid compounds, namely [CuI(4-pic)]$_n$ (n = 4; ∞; 4-pic = 4-picoline) [21]. Such behavior is associated with the reversible interconversion of the two Cu(I) isomers by exposure to solvent vapors rather than an effect of alteration of Cu···Cu distances. Blue photoluminescent (λ_{max} = 437 nm) polymeric [CuI(4-pic)]$_\infty$ exposed to toluene vapor in a sealed vial for 2 days, is converted into yellow emissive (λ_{max} = 580 nm) cubane [CuI(4-pic)]$_4$·$2C_6H_5CH_3$. The incorporation of toluene molecules permits arrangement of the tetrameric units into chains without leaving too many voids between them, and this facilitates the conversion of [CuI(4-pic)]$_4$·$2C_6H_5CH_3$ back to [CuI(4-pic)]$_\infty$ upon exposure to pentane vapor, because the copper units are already prearranged into chains [22].

Here, all the reports on thermo, vapo and mechanochromic together with those on multistimuli responsive Cu(I) compounds that appeared in the literature after the above reported pioneering works, will be summarized.

2.1. Luminescence thermochromism

Since the discovery of the temperature triggered emission of copper(I) iodide cubane clusters, many efforts have been devoted to the development of new Cu(I) thermochromic systems to be used as luminescent probes, an attractive alternative to conventional thermometers for sensing and on-line monitoring of the temperature. For practical applicability, the ideal luminescence thermochromic materials should be easy-to-detect (such as by the naked eye or portable instruments), have high sensitivity (such as large shift and fast response upon cooling or heating), wide temperature ranges, good photostability and long lifetimes. The emissive response to the temperature stimuli can be vertical (intensity) and/or horizontal (wavelength) changes.

As already discussed in the introduction, well characterized examples of thermochromic compounds are members of the [CuI(py-x)]$_4$ family whose behavior has been attributed to two emissions (high energy, HE, and low energy, LE) from two excited states of similar energies but dissimilar orbital parentages that are poorly coupled owing to the different coordinates taken by molecular distortions relative to the ground state (see Figs. 1 and 2). At room temperature, in clusters with Cu···Cu distances less than 2.8 Å, the luminescence is dominated by the LE band which has been attributed, based on experimental data [17] and recent DFT calculations [23] to a combination of a halide-to-metal charge transfer ([3]XMCT) and copper-centered d → s, p transitions and is indicated as "cluster centered" ([3]CC) to emphasize that it involves a [Cu$_4$I$_4$] cluster centered triplet excited state and is essentially independent on the nature of the ligand. At low temperature, this band is extremely weak, and the emission is dominated by the HE which has been attributed to a halide-to-pyridine ligand charge-transfer ([3]XLCT) excited state [24]. As the π* orbitals of the ligands are involved in this XLCT band, the emission at low temperature is only observed for clusters incorporating π-unsaturated ligands. In addition, the LE band shifts to longer wavelength upon cooling (from 580 nm at 298 K to 619 nm at 77 K for the [CuIpy]$_4$ cluster) and this behavior has been reported to be directly related to the Cu···Cu distances in the cluster core [Cu$_4$I$_4$] [25,26]. According to theoretical works, the Cu—Cu bonds in the excited state (LUMO) are of bonding character. As the temperature decreases, the Cu···Cu distances become shorter thus stabilizing the [3]CC excited state and shifting the emission to the red. Since no phase changes are involved, the observed thermochromic behavior is completely reversible.

In addition to this well known mechanism (hereafter indicated as "classical"), Cu(I) thermoluminescent compounds can display different behaviors as will be shown in the following section. Here thermochromic Cu(I) complexes are gathered according to different classes of ligands, and reported in Tables 1–3, together with their Cu···Cu distances, this parameter being crucial in defining their emissive behavior.

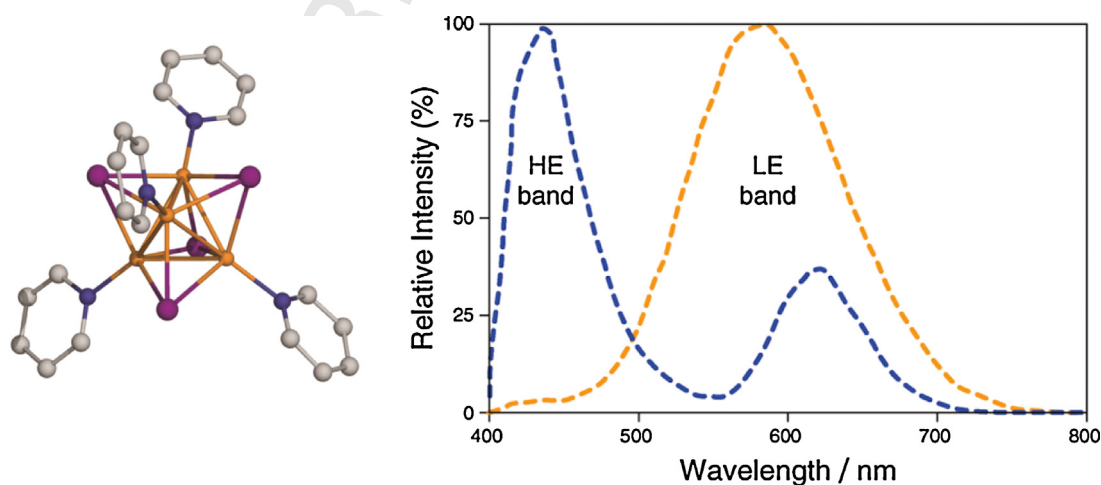**Fig. 1.** Structure of the [CuIpy]$_4$ cluster (left) and its normalized emission spectrum at 298 K (orange line) and at 77 K (blue line). Reprinted with permission from Ref. [24]. Copyright 2012, American Chemical Society.

Table 1
Summary of temperature-dependent emissive behavior of Cu(I) complexes with N-donor ligands.

Compound	T (K)	λ_{em} (nm)	Cu$\cdots$Cu distances (Å)	Reference
1	298	659		[28]
	100		3.214–3.264[a], 3.100–3.482[b]	
	77	663		
2	298	634		[28]
	100		3.201–3.245[a], 3.704–3.915[b]	
	77	659		
3	100		3.147–3.258[a], 3.848–4.636[b]	[28]
	77	565, 447		
4	298	645		[28]
	100		3.218–3.247[a], 3.813–3.987[b]	
	77	663		
5	298	656	3.195–3.257[a], 2.946[c]	[28]
	77	577		
6	298	662		[28]
	100		3.195–3.235[a], 2.989[b]	
	77	562		
7	298	564	3.172–3.230[a], 3.439[b]	[31]
	150	505		
	10	555		
8	298	494	3.128–3.249[a], 3.317[b]	[31]
	150	486		
	10	498		
9	300	542	2.710–2.892	[32]
	10	482		
10	298	410		[33]
	150		3.2275[a], 4.2198–5.3488[b]	
	18	410, 500–600		
11	298	538, 676		[34,35]
	100		3.2240[a], 3.593[b], 2.6171–2.6542[c]	
	50	534, 613		
12	298	641, 524		[35]
	100		3.2090–3.2502[a], 3.4228–3.8275[b]	
	50	632, 522		
13	450	420, 695		[36]
	298		3.8289–4.2147[b]	
	100	420, 740	3.7388–4.1812[b]	
16	298	534		[39]
	90		3.149–3.379[d], 3.154–3.458[e]	
	77	556		
17	298	496		[39]
	90		3.508[d], 3.224[e], 3.424[f]	
	77	518		
18	298	636		[39]
	90		3.447[g], 2.717, 3.518[h]	
	77	698		
19	298	612		[39]
	90		3.502[e], 3.395–3.481[a], 3.502–3.508[b]	
	77	650		
20	298	664		[39]
	90		3.135[i], 3.315–3.356[j], 2.518[k]	
	77	462		
21	298	621		[40]
	77	652		
22	298	631		[40]
	77	645		
23	298	560		[40]
	77	583		
24	298	544		[40]
	77	581		
25	298	485		[41]
	77	–		
26	298	487		[41]
	100		2.5893	
	77	412, 460		
27	298	484		[41]
	77	–		
28	298	443, 575		[41]
	100		2.8976	
	77	442, 592		
	4	377, 444		
29	298	390, 475, 505		[41]
	77	–		
30	298	470, 510		[41]
	173	–	2.4381–2.6682	
	77			

Table 1 (*Continued*)

Compound	T (K)	λ_{em} (nm)	Cu···Cu distances (Å)	Reference
31	298	417, 522		[41]
	173		2.4098–2.5577	
	77	417, 522		
	4	416, 451		
32	298	554	2.6488–3.0872	[42]
	220		2.6301–3.0406	
	160	565	2.6076–2.9914	
	100		2.5960–2.9509	
	77			
33	298	465	2.9021	[42]
	77	521		
34	298	555	2.7486–2.8840	[43]
	220		2.6902–2.8307	
	160	596	2.6709–2.8103	
	100		2.6545–2.7911	
	77			
35	298	549	2.480–2.882	[43]
	220		2.460–2.875	
	160	627	2.455–2.876	
	100		2.450–2.862	
	77			
36	298	585	2.6044–2.7794	[44]
	200		2.5966–2.7646	
	160	615	2.5925–2.7575	
	100		2.5920–2.7513	
	77			
37	298	502	2.7195	[44]
	77	609		
38	298	419	3.150	[45]
	100		3.032	
	77	419, 594		

[a]Intratrimer; [b]intertrimer; [c]cubane; [d]intralayer; [e]interlayer; [f]alternating; [g]between substructural chains; [h]within {CuI}n chains; [i]intra-1-D substructure; [j]intra-2-D substructures; [k]inter-1-D/2-D substructures; [l]298 K; [m]100 K.

2.1.1. N-donor ligands

Cu(I) pyrazolates have received great attention for their intriguing PL properties showing strong emission with microsecond lifetimes, large Stokes shifts, luminescence thermochromism, luminescence rigidochromism, and a pronounced dependence of the emission wavelength on concentration in solutions (concentration luminochromism).

In the years 2003–2005, the groups of Dias and Omary performed a systematic investigation on trinuclear Cu(I) fluorinated and non-fluorinated pyrazolates obtained by reaction of copper(I) oxide, [Cu(CH$_3$CN)$_4$][BF$_4$] or Cu(OH)$_2$ with the corresponding pyrazole [27–29]. Compounds **1–6** of formula {[3-(R),5-(R′)Pz]Cu}$_3$ (R = CF$_3$, Me, i-Pr; R′ = H, Me, Ph, CF$_3$, i-Pr) (Fig. 3) crystallize as trimers featuring planar nine-membered M$_3$N$_6$ rings and two-coordinate metal sites.

The structures of the compounds provided some clues on the ligand electronic effects on the packing of the [Cu$_3$] units. In the nonfluorinated derivatives, short intertrimer Cu···Cu distances led to the formation of dimers of trimers. In fluorinated compounds, weaker cuprophilic interactions, resulted in the formation of [Cu$_3$] units packed into chains with significantly longer Cu···Cu separations. Single crystals of **1–6** exhibit bright, broad and, all but **3**, unstructured phosphorescence even at low temperatures (Fig. 4).
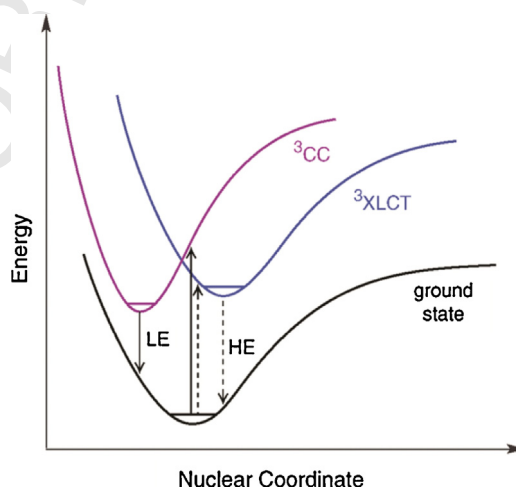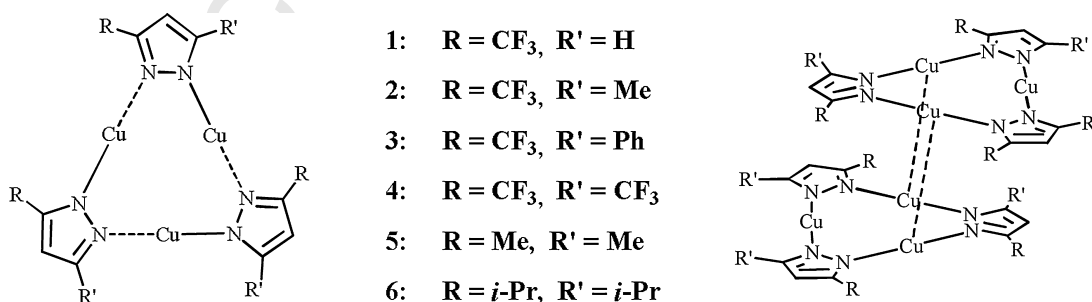

Fig. 2. Simplified potential energy surface for [CuIpy]$_4$. Reprinted with permission from Ref. [24]. Copyright 2012, American Chemical Society.

6 *E. Cariati et al. / Coordination Chemistry Reviews xxx (2015) xxx–xxx*

Table 2
Summary of temperature-dependent emissive behavior of Cu(I) complexes with P-donor ligands.

Compound	T (K)	λ_{em} (nm)	Cu···Cu distances (Å)	Reference
39	290	545		[47]
	150		2.901	
	80	587, 415		
	8	405		
39	293	550	2.8400–3.1658	[48]
	153		2.7736–3.1055	
	78	*ca.* 420, 610		
	20		2.7299–3.0587	
42	293	520	2.9478–3.1775	[48]
	153		2.863–3.129	
	78	*ca.* 420, 540		
	20		2.8041–3.0849	
41	290	560		[47]
	150	566, 424	3.14	
	100	412		
	8			
43	295	585		[46]
	77	–		
44	290	570		[49]
	150		2.704–2.743	
	80	570, 420		
45	290	580		[49]
	20	580, 420		
46 (gel)	335	580		[52]
	290	535		
	8	425		
47	298	460, 580		[53]
	153		2.525–2.943	
	77	470		
48	298	470, 560		[53]
	153		2.574–2.930	
	77	480		
49	298	450, 570		[53]
	153		2.562–3.035	
	77	460		
50	298	590	2.5758–3.0051	[54]
	77	490, 650		
51	298	626	2.4748–2.9846	[54]
	77	480, 680		

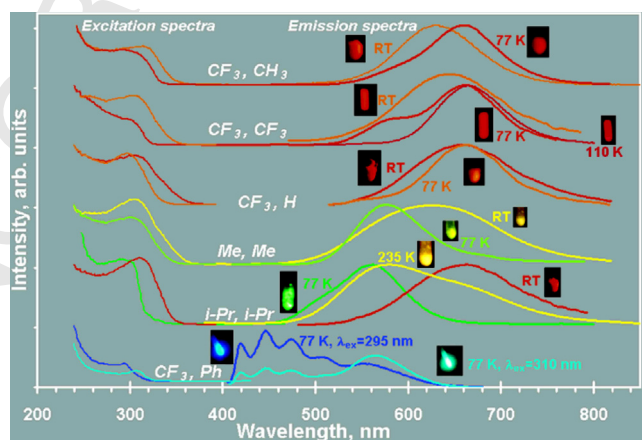Such emissions were attributed to triplet *[Cu$_3$]$_2$ intertrimeric excimers induced by Cu···Cu interactions strengthened in the phosphorescent state (Fig. 3). This assignment was in agreement with the lack of substituent effect on the luminescent behavior and was further supported by time-resolved single-crystal diffraction studies [30]. Analogously, *[Cu$_3$]$_n$ oligomeric excimers and exciplexes were considered responsible for the observed shift in the luminescence in solution at different concentrations (concentration luminochromism).

All compounds exhibit luminescence thermochromism, principally due to changes in the relative intensities of two emission bands as the result of internal conversion between two Cu···Cu bound excited states (Fig. 5). A peculiar thermoluminescent behavior was observed for **6** which shows a third bound state and three emission bands with relative intensities changing with temperature. In particular, a green emission (510 nm) dominates at low temperature, a lime green emission (560 nm) prevails between 100 and 230 K and an orange one (660 nm) is dominant at room temperature. The green and lime green bands are poorly coupled, in contrast the orange and lime green emission are likely to be in thermal equilibrium.

1:	**R = CF$_3$, R' = H**
2:	**R = CF$_3$, R' = Me**
3:	**R = CF$_3$, R' = Ph**
4:	**R = CF$_3$, R' = CF$_3$**
5:	**R = Me, R' = Me**
6:	**R = *i*-Pr, R' = *i*-Pr**

Fig. 3. Schematic structure of {[3-(R),5-(R')Pz]Cu}$_3$ **1–6** (left) and of the *[Cu$_3$]$_2$ intertrimeric excimers (right).

Table 3
Summary of temperature-dependent emissive behavior of Cu(I) complexes with S-donor ligands.

Compound	T (K)	λ_{em} (nm)	Cu···Cu distances (Å)	Reference
52	298	565	2.778–2.802	[55]
	7	452, 604		
53	298	538	2.625–2.833	[56]
	223		2.6169–2.8052	
	173	599	2.6107–2.7878	
	123		2.6079–2.7733	
	77			
54	298	526	2.672–2.814	[56]
	223		2.6594–2.7930	
	173	538	2.6501–2.7809	
	123		2.6432–2.7713	
	77			
55	298	425, 550		[57,58]
	235		2.7489–3.0302	
	195	440, 550	2.7319–3.0446	
	173		2.7309–3.0454	
	115		2.7187–3.0502	
	77			
56	298	565		[57,58]
	275		2.7172–2.8902	
	235	425, 565	2.7064–2.8812	
	115		2.6767–2.8641	
	77			
57	298	575		[59]
	173		2.6505–2.7431	
	77	430, 600		
58	298	425, 555		[59]
	173		2.8484	
	77	425, 565		
59	300	677		[60]
	153		2.831–3.326	
	5	476		
60	293	776	>3.1	[61]
	10	578, 888		
61	298	790		[62]
	113		2.66–2.71[a], 3.21[b]	
	10	590, 840		
62	293	519		[65]
	100		2.636–2.759	
	77	528		
63	293	552		[65]
	123		2.650–2.754	
	77	575		
64	293	590		[65]
	250		2.6728–2.837	
	77	545, 583		
65	293	541		[65]
	100		2.639–2.768	
	77	529, 576		

[a] For Cu_4I_4 cluster; [b] for Cu_6S_6 cluster.

Fig. 4. Luminescence spectra for single crystals of complexes **1–6**. Reprinted with permission from Ref. [28]. Copyright 2005, American Chemical Society.
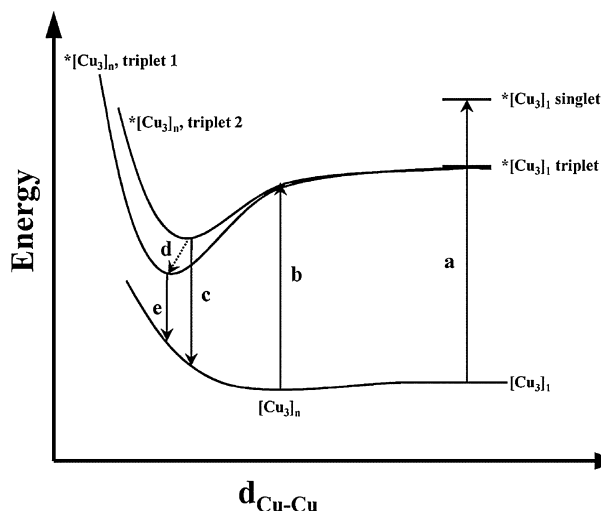
Fig. 5. Proposed photophysical model for the trinuclear Cu(I) pyrazolates. The transitions shown depict: (a) solution absorption bands; (b) solid-state excitation bands; (c) higher-energy emission bands; (d) internal conversion to a lower triplet; and (e) lower energy emission bands. Reprinted with permission from Ref. [28]. Copyright 2005, American Chemical Society.

Structural changes of the multiplex excimer were invoked also to elucidate the two-directional chromism observed for the first time by Yin et al. [31] in trimeric [Cu(Ppz)]$_3$, **7**, and polymeric {[Cu(Ppz)]$_3$[CuCN]$_3$}, **8**, obtained by reaction of CuBr with 4-(pyrid-4′-yl)-3,5-dimethylpyrazole (HPpz) and containing the [Cu(Ppz)]$_3$ entity as a building block.
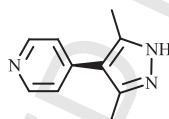
4-(pyrid-4′-yl)-3,5-dimethylpyrazole (HPpz)

Both solid compounds are emissive at room temperature with bands respectively at 564 and 494 nm, assigned to ^{3}CC excited states. The emissive blue shift of **8** with respect to **7** was explained on the basis of the higher rigidity of the framework of **8** that restrains the distortion of excimers, *[Cu$_3$]$_n$, thus leading to a smaller Stokes' shift. Solid **7** and **8** showed a two-directional emission change upon cooling. When going from room temperature to 150 K, the emission color of **7** changed from yellow-green to green (λ_{max} = 505 nm), but upon further cooling to 10 K, the yellow-green emission was recovered. A similar trend was observed for **8** that changed emission color from green to bluish-green (λ_{max} = 486 nm) on going from room temperature to 150 K and then back to green at 10 K.

This two-directional chromism was attributed to competing intra- and intermolecular cuprophilic interactions. The former, associated with contraction of the crystal, is predominant at low temperature and lead to a red shift. The latter, a thermal-dominated distortion of excited states, is more prominent in the high temperature range and lead to a blue shift of the emission. The less pronounced shift of the emission band for **8** was again explained with the higher rigidity that restrains concurrently the lattice contraction and the distortion of the excimers.

Xu and Yin et al. described the quite unique mixed-valent cluster [Cu^{II}Cu$^I_{15}$I$_{17}$(tmbpzH$_2$)$_6$], **9**, with a 3D framework prepared by reaction of CuSCN and the ligand tmbpzH$_2$ (3,3′,5,5′-tetramethyl-4,4′-bipyrazole) under solvothermal conditions in the presence of excess KI [32]. Compound **9** displays luminescent thermochromism, with a HE (482 nm) emission dominating at low temperature, and a LE band (542 nm) prevailing at high temperature.
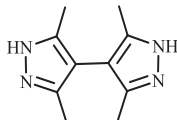

3,3′,5,5′-tetramethyl-4,4′-bipyrazole (tmbpzH$_2$)

Thiel et al. reacted enantiomerically pure 2,2′-di(1,2-pyrazol-3-yl)-(*S*)-1,1′-binaphthyl (*S*)-(pyrbinapH$_2$) with [Cu(CH$_3$CN)$_4$]BF$_4$ to give the corresponding derivative [(*S*)-pyrbinapCu$_2$]$_3$, **10**, formed by six Cu(I) centers each linking two pyrazolate units [33]. This hexanuclear copper(I) complex displays in the solid state at room temperature an emission at about 410 nm which was assigned to the naphthalene chromophore. This band shows only a moderate dependence on the temperature, increasing in intensity by a factor of 2.5 on decreasing the temperature from 293 to 18 K. However at low temperature (below 50 K) a new structured band, attributed to a singlet excited state,

developed around 500–600 nm and the complex emitted bright white light resulting from both emission bands. The yellow emission band rapidly decreased in intensity when elevating the temperature above 100 K.
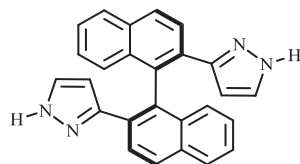

2,2'-di(1,2-pyrazol-3-yl)-(*S*)-1,1'-binaphthyl [(*S*)-(pyrbinapH$_2$)]

An interesting series of metal–organic frameworks (MOF) based on the two luminophores Cu$_4$I$_4$ and Cu$_3$Pz$_3$ was reported by Li et al. [34,35]. [Cu$_4$I$_4$(NH$_3$)Cu$_3$(L)$_3$]$_n$ (L = 3-(4-pyridyl)-5-*p*-tolyl-pyrazolate), **11**, and [Cu$_4$I$_4$(NH$_2$CH$_3$)Cu$_3$(L)$_3$]$_n$, **12**, prepared by reaction of CuI with the corresponding ligand under solvothermal conditions, exhibit at room temperature and in the solid state a dual emission in the 520–540 and in the 630–680 nm regions, originated from a thermal equilibrium between a *CC (for Cu$_4$I$_4$) and a *[Cu$_3$]$_2$ (for [Cu$_3$Pz$_3$]$_2$) excited states respectively. **11** and **12** show a different temperature-dependent luminescence: in **11** the LE band prevails in the higher temperature range (293–413 K) while at low temperature the HE band becomes dominant due to a less efficient energy transfer from HE to LE bands. In agreement with the reversibility of the thermochromic behavior and with temperature varied X-ray diffraction, the energy transfer was indicated as thermal activated rather than involving a chemical process due to phase transition. Interestingly, for **12** the LE band was found to prevail upon the whole range of temperatures (30–298 K). This behavior was related to the shorter Cu···Cu intertrimeric distances within the [Cu$_3$Pz$_3$]$_2$ luminophore in **12** and was explained in terms of more populated *[Cu$_3$]$_2$ excimeric excited states. Both for **11** and **12**, a blue shift of the LE band was observed at low temperature as already observed for other Cu$_3$ pyrazolate system [27–29]. Accordingly, such phenomenon was explained with the generation of multiple phosphorescent *[Cu$_3$]$_2$ excited states.
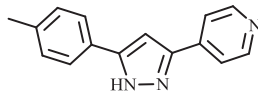

3-(4-pyridyl)-5-*p*-tolyl-1*H*-pyrazole

With the aim to avoid the overlapping of the emission bands encountered in the dual Cu$_4$I$_4$ and Cu$_3$Pz$_3$ systems, that hampers their possible use for the production of a self-calibrating Luminescent Molecular Thermometer (LMT), Li and Huang et al. recently exploited the use of a bulkier ligand (2,6-lutidine) to induce the formation of Cu$_2$I$_2$ moiety rather than the tetrameric one [36]. The authors reported the preparation of the binary cluster [Cu$_6$L$_3$(Cu$_2$I$_2$)Cu$_6$L$_3$] (H$_2$L = 3,5-bis((3,5-dimethyl-pyrazol-4-yl)methyl)-2,6-dimethylpyridine), **13**, in which the Cu$_6$L$_3$ moiety and the Cu$_2$I$_2$(2,6-lutidine)$_2$ can be recognized. In **13** the emissions of the two components are retained and provide a well-resolved dual emission with a blue band attributed to a metal/halide-to ligand charge transfer (of the Cu$_2$I$_2$ moiety) and a red cluster-centered transition (for Cu$_6$L$_3$). Accordingly, **13** exhibits two-way luminescent thermochromism with self-calibrated temperature sensing ability in the range 120–450 K, being an interesting alternative to the more expensive lanthanide-based LMTs.
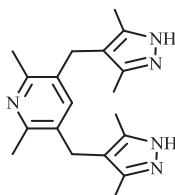
3,5-bis((3,5-dimethyl-pyrazol-4-yl)methyl)-2,6-dimethylpyridine

We mention here another LMT based on a copper(I) compound reported by Prodi et al. [37]. The trizwitterionic dicationic cluster [Cu$_5$(EtNC(S)PPh$_2$NPPh$_2$C(S)NEt)$_3$](PF$_6$)$_2$, **14**, displays excellent thermochromic luminescence with Photoluminescence Quantum Yield (PLQY) and lifetime strongly influenced by T in the range of 228–353 K regardless the presence of oxygen. The system can be used to measure temperature changes of less than 0.1 degrees in a very large temperature range that includes room temperature and the physiological temperature (310.8 K), however its low dispersibility in aqueous solutions limits the applications *in vivo*.
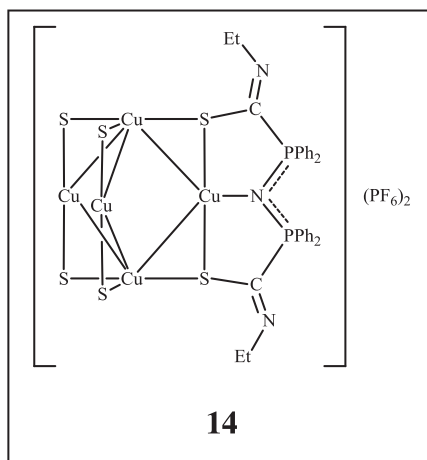
14

An interesting application of the thermochromic properties of Cu(I) pyrazolate complexes was reported by Aida et al. who investigated the self assembling through cuprophilic interactions of dendritic complexes with long alkylic chains and generic formula $Cu[C_n]L_m pz$ (n = 12, 18; m = 2, 3; L_m = the number (m) of dendritic layers; pz = pyrazolate) [38]. Solid $Cu[C_{18}]L_2 pz$, **15**, displays dichroic luminescence at room temperature when the solid is obtained from its hot melt: when the hot melt is naturally cooled it emits red (650 nm), while it emits yellow (615 nm) if slowly cooled. In both the cases, the emission was assigned to phosphorescence from a triplet metal-centered excited state. In the case of the naturally cooled hot melt, a kinetically favored crystallization of the paraffinic side chains leads to a columnar structure. In the case of the thermodynamically favored self-assembling process a certain distortion of the luminophore is assumed to be responsible of the blue shifted emission. The red luminescence can be converted into the yellow by annealing at 45 °C, and *vice versa* the yellow one into the red by annealing at 70 °C. The authors showed that the structural bistability of this complex, responsible of its phosphorescence dichroism, can be exploited to prepare a rewritable phosphorescent paper for security technological applications.
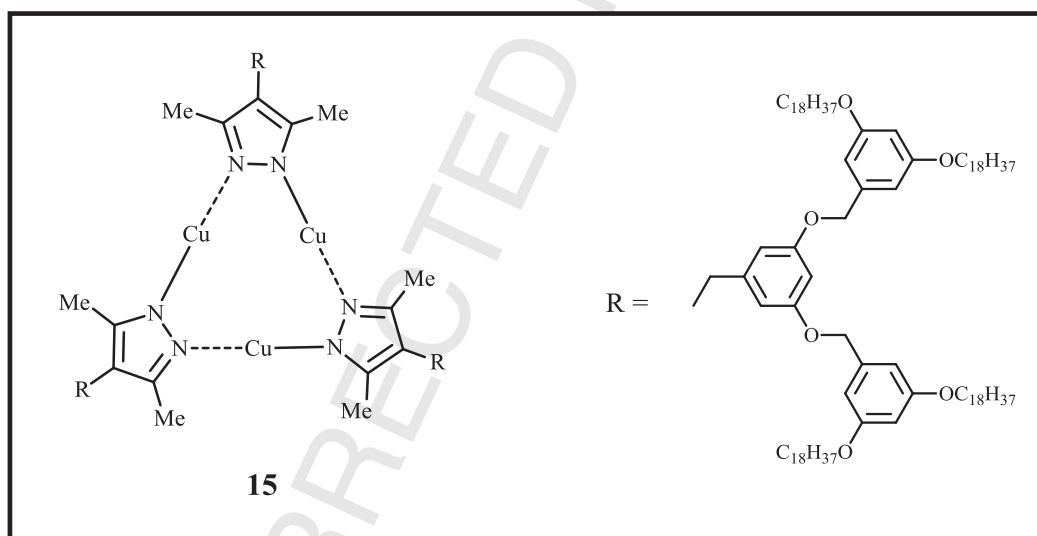

15

By changing the pyrazole with triazole ligands, Dunbar and Zubieta prepared under hydrothermal conditions, a series of Cu/trz/X systems, where trz is triazolate and X is an anionic component [39]. In particular, $[Cu_6(trz)_4Br_2]$, **16**, $[Cu_6(trz)_4Br]Cu_4Br_4(OH)$, **17**, $[Cu_3(trz)I_2]$, **18**, $[Cu_4(trz)_3]OH·7.5H_2O$, **19**, and $[Cu_5(trz)_3Cl_2]$, **20**, exhibit luminescence thermochromism. All the compounds, in the solid state and at room temperature display bright phosphorescence with broad and unstructured emissions assigned to ^{3}MLCT excited states in the 500–700 nm region. Upon cooling to 77 K a red shift in the emission bands was observed for **16**–**19** suggesting that also metal-centered or metal–metal "bond" to ligand charge transfer excited states should be taken into account. Differently, for **20** with significant cuprophilic interactions, a "classical" thermochromism was observed (a blue shift from 664 nm at room temperature to 462 nm at 77 K).

Näther et al. reported on the luminescence thermochromism of $[(CuCl)_3(2,3\text{-dmpyz})_2]$, **21**, $[(CuCl)_2(2,3\text{-dmpyz})]$, **22**, $[(CuI)(2,3\text{-dmpyz})]$, **23**, $[(CuI)_2(2,3\text{-dmpyz})]$, **24** (2,3-dmpyz = 2,3-dimethylpyrazine), obtained by reaction of CuX (X = Cl, I) with the N-donor ligand [40]. A dependence on the nature of the halide atom was found in the room temperature solid state emission spectra, with maxima at 544–560 nm for the iodine-containing polymers and at 621–631 nm for the chlorine ones. The nature of the photoluminescence was attributed to a combination of several processes such as ^{3}MLCT, ^{3}MC and ^{3}XLCT transitions, this latter supported by the difference in the emission positions according to the different halide atoms. Moreover fluorescence originating from ligand centered transitions were also suggested as possible contributors to the total luminescence emission. Upon cooling at 77 K a red shift in the emission bands was observed for all compounds and was explained according to a predominance of "cluster centered" and XLCT transitions.

Pike, Patterson et al. described the synthesis and luminescent behavior of various networks obtained by reaction of CuCN with substituted piperazines and hexamethylenetetramine (HTMA). Some of these compounds $((CuCN)_2(Me_2 Pip)$, **25**, $(CuCN)_4(Me_2 Pip)$, **26**,

(CuCN)(Ph$_2$CHPip), **27**, (CuCN)$_2$(Ph$_2$CHPip), **28**, (CuCN)$_3$(HMTA)$_2$, **29**, (CuCN)$_5$(HMTA)$_2$, **30**, and (CuCN)$_5$(HMTA), **31** (Me$_2$Pip = N,N'-dimethylpiperazine and Ph$_2$CHPip = N-(diphenylmethyl)piperazine)) are thermochromic [41]. At room temperature the solid compounds show a HE emission band (of MC and MLCT mixed character) in the 440–460 nm region and a weak LE band in the 470–575 nm range, which in some cases are overlapped originating a single emission. Upon cooling to 77 K, it was observed a further significant increase of the HE band with respect to the LE band that diminishes and in some cases disappears. Although close Cu···Cu contacts are present in many of the reported samples, no correlation with luminescence behavior was suggested since CuCN and **25**, lacking Cu···Cu interactions, display similar photophysical behavior.


N,N'-dimethylpiperazine (Me$_2$Pip), N-(diphenylmethyl)piperazine (Ph$_2$CHPip), hexamethylenetetramine (HMTA)
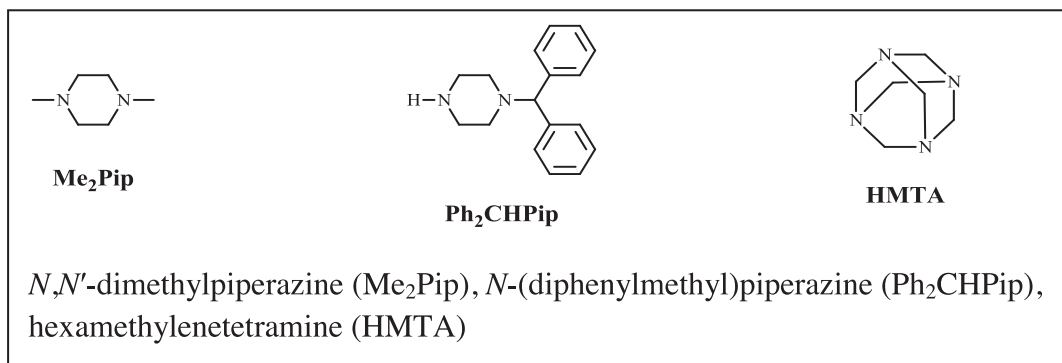
Sun et al. investigated the temperature-dependent luminescent properties of [Cu$_6$I$_6$(dmimb)$_3$]$_n$ (dmimb = 1,4-di(2-methyl-imidazol-1-yl)butane), **32**, and [Cu$_4$I$_4$(dimbe)]$_n$ (dimbe = 1,3-di(imidazol-1-yl)benzene), **33**, prepared by reaction of CuI with the corresponding ligand under solvothermal conditions [42]. X-ray diffraction studies of **32** and **33** revealed different structural motifs, containing the [Cu$_6$I$_6$] and the rare "S-shaped-double-bowl" [Cu$_{10}$I$_{10}$] clusters, respectively. Solid **32** exhibits at room temperature an emission at 554 nm, that was assigned to the ^{3}CC excited state. This band was red-shifted at 77 K (λ_{em} = 565 nm) due to the shortening of the Cu···Cu distances upon cooling (2.897 Å at 298 K vs. 2.787 Å at 100 K), as revealed by multi-temperature X-ray analysis. A different emissive behavior was found for solid **33**, characterized at room temperature by the presence of ^{3}XLCT (λ_{em} = 465 nm) and at 77 K by ^{3}CC excited states (λ_{em} = 521 nm). In this case the observed temperature-dependent luminescence was ascribed to changes in the relative intensities between the two excited states.

1,4-di(2-methyl-imidazol-1-yl)butane (dmimb), 1,3-di(imidazol-1-yl)benzene) (dimbe)
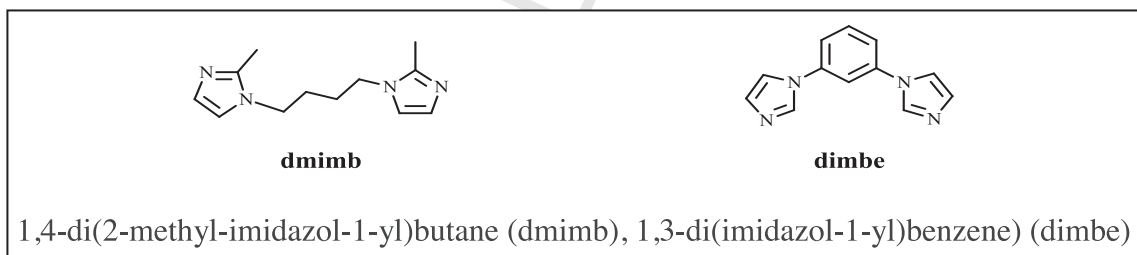
The same group reported on the solvothermal reaction of CuI with dmimpr or dimb (dmimpr = 1,3-di(2-methyl-imidazol-1-yl)-propane, dimb = 1,4-di(imidazol-1-yl)butane) that yielded the coordination polymers [Cu$_4$I$_4$(dmimpr)$_2$]$_n$, **34** and [Cu$_6$I$_6$(dimb)$_3$]$_n$, **35** [43]. X-ray diffraction analysis revealed, for the Cu$_4$I$_4$ cluster in **34**, Cu···Cu distances shorter or comparable to the 2.8 Å critical value. In polymer **35** both cubane Cu$_4$I$_4$ and rhomboid-type Cu$_2$I$_2$ clusters were detected, with Cu···Cu contacts of 2.882 and 2.480 Å, respectively. Solid-state emission spectra at room temperature of the two compounds showed an intense emission band at 555 nm for **34** and at 549 nm for **35**, assigned to the ^{3}CC excited states. By lowering the temperature to 77 K, a color change was appreciated by naked eye and a red-shift of 41 nm and 78 nm was observed for **34** and **35**, respectively. By means of multi-temperature X-ray crystal structure analyses it was established that the emission red shifts are correlated to the decrease of Cu···Cu distances with the temperature. Moreover **34** showed a good linear relationship between the maximum emission wavelength and the temperature, while in **35**, a similar correlation was not observed due to the presence of the two Cu$_4$I$_4$ and Cu$_2$I$_2$ clusters.


1,3-di(2-methyl-imidazol-1-yl)-propane (dmimpr), 1,4-di(imidazol-1-yl)butane (dimb)
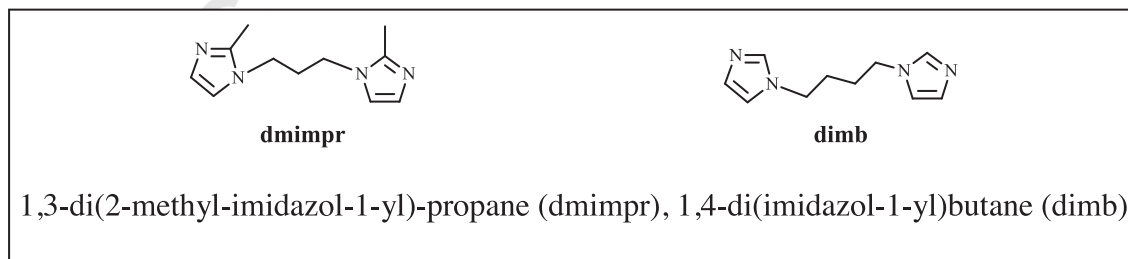
Another example of the red-shift of the ^{3}CC band upon cooling due to Cu···Cu shrinkage was reported by the same group for [Cu$_4$I$_4$(bpmp)$_2$]$_n$, **36**, and [Cu$_4$I$_4$(bpmp)$_3$]$_n$, **37**, (bpmp = 1,4-bis(pyridin-4-ylmethyl)piperazine), obtained by reaction of CuI with bpmp
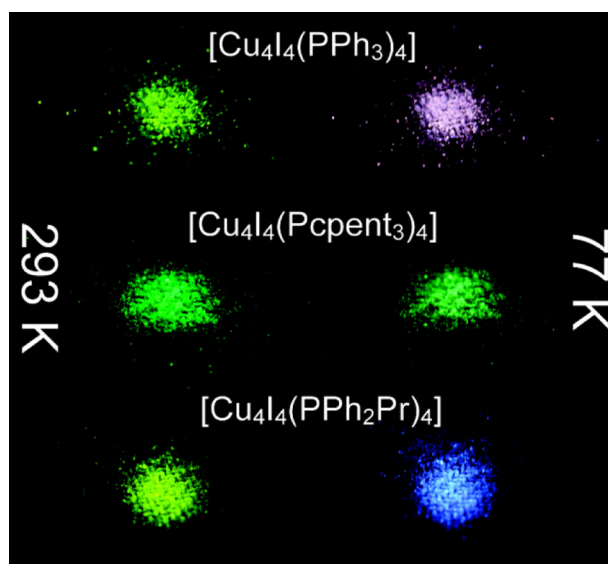
Fig. 6. Photos of powder of clusters **38–40** under UV irradiation at r.t. (left) and in liquid nitrogen (right). Adapted with permission from Ref. [47]. Copyright 2011, American Chemical Society.

under solvothermal conditions or by mechano-chemical syntheses [44]. X-ray diffraction studies showed for the two polymers different structural motifs, containing the cubane and the stairstep Cu_4I_4 clusters in **36** and **37**, respectively, with Cu···Cu distances shorter than 2.8 Å in both cases. At room temperature, the complexes were characterized by solid-state emission bands at 585 nm (for **36**) and 502 nm (for **37**), assigned to the ^3CC excited state. Upon cooling at 77 K, a red-shift of 30 nm was observed for **36**, while a less pronounced shift of 7 nm was detected for **37** in agreement with its stairstep structural motif.
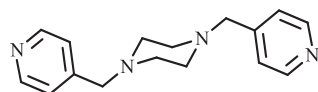
1,4-bis(pyridin-4-ylmethyl)piperazine (bpmp)

Boomishankar et al. prepared the cationic MOF $\{[Cu_6I_5(L)_2](OH)\cdot 3DMF\, 2.5\text{-}MeOH\}_n$, **38**, by reaction of CuI with the tridentate thio-phosphoramide ligand L (L = $(NHAQ)_3P=S$; AQ = 3-quinolinyl) [45]. The crystal structure revealed the presence of $[Cu_6I_5]^+$ clusters with each Cu center tetrahedrally coordinated to three I⁻ ions and one ring N-donor from the ligand. Differently from cubane clusters, solid **38** displays at 298 K a ligand-centered fluorescence band (HE, $\lambda_{em} = 419$ nm). At 77 K a phosphorescent emission (LE, $\lambda_{em} = 594$ nm) arising from ^3CC with mixed XMCT and Cu centered d → s, p transitions of the $[Cu_6I_5]^+$ cluster was observed, together with the weak HE band. The population of the triplet states was suggested to arise from an ISC process at low temperature.
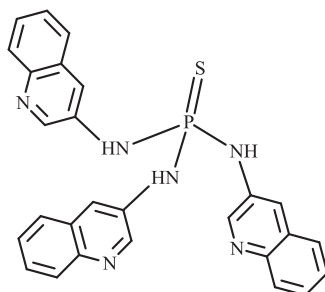
$(NHAQ)_3P=S$; AQ = 3-quinolinyl

2.1.2. P-donor ligands

Boilot, Perruchas et al. reported detailed experimental (structural and optical) and theoretical investigation (DFT calculations) to elucidate the photophysical behavior of phosphine-based $[CuIL]_4$ clusters [46,47]. In particular, clusters **39–41** with L = PPh_3
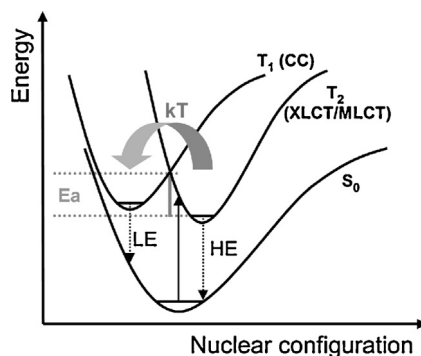
Fig. 7. Simplified energy level diagram of clusters 39–41. Reprinted with permission from Ref. [47]. Copyright 2011, American Chemical Society.
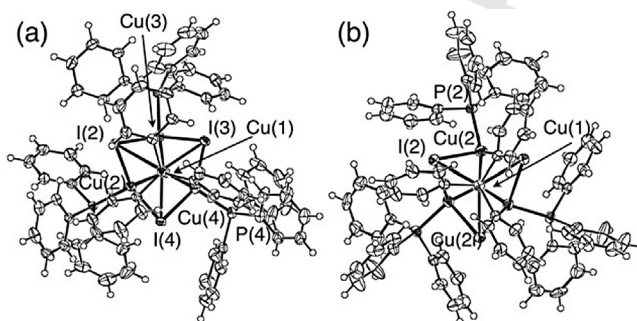

Fig. 8. Structures of polymorphs 39 (left) and 42 (right). Reprinted with permission from Ref. [48]. Copyright 2010, Royal Society of Chemistry.

(triphenylphosphine, 39), Pcpent₃ (tricyclopentylphosphine, 40) and PPh₂Pr (diphenylpropylphosphine, 41) were synthesized by reaction of CuI with the corresponding phosphine. Their luminescence behavior as a function of temperature was determined, revealing the "classical" mechanism but with important differences with the corresponding pyridine cubanes. The three compounds show at room temperature a yellow-green LE emission (523–560 nm region) which was assigned to ^{3}CC excited state of mixed iodide-to-copper charge transfer (XMCT) and copper-centered 3d → 4s, 4p transitions. At low temperature the appearing of a blue HE emission (405–412 nm region) was observed for 39 and 41 but not for 40 which was in fact not thermochromic. The intensity of this HE band increases progressively with the concomitant extinction of the LE band and at 8 K is the only feature present in the spectrum. This band was directly correlated with the presence of π* orbitals of the ligand, and it was attributed to a ligand centered excited state with mixed ^{3}XLCT/^{3}MLCT character, in contrast to [CuIpy]₄ in which pure ^{3}XLCT excited state is at the origin of this emission (Fig. 6). The thermochromic luminescence of clusters 39 and 41 derives from the thermal equilibrium between the ^{3}CC and the ^{3}XLCT/^{3}MLCT excited states that, in contrast with the pyridine derivative, are highly coupled displaying same excitation profiles and low activation energy (Fig. 7). Interestingly, the presence of the LE emission band is not strictly correlated to short Cu···Cu contacts, being in fact present also in 40 and 41 for which Cu···Cu distances of 3.276 Å and 3.14 Å were measured, respectively. Such long distances, correlated with the steric effect of the ligands and/or to crystal packing, explain the lack of red shift of the LE band of 41 by lowering the temperature, contrarily to what observed for 39 having 2.90 Å Cu···Cu distances which becomes closer to the 2.8 Å value.
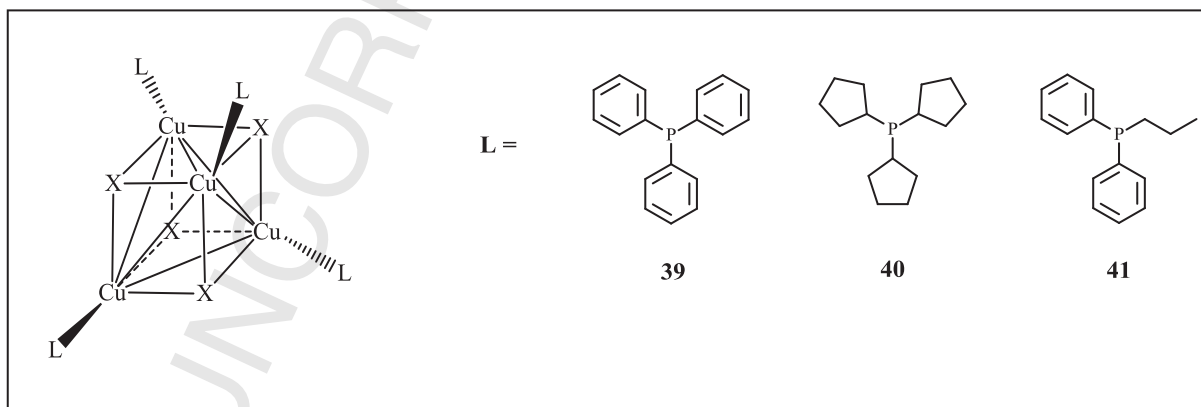
In 2010, Ozawa and Toriumi et al. investigated the relationship between the structural changes in the ^{3}CC excited state and the "classical" luminescence thermochromism of two [CuI(PPh₃)]₄ polymorphs by performing a multi-temperature X-ray crystal structure analysis [48]. [CuI(PPh₃)]₄ was prepared by reaction of CuI with PPh₃. The already known monoclinic form 39 was crystallized from CHCl₃, while a new cubic form 42 was obtained by recrystallization from a diluted toluene solution (Fig. 8). At room temperature solid 39 shows intense
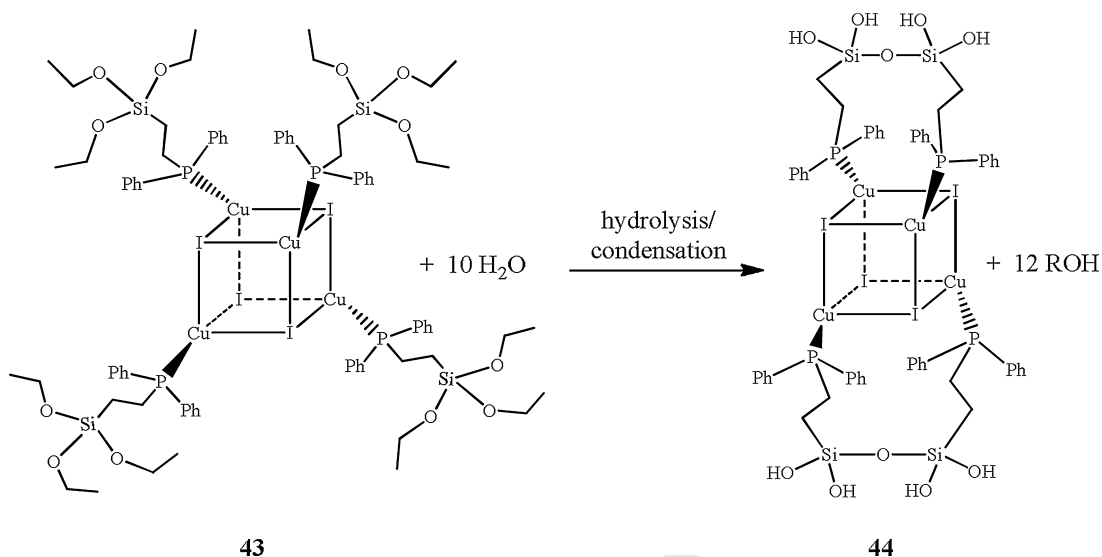
Scheme 1. Synthetic route to cluster **44** [49].
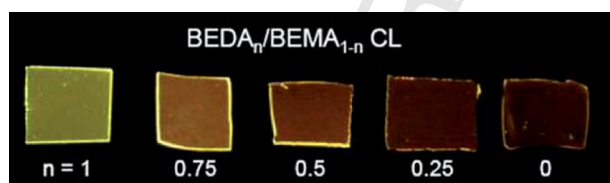
Fig. 9. Photos of self-standing films of the BEDA$_n$/BEMA$_{1-n}$ **41** ($n = 1, 0.75, 0.5, 0.25, 0$) composite materials under UV irradiation. Reprinted with permission from Ref. [51]. Copyright 2013 Royal Society of Chemistry.

green-yellow luminescence ($\lambda_{max} = 550$ nm) which is red-shifted at 78 K ($\lambda_{max} = 610$ nm). Solid **42** displays at 293 K blue-green emission ($\lambda_{max} = 520$ nm) which is slightly red shifted at lower temperature ($\lambda_{max} = 540$ at 78 K). The red-shift of the LE emission band of both complexes was correlated with the shrinkage of the Cu$_4$ core size (about 11% smaller than those at room temperature), due to changes in the orientation of the phosphine ligands that affect the crystal packing and that are induced by temperature variation. The smaller Cu$_4$ size in **39** showed the larger energy shift.

Boilot, Perruchas et al. prepared the cluster derivative [Cu$_4$I$_4$(PPh$_2$(CH$_2$)$_2$Si(OH)$_2$OSi(OH)$_2$(CH$_2$)$_2$PPh$_2$)$_2$] **44** [49] by hydrolysis of [CuIL]$_4$ cubane **43** containing a phosphine functionalized with an alkoxy moiety (Scheme 1). **44** exhibits a peculiar emissive behavior in the solid state. The characteristic cluster-centered ^{3}CC emission observed at room temperature ($\lambda_{em} = 570$ nm) progressively increased in intensity and narrowed by lowering the temperature, whereas a HE band ($\lambda_{em} = 420$ nm, ^{3}XLCT transition) of low intensity appeared at 80 K. This was attributed to a lack of communication between the two excited states caused by the efficient hydrogen-bonding network observed between the clusters in the crystal structure, which induces "constraints" in the solid state. Moreover the chelating character of the ligand, which limits the flexibility of the cluster, avoid shortening of Cu···Cu bond by lowering the temperature, accordingly no red shift of the LE band was observed.

44 was further reacted with tetramethoxysilane to give the condensation product **45**, characterized by a different hydrogen bonding network in the solid state and that displays the "classical" thermochromic luminescence behavior of the [CuIL]$_4$ clusters.

Thin films of potential interest for applications as LMT or sensors were obtained from **43** and **45** by sol–gel polymerization technique, with the thermochromic properties of their precursors maintained within the film [46,49]. Transparent films were also obtained by incorporation of **41** into Bisphenol-A-Ethoxylate DiAcrylate (BEDA) UV-polymerizable acrylic resin [50] that protected the cluster from non-radiative phenomena affording a composite material that displayed a perfect control of thermochromism with an intensity of the luminescence almost constant in the 290–130 K range.

Systems capable of controlling selectively the light emission by changing the rigidity of the environment are very promising in the field of photoactive materials as local probe to detect the medium rigidity. By exploiting the rigidochromic properties of **41** and varying the rigidity of the hosting matrix, Perruchas et al. prepared photoluminescent composite materials exhibiting different emission colors using the same luminescent guest [51]. **41** was dispersed in a series of photopolymerizable matrices exhibiting different glass transition temperatures (T_g). These matrices were obtained by blending at different molar ratios two chemically similar acrylic monomers presenting different flexibility, namely BEDA and Bisphenol-A-Ethoxylate DiMethAcrylate (BEMA). A change of the emitted color ranging from yellow to orange was observed by decreasing the T_g value of the polymeric matrix (with T_g values decreasing by increasing the BEMA content; Fig. 9). This trend is in agreement with the luminescence rigidochromism of the copper iodide cluster which emits at lower energy by increasing the medium flexibility due to a decreased energy of the *CC excited state relative to the ground state. For the materials with
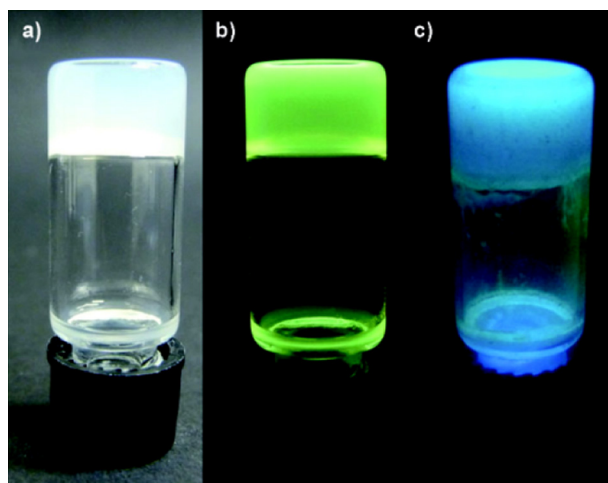
Fig. 10. Photos of **46** gel at (a) r.t. in ambient light, (b) r.t. under UV irradiation, and (c) after cooling in liquid nitrogen and under UV irradiation. Reprinted with permission from Ref. [52]. Copyright 2013, WILEY-VCH Verlag GmbH & Co. KGaA, Weinheim.

BEMA content higher that 50%, emission values (around 605 nm) close to the one in solution were observed meaning that the polymeric network induces almost no constraint to the cluster.

BEDA
Bisphenol-A-ethoxylate diacrylate (n=2)

BEMA
Bisphenol-A-ethoxylate dimethacrylate (n=15)
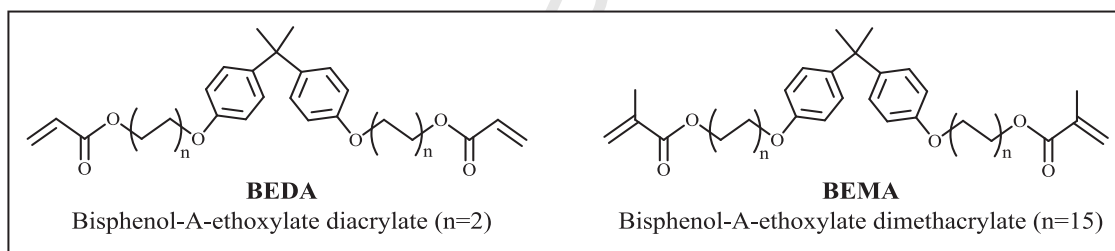
Perruchas, Camerel et al. functionalized the $[CuIL]_4$ clusters with a cholesteryl phosphine ligand able to induce gelation to give a new hybrid gelator **46** with intriguing photophysical properties [52]. **46**, prepared by reaction of CuI with L in CH_2Cl_2, revealed to be a good gelator of cyclohexane, forming a stable and robust gel with thermally reversible sol-gel transition.


46

L =
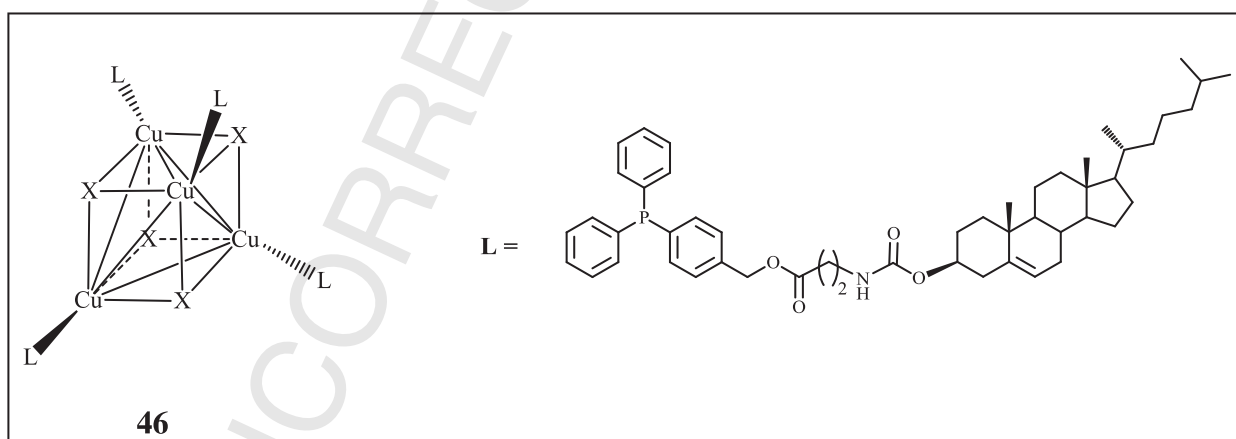
The gel is highly emissive and displays the "classical" luminescence thermochromism (λ_{max} equal to 535 and 435 nm at 290 and 8 K respectively) confirming that the cubane structure is maintained in the gel (Fig. 10). The same behavior was also observed for powders and xerogels of **46**. The gelation process of **46** was followed by photoluminescence measurements. A suspension of **46** in cyclohexane was heated up to 338 K forming a weakly emissive (580 nm) clear solution which was then cooled down to room temperature. Remarkably, emission spectra showed a gradual intensification (up to 60 times the original value) and a blue shift (535 nm) of the emission during the cooling process. The accomplishment of gelation process was assessed by the stabilization of the emission intensity. Thanks to this rigidochromic behavior, this cluster was indicated as a convenient probe for gelation processes, leading to an on/off system in which emission is exalted in the gel state.

47: R = phenyl
48: R = cyclohexyl
49: R = ethyl
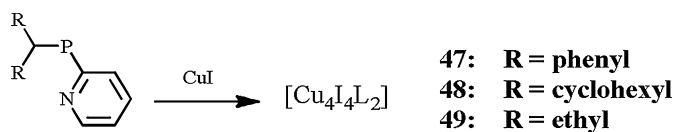
Scheme 2. Synthetic route to clusters **46–48** [53].

Thompson et al. synthesized three "classical" thermoluminescent clusters of formula $Cu_4I_4L_2$ by reacting CuI with PN̂-type ligands 2-[(diRphosphino)methyl]pyridine (**47**, R = phenyl; **48**, R = cyclohexyl; **49**, R = ethyl) (Scheme 2) [53]. By structural characterization it was found that the compounds adopt an octahedral geometry for the Cu_4I_4 core with both short (bridged by μ^2-iodide) and long (flanked by PN̂-type ligand) Cu···Cu distances. The solid compounds showed at room temperature a predominant HE blue luminescence (in the 450–470 nm region) with variable amount of LE emission (560–580 nm) associated with different steric demands of the phosphine groups. By optical characterization and DFT calculations for the HE and the LE emission an assignment to ^{3}XLCT and ^{3}CC excited states, similar to that of the [CuIpy]$_4$ analogs, was formulated. Particularly striking is compound **47**, for which a significant contribution of the LE band at room temperature together with the more intense HE emission is responsible for the white emission color observed at room temperature by naked eye. When lowering the temperature to 77 K, the LE emission was no longer detected for the three clusters. The peculiar emissive behavior of the three compounds was ascribed to the effects of unequal Cu···Cu bond distances and to the stabilization of the molecular geometry of the ^{3}XLCT excited state in the rigid coordination environment enforced by the PN̂-type ligands. The role of the phosphine ligands is crucial in the modulation of the thermochromic emission properties since the contractions of Cu···Cu distances in the Cu_4I_4 core during the formation of the ^{3}CC excited state are favored by the distortion of the bidentate ligand. Derivatives bearing bulky R groups on the PN̂ ligand did not show neither LE emission nor luminescence thermochromism in the solid state.

A study on the effect of the temperature on the luminescent properties was reported for two complexes with bridging PP̂-type ligand [(CuI)$_4$(dcpm)$_2$] (dcpm = bis(dicyclohexylphosphino)methane), **50**, and [(CuI)$_3$(dcpm)$_2$], **51** [54]. The compounds display only a LE emission at room temperature and both the HE and LE at 77 K. The short Cu···Cu distances (2.5758 and 2.4748 Å for **50** and **51** respectively) were considered at the basis of the observed "classical" thermochromic luminescent behavior.


bis(dicyclohexylphosphino)methane (dcpm)
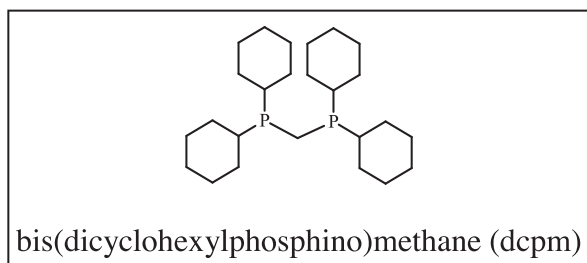
2.1.3. S-donor ligands

In 2005 Kim et al. reported the first sulphur coordinated Cu_4I_4 cluster showing "classical" thermochromic behavior [55]. In [Cu$_4$I$_4$L$_2$]$_n$ polymer (L = 1,12-diphenyl-5,8-dioxa-2,11-dithiadodecane), **52**, the cubane clusters are connected to four ligands by Cu—S bonds forming a layered structure. In agreement with Cu···Cu distances shorter than 2.8 Å, at room temperature, the solid state spectrum of **52** displayed a broad emission band (λ_{max} = 565 nm) that was assigned to a CC excited-state. At 7 K the most prominent LE band was red-shifted to 604 nm and a second HE much weaker emission at 452 nm was observed.


1,12-diphenyl-5,8-dioxa-2,11-dithiadodecane
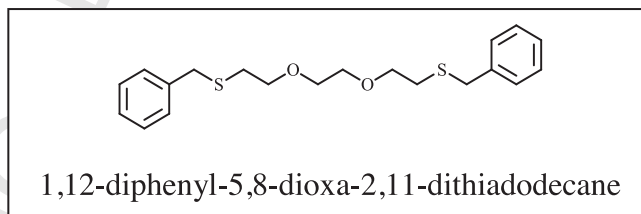
The same group, aiming at elucidating the relationship between luminescence thermochromism and Cu···Cu distances [56] prepared and characterized two thermochromic coordination polymers, namely [Cu$_4$I$_4$L$_2$]$_n$, **53**, and [Cu$_4$I$_4$L$_2$]$_n$, **54** (**53** characterized by a 2D network and **54** by a 1D zigzag loop chain) (L = 2-(cyclohexylthio)-1-thiomorpholinoethanone). At room temperature, solid state emission spectra of **53** and **54** displayed a broad band with maxima at 538 and 526 nm, respectively, which were assigned to ^{3}CC excited state. By decreasing the temperature, the emission of **53** changed from yellow to red (λ_{max} = 599 at 77 K) while for **54** an only 12 nm red-shift was observed. This different thermochromic behavior was explained on the basis of multi-temperature X-ray diffraction data which revealed a pronounced contraction of the longer Cu···Cu distances, whereas shorter distances were almost unaffected by lowering the temperature.

53
2D Network

54
1D Zigzag Loop Chain
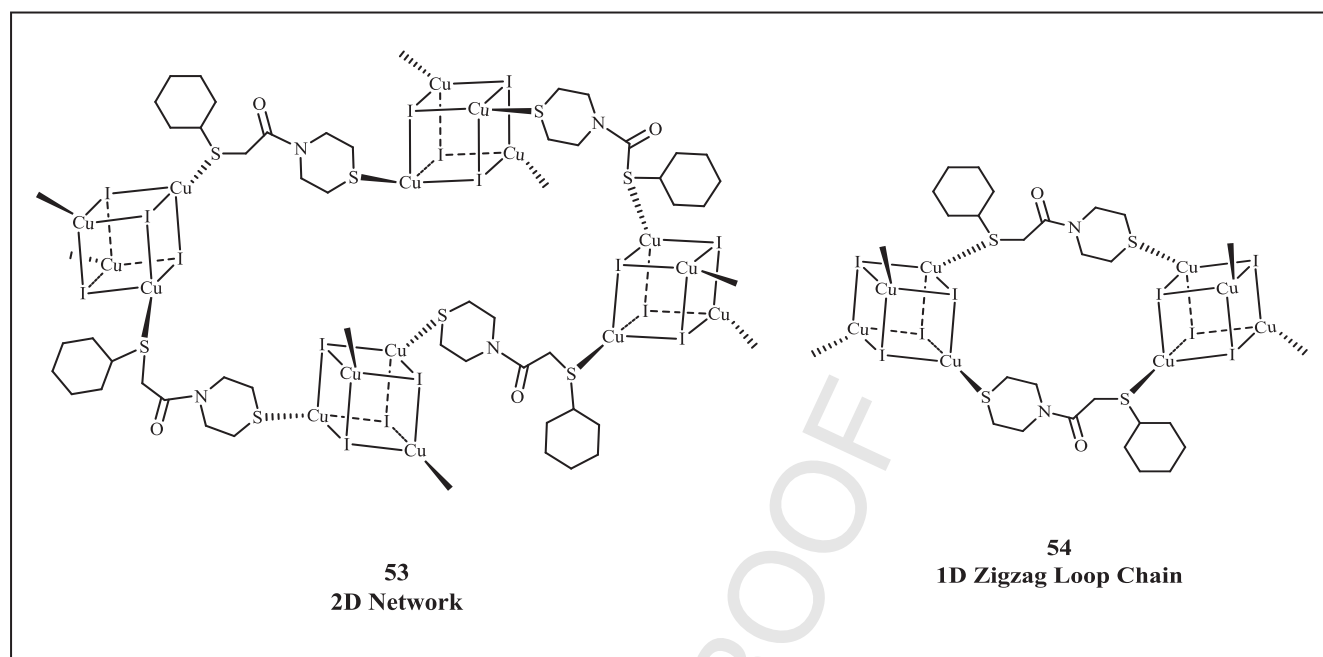
Harvey, Knorr et al. performed an experimental and theoretical investigation on the luminescence properties of coordination polymers obtained by reaction of CuX (X = Br, I) with mono- and polydentate thioethers ligands [57–59]. Reaction of the CuX salts with Et_2S, $PhS(CH_2)_4SPh$ or $PhSCH_2C\equiv CCH_2SPh$ afforded $[Cu_3Br_3(SEt_2)_3]_n$, **55** (a 1D chain containing rhomboid Cu dimers connected by two bridging ligands to open stepped cubane Cu_4Br_4 motifs), $[Cu_4I_4(SEt_2)_2(\mu\text{-}SEt_2)]_n$, **56** and $[Cu_4I_4\{\mu\text{-}PhS(CH_2)_4SPh\}_2]_n$, **57** (with Cu_4I_4 cubane clusters), and $[(Cu_6I_6)\{\mu\text{-}PhSCH_2C\equiv CCH_2SPh\}_3]_n$, **58** (containing Cu_6I_6 clusters). The solid-state luminescence spectrum of **55** at room temperature exhibit two emissions centered at 425 and 550 nm. At 77 K, the 550 nm emission is accompanied by a long shoulder at 650 nm and these two features were assigned to the Cu_4Br_4 center and to the $Cu_2Br_2S_2$ core, respectively. Compound **56** shows at room temperature an emission at 565 nm of CC origin, which, at low temperature, is intensified and sharpened. The narrower emission upon cooling was attributed to the rigidity of the ligand which allows small excited state distortions. In agreement, the use of a more rigid ligand in polymer **58** with respect to **57**, not only led to different clusters (Cu_6I_6 vs. Cu_4I_4), but also induced the largest narrowing of the emission on decreasing the temperature.

An example of luminescence thermochromism arising from a Cu_6S_6 cluster was reported by Karasawa et al. [60] who prepared the $[Cu_6(6\text{-}mpyt)_6]$ (6-mpyt = 6-methyl-2-pyridinethiolato) compound **59** by reaction of $CuSO_4$ with 1H-6-methylpyridine-2-thione in MeOH or by reaction of $Cu(ClO_4)_2$ with 2,2′-bis(6-methylpyridyl)disulfide. X-ray analysis revealed that the six copper atoms form a distorted octahedral core with relatively short Cu···Cu distances (2.831 and 3.326 Å). The compound shows the "classical" thermochromism with one band at 677 nm in its solid state emission spectrum at 300 K, which was assigned to a ^3CC excited state. By lowering the temperature, a gradual red-shift and a decrease in intensity in this emission band was observed together with the appearance of a HE band (of MLCT character) at 476 nm that became predominant at 5 K. The intensity of the two bands were complementary by changing the temperature
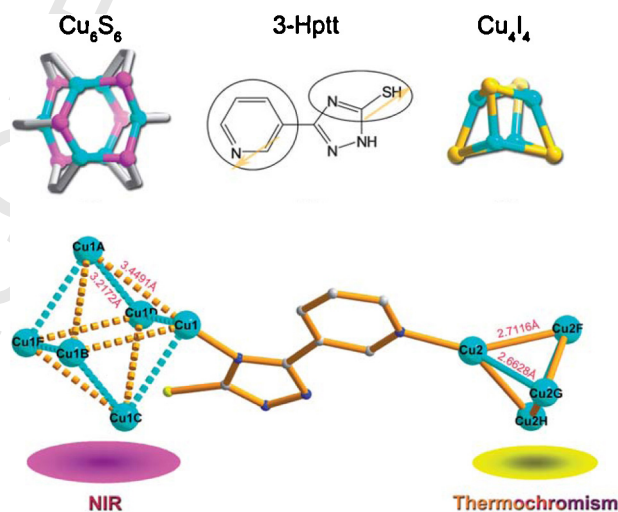

Fig. 11. Schematic representation of the assembly of a multi-metal-cluster MOF, taking 3-Hptt as linear linker and Cu_6S_6 and Cu_4I_4 clusters as octahedral or tetrahedral connecting nodes. Adapted with permission from Ref. [62]. Copyright 2013, Royal Society of Chemistry.

and it was suggested that the two levels originating the bands were populated through the same thermal activation process producing the luminescence thermochromism.

1H-6-methylpyridine-2-thione and 2,2'-bis(6-methylpyridyl)disulfide
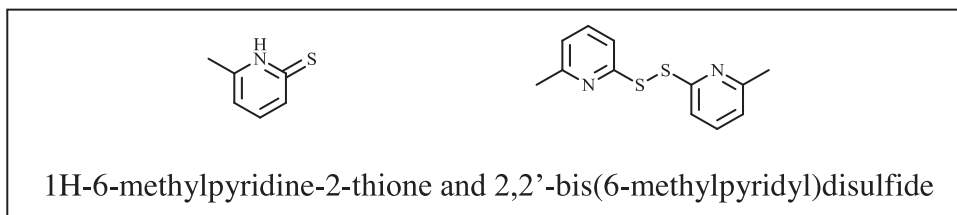
The Cu_6S_6 cluster $[CuI(4\text{-ptt})]_6 \cdot 8DMF \cdot 7H_2O$ (4-Hptt = 5-(pyridin-4-yl)-1H-1,2,4-triazole-3-thiol, DMF = N,N-dimethylformamide), **60**, exhibiting unusual near-infrared (NIR) thermochromic emission was reported by Hong et al. [61]. The compound displays at room temperature an emission at λ_{max} = 776 nm which was deconvoluted as the overlap of two peaks at 763 and 789 nm which were assigned to a ^{3}MLCT and a ^{3}CC transition, respectively. At 10 K, a blue shift and an intensification of the CT band was observed due to a better packing of the ligands and hydrogen bonding. The reduced intensity and the red shift (888 nm) of the CC band at low temperature was attributed to a distortion occurring in the excited state in which the metal centers adopt a more flattened coordination geometry.

5-(pyridin-4-yl)-1H-1,2,4-triazole-3-thiol (4-Hptt)
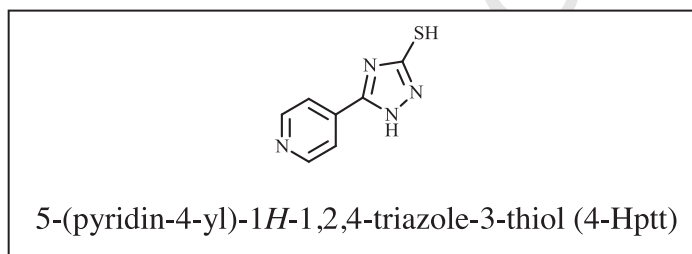
Aiming at obtaining a material with dual emission, the same group prepared the 3D MOF $[(Cu_4I_4)_3(CuI_6)_2(3\text{-ptt})_{12}]_n \cdot 24nDEF \cdot 12nH_2O$, **61**, with connecting nodes containing the Cu_4I_4 and Cu_6S_6 clusters as multi-luminophores [62]. The complex was prepared by reacting CuI with the organic ligand 5-(pyridin-3-yl)-1H-1,2,4-triazole-3-thiol (3-Hptt), that being less sterically hindered than the 4-Hptt previously reported [61], allowed the formation of both types of clusters (Fig. 11). Single crystal X-ray analyses revealed that the Cu···Cu distances in the Cu_4I_4 moiety are shorter than 2.80 Å, indicating strong cuprophilic interactions. Solid **61** displays at room temperature a broad emission at 790 nm, which was the result of the overlap of a band at about 770 nm assigned to the ^{3}CC of Cu_6S_6, and a broad emission above 800 nm originated from the ^{3}CC excited state of Cu_4I_4.

Upon cooling to 10 K an intense band was found at 590 nm corresponding to the ^{3}XLCT in Cu_4I_4 together a weak emission at 840 nm assigned to the ^{3}CC of Cu_6S_6. It was thus concluded that the "classical" thermochromic behavior was originated from the Cu_4I_4 moiety, being the Cu_6S_6 cluster only responsible for the red-shifted and the quenching of the NIR emission associated with the distortion occurring in the ^{3}CC excited state.

2.2. Luminescence vapochromism

The specific and convenient detection of compounds of interest in the environment represents one of the current challenges in chemistry. Detection of volatile organic compounds (VOCs) *via* chemical "sniffing" requires an interaction between the VOC and a detector substrate, resulting in a measurable change. Various d^8 and d^{10} metal complexes have been found to show vapor-triggered luminescence color changes with mechanism that usually involve reversible *rearrangements* catalyzed by solvent vapor or interstitial solvation of transition metal complexes and far less frequently, the *exchange* of ligands coordinated to metal centers. When metal coordination moieties are packed in the solid state, intermolecular interactions such as metallophilic contacts, π—π stacking, and hydrogen bonding in the solid-state stacked structures can be perturbed by interactions with interstitial solvate molecules. On the other hand exposure of solid metal complexes to vapors of VOCs may result in direct reaction of the VOC molecules with the complexes or induce coordination substitution reaction through metal–solvent bonds. The energy level of excited state is thus modified, inducing distinct changes in luminescence color or brightness [2].

For practical application as VOC luminescence sensors, apart from reversibility and selectivity, sensitivity, response time and durability are also important.

Studies on Cu(I) luminescent VOC responsive materials have appeared in the literature many years after the first pioneering work of Ford et al. [21]. It was only in 2010 that Pike et al. reported the reaction of various amine (L) vapor with solid CuCN at room temperature to produce adducts of the stoichiometry $CuCN \cdot L_n$ with n = 0.75–2.0 with visible colored luminescence responses highly dependent on the exact nature of the amines [63]. DFT calculations indicated that the HOMO of the $CuCN \cdot L_n$ compounds is mostly comprised of the $3dz^2$ orbital of the metal, while the LUMO is a mixture of 4p orbitals of Cu(I) and π* orbitals of the cyano ligand, thus indicating that emission has mixed MC and MLCT character. In contrast to the authentic $(CuCN)L_n$ compounds prepared by reaction of CuCN in neat heated amine which only partially lose amine over a period of weeks under vacuum, the vapor-exposed samples were found to quickly lose their visible luminescence when placed under vacuum. The binding of amine into solid copper(I) cyanide is thus a totally reversible process. The ligand induced CuCN emission shift from the UV (392 nm) into the visible region was suggested as potential for a sniffing detection system for amines or other nucleophilic VOCs.
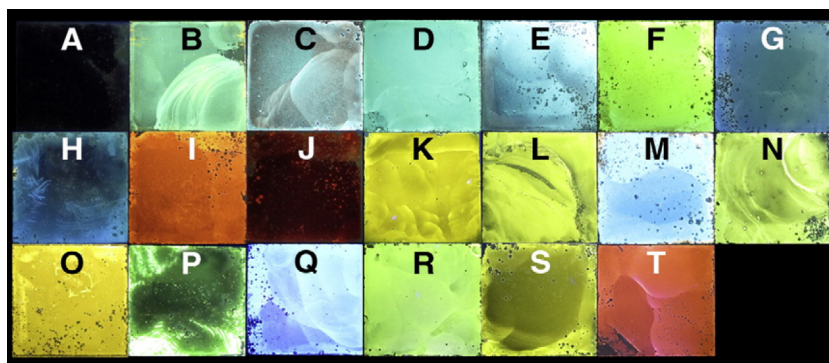
Fig. 12. Previously VOC-exposed CuI films on glass placed under 365 nm irradiation. A, no exposure; B, pyridine; C, 2-Me-pyridine; D, 3-Me-pyridine; E, 4-Me-pyridine; F, 2-Br-pyridine; G, 3-Cl-pyridine; H, 3-Br-pyridine; I, 2-Ph-pyridine; J, 4-acetylpyridine; K, piperidine; L, N-Me-piperidine; M, N-Et-piperidine; N, morpholine; O, N-Me-pyrrolidine; P, N,N'-Me$_2$-piperazine; Q, N,N'-Et$_2$-piperazine; R, Me$_2$S, S, Et$_2$S; T, tetrahydrothiophene. Reprinted with permission from Ref. [64]. Copyright 2013 Elsevier B.V. All rights reserved.
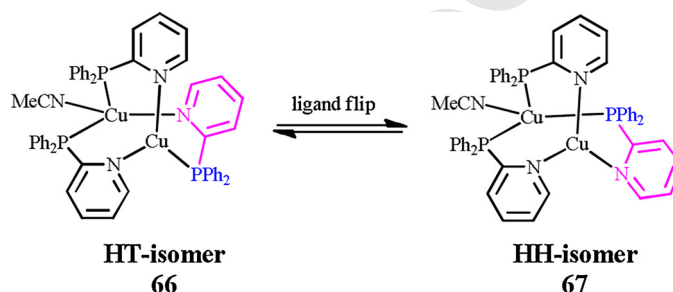
Scheme 3. HH and HT isomers [66].

Similarly, in 2014 Pike et al. reported a study on the use of CuI films as viable VOC sensors aimed at the development of CuI film surfaces for real-time photoluminescence detection of amine and sulfide vapors in the environment [64]. CuI films, prepared by casting from CH$_3$CN solution on microscope cover glasses, were exposed for 5–15 min to saturated atmospheres of amine or sulfide vapors in sealed containers. Steady-state PL spectra, both at room temperature and 77 K, were measured immediately after exposure. A wide range of luminescence behavior was observed, with emission wavelength varying from blue (447 nm in the case of 3-BrPy) to orange (620 nm for tetrahydrothiophene, THT displaying also a green 530 nm emission) and was often distinctive even for chemically similar VOCs, demonstrating the potential selectivity of CuI detection (Fig. 12).

On the basis of the observed multiple emission of CuI-THT, suggesting the presence of various phases, the same group further investigated this derivative [65]. According to the stoichiometry and the temperature six different phases were recognized and isolated from the reaction of CuI with THT in MeCN. In particular, (CuI)$_4$(THT)$_2$, **62**, (CuI)$_{10}$(THT)$_7$(MeCN), **63**, and two polymorphs of (CuI)$_4$(THT)$_4$, (**64** and **65**) are luminescent with modest but fully reversible thermochromic behavior. At room temperature, solid compounds showed a LE band in the 519–590 nm region, attributed to ^{3}CC transitions. At 77 K the emission band of **62** and **63** red-shifted of 9 and 23 nm, respectively. The broad emission of **64** and **65** (590 nm and 541 nm respectively at room temperature) were found to split at 77 K into two coupled excitation/emission band pairs. On the basis of the energy Stokes shifts and lifetimes, different contribution from ^{3}XMCT and ^{3}MC were suggested for the compounds' CC emissions.

Wang et al. reported a dinuclear copper(I) complex that undergoes methanol-responsive luminescence change through structural isomerization [66]. Compound [Cu$_2$(dppy)$_3$(MeCN)](BF$_4$)$_2$ (dppy = diphenylphosphino-pyridine), **66**, was prepared by reaction of [Cu(MeCN)$_4$]BF$_4$ with dppy in 2:3 ratio in MeCN. The compound emits bright blue light (489 nm) in the solid state at room temperature. By recrystallization of **66** from a mixed solvent of CH$_2$Cl$_2$–MeOH, [Cu$_2$(dppy)$_3$(MeCN)](BF$_4$)$_2$·MeOH (**67**·MeOH), showing a solid state green emission (520 nm) at room temperature, was obtained. X-Ray single crystal structural analysis revealed that the two compounds are linkage isomers, **66** having a head-to-tail (HT) arrangement of the three bridging dppy ligands while **67** a head-to-head (HH) configuration (Scheme 3).

The conversion from **66** to **67**·MeOH could also be performed by exposure of solid **66** to MeOH vapor, and the process was fully reversed when the methanol adduct was recrystallized from MeCN/Et$_2$O. The linkage isomerization reaction is accompanied by a significant increase of the Cu···Cu separation, from 2.721 Å in **66** to 2.7961 Å in **67**·MeOH, however, in **67** relevant π–π interactions between phenyl and pyridyl planes takes place lowering the LUMO energy level and resulting in a red shift of the emission with respect to **66**.

Pike et al. prepared compounds [(CuI)$_2$(N,N'-diethylpiperazine)], **68**, [(CuI)$_2$(N,N'-dibenzylpiperazine)], **69**, and [(CuI)$_2$(N,N'-bis-phenethylpiperazine)], **70**, by reaction of CuI with the corresponding N,N'-disubstituted piperazine in MeCN [67]. The structures of the compounds consist of chains with piperazine-linked Cu$_2$I$_2$ rombs. All complexes are photoluminescent at 77 K, and all but **69**, photoluminescent at room temperature, showing bands at wavelengths of less than 500 nm which, according to spectroscopic studies and DFT calculations, were associated to cluster-centered (XMLT/metal centered) excitations for the aliphatic amines and MLCT (d → π*) for aromatic amine. The complexes act as sensor materials, undergoing irreversible changes in their luminescence emission in response to gas phase aliphatic and aromatic amines (Nu) associated with the formation of cubanes (CuI)$_4$Nu$_4$ through replacement of the piperazine
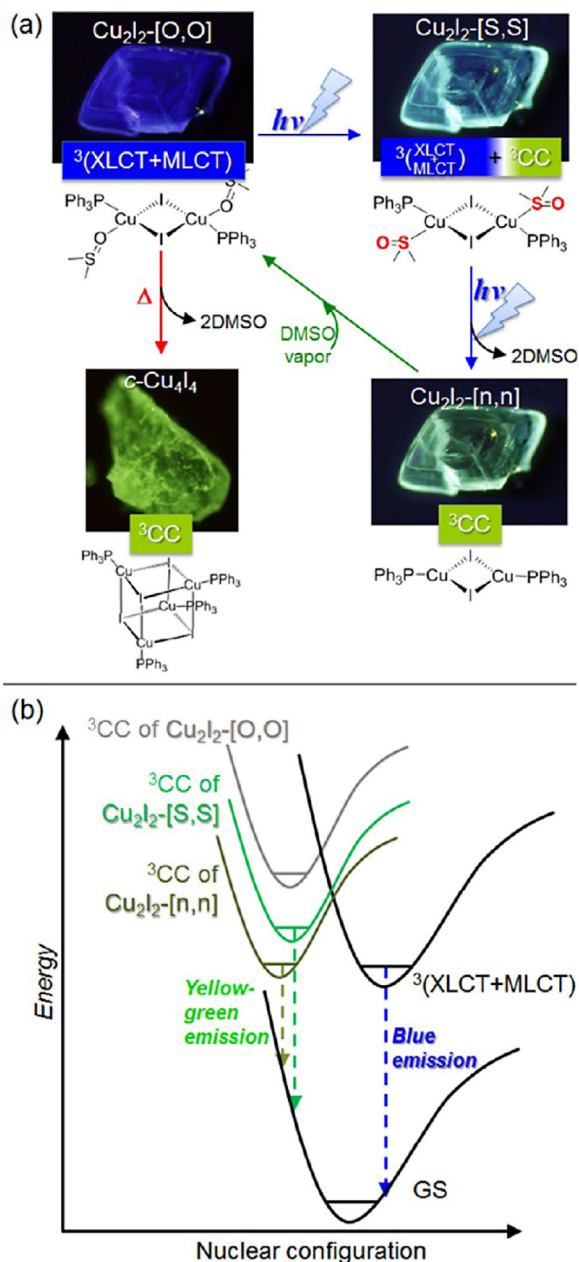
Fig. 13. (a) Possible Mechanism of Light-, Vapor-, and Heat-Induced Structural Transformation of Cu_2I_2-[O,O]. (b) Simplified Energy Level Diagram of the Three Possible Forms, Cu_2I_2-[O,O], Cu_2I_2-[S,S], and Cu_2I_2-[n,n]. Reprinted with permission from Ref. [68]. Copyright 2013, American Chemical Society.

ligands. Depending on the nucleophile, luminescent materials with emission colors ranging from blue (Nu = 2-methylpyridine) to red (Nu = morpholine) were obtained. This behavior was not observed for the other complexes prepared in the same article with less sterically demanding piperazines all containing 4-coordinated copper(I).

Kato et al. reported the light-, vapor-, and heat-induced structural transformation of the halide-bridged rhombic dicopper(I) complex [$Cu_2(\mu$-I$)_2$(DMSO)$_2$(PPh$_3$)$_2$], **71**, prepared by reaction of CuI with PPh$_3$ in DMSO [68]. Single-crystal X-ray diffraction measurements revealed that the DMSO ligand is coordinated to the Cu(I) ion *via* the O atom. Such O-coordinated linkage isomer, Cu_2I_2-[O,O], shows in the solid state at room temperature bright blue phosphorescence (λ_{em} = 435 nm) from the ^{3}XLCT and ^{3}MLCT mixed excited state. Upon thermal (423 K for 1 day) removal of DMSO, the conversion of Cu_2I_2-[O,O] to the cubane complex (c-Cu_4I_4), showing yellow-green emission from the ^{3}CC excited state, was observed. The c-Cu_4I_4 complex was not converted to the original Cu_2I_2-[O,O] by exposure to DMSO vapor even at the relatively high temperatures. It was also found that under UV irradiation, the blue phosphorescence rapidly disappears and a new green emission band simultaneously appears at 500 nm. With prolonged irradiation, the emission color was gradually change to yellowish-green (λ_{em} = 540 nm). The initial blue phosphorescence of Cu_2I_2-[O,O] was recovered by exposure of the UV-light-irradiated sample to saturated DMSO vapor for several hours at 298 K. IR spectra acquired under UV irradiation suggested that linkage isomerization of the ambidentate DMSO ligand from the O-coordinated isomer, Cu_2I_2-[O,O], to the S-coordinated isomers, Cu_2I_2-[S,S] *via* Cu_2I_2-[O,S], occurs under UV irradiation. By prolonged UV irradiation, the DMSO removed dinuclear complex [$Cu_2(\mu$-I$)_2$(PPh$_3$)$_2$] (Cu_2I_2-[n,n]) is possibly obtained (Fig. 13). Theoretical calculations suggested that both the linkage isomerization from O-coordination to S-coordination and

the release of the DMSO ligand cause contraction of the rhombic $Cu_2(\mu\text{-}I)_2$ core, making the $Cu\cdots Cu$ interaction more effective. This contraction facilitates generation of the ^3CC emissive state by thermal excitation from the ^3XLCT and ^3MLCT mixed transition state, resulting in longer wavelength emission.

Li et al. reported the synthesis and characterization of MOF $[(CuCN)_3L\cdot(H_2O)(CH_3CH_2OH)]_n$ (L = 2,6-bis((3,5-dimethyl-1H-pyrazol-4-yl)methyl)pyridine), **72**, and of its thermally desolvated analog **73** [69]. Solid **72** shows a broad band at 490 nm which was assigned to a mixture of intra/interligand charge transfer and MLCT, with partial contribution of $Cu\cdots Cu$ bonding. Desolvated **73** exhibits blue luminescence at around 450 nm, which was attributed to ILCT. **73** is capable of qualitative heterogeneous solid–liquid sensing for several VOC solvents through reversible emission color changes. The guest-dependent luminescent variation of the **73**·solvent series, prepared by immersing **73** in different VOC solvents, was found by powder X-ray diffraction (PXRD) to be connected with the incorporation of the guest molecules in the MOF host. The solid–liquid sensing behavior to MeCN solvent, not only induced the largest shift (about 80 nm) of the emission peak, with a visual change from blue to yellow, but also shifted the emission peak of the **73**·MeCN sample back to the original value after drying in air, suggesting an easy access and departure of MeCN molecules into the channels of the dynamic MOF sensor. Based on this observation, a thin film device for quantitative real-time solid–gas monitoring of MeCN vapor was assembled. The emission of the dynamic MOF sensor **73** responded gradually to the continuously increasing concentration of the MeCN vapor eventually matching that of **73**·MeCN realized in the solid–liquid sensing process. The **73**·MeCN sample could be easily reactivated and reused for many cycles of detection–activation without the loss of sensing ability.
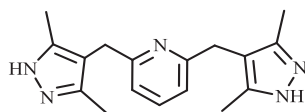
2,6-bis((3,5-dimethyl-1H-pyrazol-4-yl)methyl)pyridine

The preparation of the dimeric Cu(I) complex $[Cu_2(PPh_3)_4(MeCN)_2(Bpy)](BF_4)_2$ (Bpy = 4,4′-dipyridyl), **74a**, by reaction of $[Cu(MeCN)_4]BF_4$ with two equivalents of PPh_3 and a half-equivalent of Bpy in either CH_2Cl_2 or acetone was reported by Royzman et al. [70]. The compound shows in the solid state at room temperature intense (PLQY 45%) emission (λ_{em} = 486 nm) associated to MLCT behavior. The MeCN ligands can be readily removed from **74a** by heating in a vacuum oven at 393 K, producing $[Cu_2(PPh_3)_4(Bpy)](BF_4)_2$, **74b**, with reduced QY (7%) at 568 nm. **74b** reversibly absorbs many vapor phase nucleophiles (Nu), as revealed by thermogravimetry. Intense luminescence emission was restored for **74b**/Nu, Nu = MeCN (λ_{em} = 492 nm), acetone (λ_{em} = 548 nm), tetrahydrothiophene (THT) (λ_{em} = 529 nm), and Et_2S (λ_{em} = 499 nm). In contrast, exposure to Nu = water, morpholine, 3-methylpyridine, piperidine, or quinoline seemed to further attenuate the weak **74b** emission according to Cu(I) exciplex formation with trapped Nu molecules. In order to further study Nu uptake and emission response, films of **74b** were produced by casting CH_2Cl_2 solutions of **74a** onto glass. Fresh films were exposed to saturated MeCN, acetone, THT, and Et_2S vapor. The intense emission associated with these exposed films matched that of the powders. Formation of emissive **74b**/Nu adducts, while reversible for powder samples, is irreversible for the films. Neither application of vacuum nor heating reverse adduct formation.

The synthesis and structural characterization of an hexanuclear Cu(I) cluster $\{Cu_3(L)_2\}_2$ (L = 4,4′,4″-[1,3,5-phenyl-tri(methoxy)]-tris-benzoic acid]), **75**, by in situ reduction of Cu(II) to Cu(I) treating $Cu(NO_3)_2\cdot 2.5H_2O$ and L in DMF at solvothermal condition, were reported by Maji et al. [71]. Single-crystal X-ray crystallographic studies revealed that the carboxylate groups control the $Cu\cdots Cu$ interionic distance which eventually results in cuprophilic interactions. Solid state room temperature emission spectrum showed intense (PLQY 27.6%) yellow emission (λ_{em} = 560 nm) which was suggested of hybrid LMCT and cluster centered character. The emission properties of **75** were further explored to sense electron rich and deficient solvent vapors including nitroaromatics. It was found that vapors of compounds containing
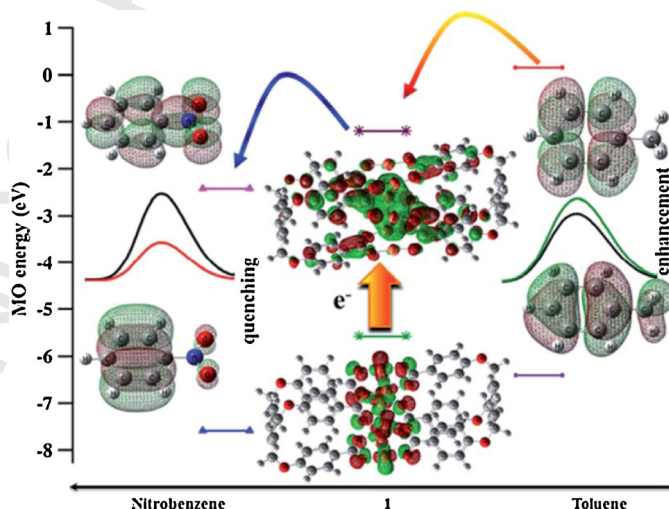

Fig. 14. Excited state electron migration mechanism. Reprinted with permission from Ref.[71]. Copyright 2014, Royal Society of Chemistry.

electron deficient groups like nitrobenzene (NB), o-dinitrobenzene (o-DNB) and 2,4-dinitrotoluene (DNT) quench the emission of **75** (in the order NB > o-DNB > DNT), while an emission intensification was produced for those having electron donating groups like toluene, o-xylene and p-xylene. Quenching or enhancement being affected by electron availability and vapor pressure of the solvent. The observed trend was explained by a donor–acceptor electron transfer mechanism in agreement with the relative orbital energy levels of the cluster and analyte obtained from DFT calculations. In the case of an electron-withdrawing analyte, the LUMO is a low lying π^*-type orbital and its energy is below the LUMO of **75**. Upon excitation, electrons are transferred from the LUMO of **75** to the LUMO of analyte resulting in quenching. In the case of the electron donating analytes the LUMO is above the LUMO of **75** and electrons can flow from the LUMO of analytes to the LUMO of complex, resulting in emission enhancement (Fig. 14).

4,4′,4″ -[1,3,5-phenyl-tri(methoxy)]-tris-benzoic acid
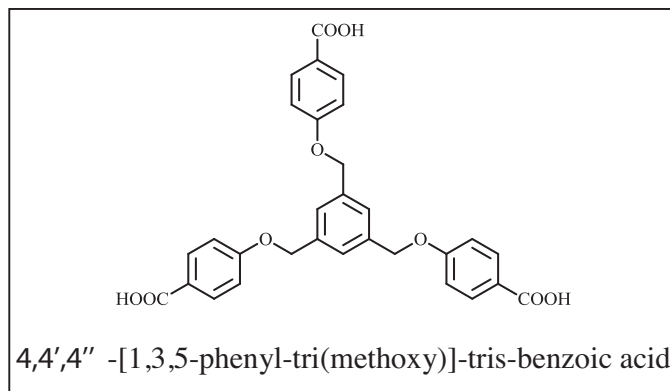
A porous Cu(I)-MOF as colorimetric sensor to detect water and formaldehyde species in a single-crystal-to-single-crystal fashion was reported by Dong et al. [72]. $Cu_2(L)_2I_2 \cdot MeCN \cdot MeOH \cdot 1.5H_2O$ (L = 1-benzimidazolyl-3,5-bis(4-pyridyl)benzene), **76**, was prepared by reaction of L with CuI in a $MeCN/CH_2Cl_2/MeOH$ mixed-solvent system, as bright yellow crystals.

1-benzimidazolyl-3,5-bis(4-pyridyl)benzene
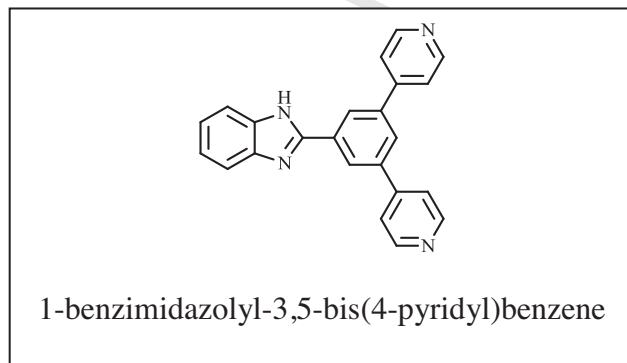
On standing at room temperature for a while, a single crystal-to single crystal transformation to $Cu_2(L)_2I_2 \cdot 4H_2O$, **77**, occurs due to the escape of the encapsulated MeCN and MeOH in **76**, and the entrance into the cavities of water molecules from air. Based on these results the potentiality of **76** as humidity sensor was tested and the sensing process was monitored by solid-state emission spectra. The 607 nm emission of **76**, originated from a ^3CC transition having mixed XMCT character, was strongly quenched by increasing humidity exposition time due to non radiative energy transition. In addition, the emission maximum was slightly red-shifted (613 nm), in consequence to slight variation of the bond distances within the Cu_2I_2 cluster core. It was also observed that when crystals of **77** were exposed to formaldehyde vapor for around 24 h at room temperature a single crystal-to single crystal transformation to $Cu_2(L)_2I_2 \cdot 2(HCHO)(H_2O)$, **78**, occurred. HCHO encapsulation caused dramatic changes in emission spectra, with an intensification and a blue shift (from 613 to 598 nm) of the emission band in the HCHO-loaded samples due to a structural rigidity enhancement imposed by the host–guest interactions and to variations of the Cu_2I_2 core. Based on this results, this Cu(I)-MOF was indicated as a potential candidate for a portable sensing device for formaldehyde pollutant.

Besides the above reported Cu(I) compounds, there are some reports on the vapochromic behavior, displayed by mixed Cu(I)-Au(I) derivatives. Catalano et al. reported the first gold(I)-copper(I) complex showing vapochromic behavior associated with "on-off" Au$\cdots$Cu interactions induced by ligand exchange reaction [73]. $[Au(im(CH_2py)_2)_2(Cu(MeCN)_2)_2](PF_6)_3$, **79**, was prepared by reaction of $[Au(im(CH_2py)_2)_2]PF_6$ with 2 equiv of $[Cu(MeCN)_4]PF_6$. Upon exposure of solid **79** to MeOH vapor, an attenuation and a red shift of the emission from blue (462 nm) to green (520 nm) was observed due to the exchange of all MeCN molecules and the formation of $[Au(im(CH_2py)_2)_2(Cu(MeOH))_2](PF_6)_3$, **80** (Scheme 4).

The molecular structures of **79**·2MeCN and **80**·2MeOH 2Et$_2$O, determined by single-crystal X-ray diffraction, revealed long (4.596 Å) and short (attractive) (2.7195 Å) Au$\cdots$Cu separations in the two compounds respectively. The attractive interaction between individual metals in **80** was indicated as the consequence of the replacement of two MeCN molecules per Cu(I) center by only one methanol ligand, making one coordination site of the copper(I) centers available for metal–metal bonding. Exposure of **80** to atmosphere produced a partial loss of MeOH accompanied by a luminescence shift to 543 nm. The uptake and loss of MeOH vapor is rapid and reversible. Exposure of **80** to vacuum afforded complete loss of MeOH, with luminescence shift to 573 nm. **79** was regenerated by treatment of **80** with MeCN vapor,
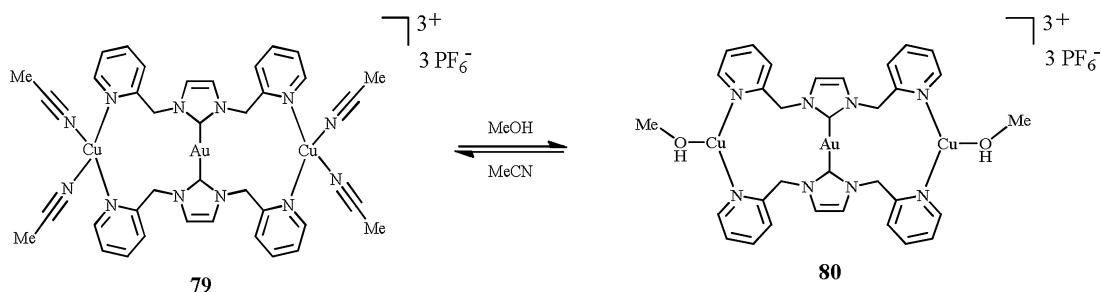
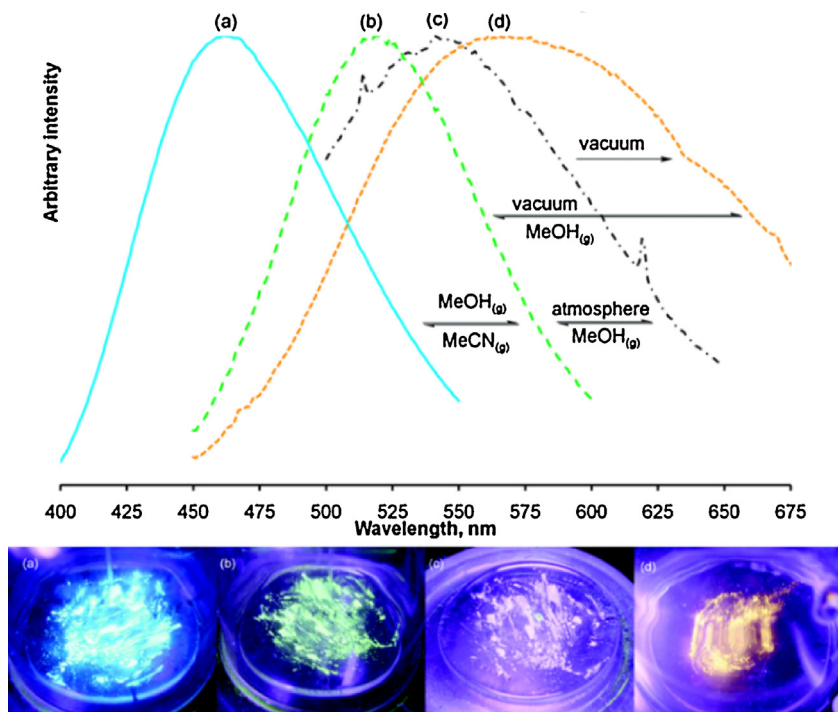**Scheme 4.** Interconversion between complexes **79** and **80** (solvent indicate their vapors) [73].

Fig. 15. (top) Normalized solid-state emission spectra showing transformations and (bottom) photographs of (a) **79**, (b) compound **80** formed by treating **79** with MeOH vapor, (c) MeOH-treated **79** exposed to atmosphere, and (d) MeOH-treated **79** exposed to vacuum. Reprinted with permission from Ref.[73]. Copyright 2010, American Chemical Society.

the interconversion being followed by powder X-ray diffraction. Compound **79** also reacts with acetone and H_2O vapors, leading to species that produce yellow-orange (591 nm) and green (519 nm) emission respectively (Fig. 15).

Vapochromic behavior induced by modulation of metallophilic interactions by organic solvent was observed for another Au-Cu bimetallic complex [74]. $[Au_2Cu_2(C_2OHC_5H_8)_4]_n$, **81**, was prepared by reaction of $Au(SC_4H_8)Cl$, $Cu(NCMe)_4PF_6$, and 1-ethynylcyclopentanol in the presence of NEt_3. Four crystalline polymorphs, with different PL behavior, could be isolated by recrystallization in different solvents: MeOH **81a**; EtOH, acetone, or $CHCl_3$ **81b**; toluene **81c**; and diethyl ether or ethyl acetate **81d**. Form **81a** displays very weak yellow luminescence in the solid state (582 nm), while **81b** exhibits a slight increase in emission intensity with a very similar peak wavelength (566 nm). **81c** and **81d** show a bathochromic shift (620 and 609 nm respectively) and an intensification of the emission. The structures of **81b–d** were determined by single-crystal X-ray diffraction and the enhancement of the emission intensity was suggested to be correlated with the increasing role of metal—metal bonding which makes emission progressively more metal-centered in the order **81b** < **81c** < **81d**. It was found that the vapors of certain solvents can induce solid-state isomerization accompanied by switching of luminescence: exposure of solid **81d** to MeOH vapor at room temperature resulted in a dramatic drop in the emission intensity due to the transformation of **81d** into **81a**. The reverse isomerization was induced by treatment of **81a** with diethyl ether or ethyl acetate vapors. MeOH vapor influenced also the emissive behavior of **81b** and **81c**, causing a significant decrease in photoemission and a shift to the yellow region in the case of **81c**. **81b** and **81c** were also quickly converted into **81d** thermally at *ca.* 408 and 388 K, respectively (Scheme 5).

Koshevoy et al. reported three heterometallic Au(I)–Cu(I) complexes showing distinct switching of luminescence upon exposure to polar solvent vapors [75]. Compound $[HC(PPh_2)_3Au_3Cu(C_2COHPh_2)_3]PF_6$, **82**, was synthesized *via* treatment of $(AuC_2COHPh_2)_n$ with $(PPh_2)_3CH$ ligand in the presence of Cu^+ ions and NEt_3. Addition of Cl^- or Br^- anions to the compound resulted in the formation of neutral $[HC(PPh_2)_3Au_3CuX(C_2COHPh_2)_3]$ derivatives (X = Cl (**83**), Br (**84**)). Treatment of solid solvent-free **82** with methanol vapors for 30 min resulted in a *ca.* 50 nm hypsochromic emission shift (from 557 to 501 nm) and by a 3-fold increase of the intensity, reaching a value of 60%. A remarkable hypsochromic shift of the corresponding emission band was also observed for interaction of the solid solvent-free samples of **83** ($\lambda_{em} = 550$ nm) with acetone ($\lambda_{em} = 480$ nm) and **84** ($\lambda_{em} = 550$ nm) with THF ($\lambda_{em} = 491$ nm) vapors. X-ray powder diffraction studies revealed that the initial solvent-free powders are X-ray amorphous and treatment with solvent vapors induce reorganization of
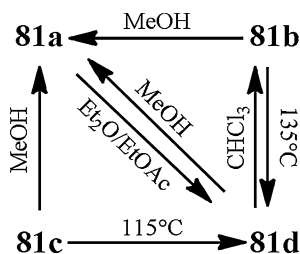
Scheme 5. Summary of the observed interconversions among **81a–d** (solvent indicate their vapors) [74].

the solid to give the crystalline phases and that it is this amorphous-crystalline conversion at the basis of the observed vapoluminescence. Solvation of complex **82** is virtually irreversible, as a prolonged vacuum does not have any appreciable effect on the properties of the sample treated with MeOH vapors. Clusters **83** and **84** tend to lose slowly absorbed solvent molecules. However, complete reversibility could not be achieved even upon exposure of these compounds to high vacuum and pure solvent-free systems were not observed.

2.3. Luminescence mechanochromism

In recent years, mechanochromic luminescent materials which exhibit reversible modification of the emission wavelength in response to external mechanical forces (grinding, shearing, compressing, or rubbing) have attracted great attention for both fundamental research and for their potential applications in luminescence switches, mechanosensors, mechanohistory indicators, security papers, optoelectronic devices, and data storage in various fields [76]. The importance of such smart materials is testified by the ever growing numbers of publications on this subject. However, the majority of reports concern organic systems [77], with examples based on transition-metal complexes still relatively limited and mainly based on Au(I) and Pt(II) complexes with few examples of Ag(I), Cu(I) and Zn(II) derivatives [76]. In these systems, the observed mechanoluminescence is correlated with disruption of an intermolecular metal···metal contact or inter-ligand π—π stacking, or a change in molecular conformation. The subsequent reversion to the original solid-state emission is usually achieved upon thermal treatment or recrystallization.

Concerning Cu(I) based compounds (see Table 4), pyrazolate complexes of the Cu_3pz_3 type, possessing a planar configuration prone to form excimer with PL behavior strictly correlated to intermolecular Cu···Cu interactions, seem ideal candidate to show pressure-triggered luminescent properties.

In 2010 Gong et al. aiming at understanding the relationship between the intermolecular Cu···Cu distance and phosphorescent properties of copper(I) complexes, prepared three trimeric copper(I) pyrazolates, namely $\{[3,5-(Me)_2-4-(Ph)Pz]Cu\}_3$, **85**, $\{[3,5-(Me)_2-4-(1-Naph)Pz]Cu\}_3$, **86**, and $\{[3,5-(Me)_2-4-(9-Anthr)-Pz]Cu\}_3$, **87**, in which substituents with different volumes were used to tune the distance of intertrimer units [78]. High pressure experiments were also performed in order to continuously modify the distance between two adjacent molecules.

Table 4
Summary of mechanochromic emissive behavior of Cu(I) compounds.

| Compound	Before grinding		After grinding	Proposed mechanism	Reference
	Cu···Cu (Å)	λ_{em} (nm)	λ_{em} (nm)		
88	3.087–3.175[a]	620, 390 (HE/LE = 4.0)	730, 370 (HE/LE = 0.28)	Grinding induced amorphization with shortening of Cu···Cu distances	[79]
89a	3.135–3.141[a]	630, 390 (HE/LE = 4.8)	730, 370 (HE/LE = 0.19)	Grinding induced amorphization with shortening of Cu···Cu distances	[79]
89b	3.123–3.168[a]	630, 380 (HE/LE = 7.4)	730, 370 (HE/LE = 0.21)	Grinding induced amorphization with shortening of Cu···Cu distances	[79]
89c	3.088[a]	650, 390 (HE/LE = 10.6)	(HE/LE = 0.16)	Grinding induced amorphization with shortening of Cu···Cu distances	[79]
90		540	573	Solvent removal causes contraction of Cu···Cu distances	[80]
91	2.854[b]	539	700	Crystal to amorphous transition with alteration of Cu···Cu and π···π interactions	[81]
92		512	490	Crystal to amorphous transition with alteration of Cu···Cu and π···π interactions	[82]
93a	3.220–3.254[c]	535	595	Crystal to amorphous transition with alteration of Cu···Cu and π···π interactions	[83]
93b	3.205–3.201[c]	552	599	Crystal to amorphous transition with alteration of Cu···Cu and π···π interactions	[83]
93c	3.654[c]	615	605	Crystal to amorphous transition with alteration of Cu···Cu and π···π interactions	[83]

[a]Intermolecular; [b]between helical chains; [c]between two adjacent layers.

Schematic structure of complexes **85-87**
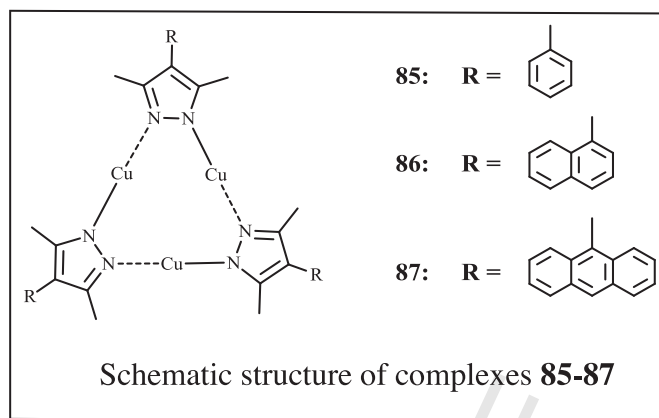
At ambient temperature and pressure, powders of the three compounds display a dramatically different emissive behavior. **85** and **86** show strong phosphorescence (at 620 and 638 nm, respectively) and weak fluorescence (at 440 and 420 nm, respectively). **87** displays only fluorescence at 430 nm and 530 nm. Photophysical measurements and theoretical studies revealed that the intertrimer Cu···Cu interactions, tuned by pyrazolate substituents, strongly influence the compounds' phosphorescence which was assigned to the excited-state of dimers/polymers of trimers ($^*[Cu_3]_n$) with LMCT characteristics. A direct evidence to support this assignment was the observation that the phosphorescence intensity of **85** increased about 6-fold at 2.36 GPa, in comparison with that under ambient conditions. Such intensification was explained with reduced intertrimer Cu···Cu distances resulting in more intense cuprophilic interactions, favoring the form of dimers or polymers. On the contrary, the slight pressure dependence of the phosphorescence intensity of **86** was explained on the basis of slight changes of the intertrimer Cu···Cu distances with increasing pressure. With regard to **87**, no phosphorescence was observed because intertrimer Cu···Cu distances were too large to allow significative interactions. All these results unambiguously proved that intermolecular Cu···Cu interactions played the most important role in the photophysical properties of the trimer copper(I) pyrazolates. However, this pressure triggered luminescence behavior cannot be strictly classified as mechanochromism since it regards only enhancement of the emission and not a wavelength shift. Cu(I)-pyrazolate type complexes have in fact solid-state phosphorescent emission lying in the LE region (orange or red) thus pressure induced shortening of Cu···Cu distances has almost no visual result. Pyrazolate-compounds with mechanically induced shift of the emission have been reported only very recently [79]. Li et al. prepared, by solvothermal reaction, $[Cu_3(EBPz)_3]$ (EBPz = ethyl-4-benzoate-3,5-dimethylpyrazolate), **88**, and three polymorphs of $[Cu_3(MBPz)_3]$ (MBPz = methyl-4-benzoate-3,5-dimethylpyrazolate), **89a–c**. All solid compounds display at room temperature dual emission with an intense HE ligand-based fluorescent band (380–390 nm) and a much weaker LE cluster-centered phosphorescence (620–630 nm). The weakness of the LE band is unusual for pyrazolate excimers having short Cu···Cu distances as is in the present case, and it is related to the presence of the para ester group which, acting as an auxochrome, intensify the ligand localized HE band. All solid compounds display luminescence mechanochromism associated with variation of the relative intensity of the HE and LE bands, the LE band becoming predominant in the spectra of all ground samples. The process is completely reversible by heating at 403 K for 2 h or adding few drops of EtOH to the ground samples. This grinding-triggered luminescent behavior is associated to a crystal-to-amorphous transformation (XRPD evidences) with shortening of intermolecular Cu···Cu distances.

TD-DFT calculations indicated that the emissive singlet and triplet excited states lie close in energy, suggesting the possibility of Reverse Inter System Crossing (RISC; see Section 3 for more details) which would agree with the long fluorescent lifetimes measured for the HE band.
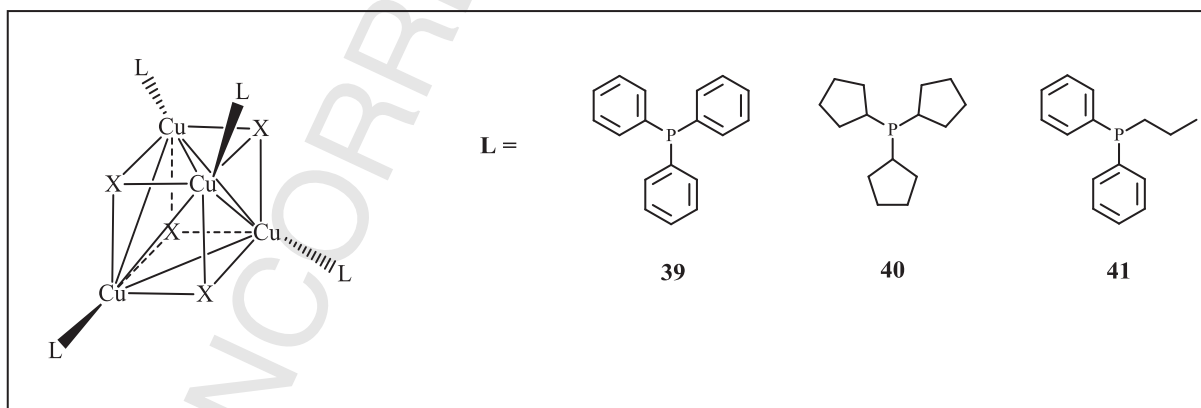
Exploiting the modulation of Cu···Cu interactions, Hong et al. realized a stimuli-responsive material with AND logic function [80]. Here our interest concerns the mechanochromic behavior of the compound having decided, as stated in the introduction, not to include studies on solvent triggered emission changes.

$[CuI(Hdppa)]_4 \cdot H_2O \cdot EtOH$ (Hdppa = 3-(diphenylphosphino)propionic acid), **90**, displays, at room temperature in the solid state, highly efficient (PLQY 92.8%) green emission ($\lambda_{em} = 540$ nm). When ethanol solvent was removed upon grinding or heating at 323 K in vacuum, the luminescence changed to an intense (PLQY 86.8%) yellow emission ($\lambda_{em} = 573$ nm). After treating it with a few drops of EtOH and
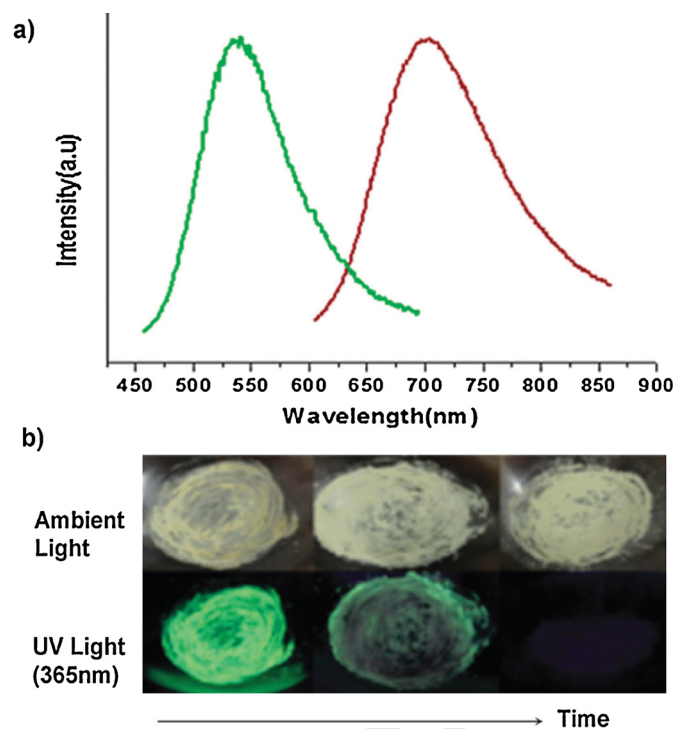
Fig. 16. (a) Normalized solid-state emission spectra for the unground (green line) sample and ground (red line) sample; (b) photographs of **91** show luminescence changes with grinding time at room temperature under ambient light and UV lamp, respectively. Reprinted with permission from Ref. [81]. Copyright 2013, Royal Society of Chemistry.

drying, the emission was reverted to the original green emission. The color conversion process is fully reversible as demonstrated through numerous cycles without any decomposition. According to previous reports, the emission bands at room temperature were attributed to the ^{3}CC excited state. The observed color changes were associated with variation in Cu$\cdots$Cu distances which are reduced upon grinding and restored to the original value upon treatment with drops of EtOH. In ground sample the closer Cu$\cdots$Cu interactions allow for an effective overlap of the d orbitals between Cu atoms therefore the higher energy of the HOMO results in the lowering of the HOMO–LUMO energy gap and an increase in the emission wavelength.

Zhang et al. reported the solvothermal preparation and characterization of two Cu(I) coordination polymers with mechanical-grinding-triggered-luminescence change, namely [Cu(dm-bim)]$_n$ (dm-bim = 5,6-dimethylbenzimidazolate), **91** [81] and [CuBH(dm-bim)$_3$]$_n$·(solvent)$_x$, **92** [82]. In the solid state at room temperature **91** shows a green emission at 539 nm which was assigned to a ^{3}MLCT with contribution from 3d → 4s cluster-centered excited states. When ground, **91** displays an obvious red shift about 160 nm (λ_{em} = 700 nm, Fig. 16a).

Solid **92** emits at room temperature at 512 nm according to an ^{3}MLCT excited state. After grinding, the emission spectrum of **92** showed a blue shift of about 20 nm (Fig. 17).

For both compounds X-ray powder diffraction analysis indicated a crystal-to-amorphous phase conversion caused by the strong grinding. The luminescent shifts were suggested to be related to alteration of Cu$\cdots$Cu and $\pi\cdots\pi$ interactions. The crystalline phase of **91** could be recovered only after one month, from a mixed chloroform and benzene solvent, while grounded **92** was easily reconverted to its crystalline form a mixed chloroform and acetone solvent.

In 2014 Li et al. reported the synthesis and characterization of three 2D mechanochromic luminescent isomeric porous coordination polymers, Cu(4-pt)·G, **93**, (G = toluene, **93a**; ethanol, **93b**; toluene, **93c**; 4-pt = 5-(4-pyridyl)tetrazole) [83]. Solid samples of **93a**, **93b**, and **93c** show at room temperature emission bands centered at 535, 552, and 615 nm, which were assigned to MLCT [Cu → π^*(tetrazolate)] involved with the Cu$\cdots$Cu [3d → 4s] cluster-centered excited states. The emission properties of the three compounds were unaffected by gently grinding, however, upon strong grinding a weak orange emission appeared for all of them. The X-ray powder diffraction patterns indicated a loss of crystallinity of the compounds when strongly ground, the amorphous state being generated by the disordered sliding between the Cu(4-pt) layers in the structures with alterations of weak Cu$\cdots$Cu and $\pi-\pi$ interactions, thus changing the PL properties of the compounds. The crystalline state could be restored in one month by immersion of ground samples in CHCl$_3$.
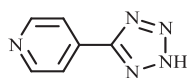

5-(4-pyridyl)tetrazole) (4-pt)
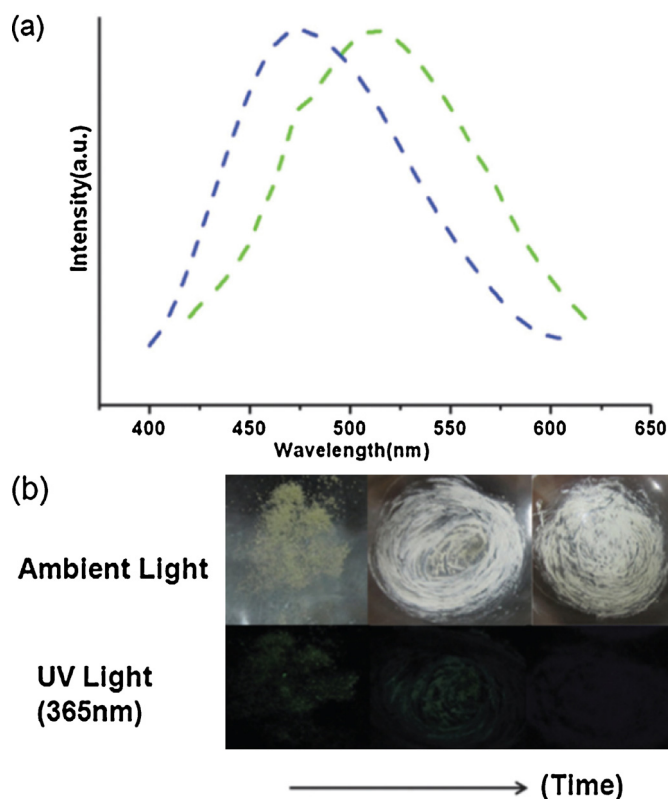
Fig. 17. (a) Normalized solid-state emission spectra for the unground (green line) sample and ground (blue line) sample; (b) photographs of **92** show luminescence changes with grinding time at room temperature, under ambient light and UV lamp. Reprinted with permission from Ref. [82]. Copyright 2014, Royal Society of Chemistry.

2.4. Multistimuli responsive luminescence

Currently most of the reported stimuli-responsive luminescent materials tune their colors only in response to a single stimulus. However, for practical application, materials that independently respond to multiple stimuli are highly desirable and have recently aroused significant interest.

A molecular Cu(I) iodide cubane cluster, namely $[CuI(PPh_2(CH_2CH=CH_2))]_4$, **94**, with mechanochromic and thermochromic luminescence properties was reported by Perruchas et al. in 2010 [84]. At 275 K the solid state emission spectrum of the cluster before grinding shows a weak green emission ($\lambda_{em} = 530$ nm). After grinding, a much more intense yellow emission ($\lambda_{em} = 580$ nm) was observed. The original weak green emission was restored by heating the crushed powder at 373 K for 30 min or upon dissolution in CH_2Cl_2 and subsequent evaporation of the solvent. For both uncrushed and crushed clusters, the emission bands were attributed to a ^3CC excited state. Photophysical, X-ray diffraction and NMR analysis of the cluster before and after the grinding process suggested that the mechanochromic behavior originates from local distortions in the crystal packing where the intermolecular arrangement is modified, thus affecting the $Cu\cdots Cu$ distances of the $[Cu_4I_4]$ cluster core. The phenomenon is reversible since, upon exposure to solvent or heating, this compound recovers its original crystalline phase and emission properties. Both uncrushed and crushed clusters display the "classical" thermochromic luminescence properties of Cu(I) cubanes with phosphine ligands. Based on such thermochromic behavior, the preservation of the $[CuIL]_4$ cubane in the crushed compound was confirmed.
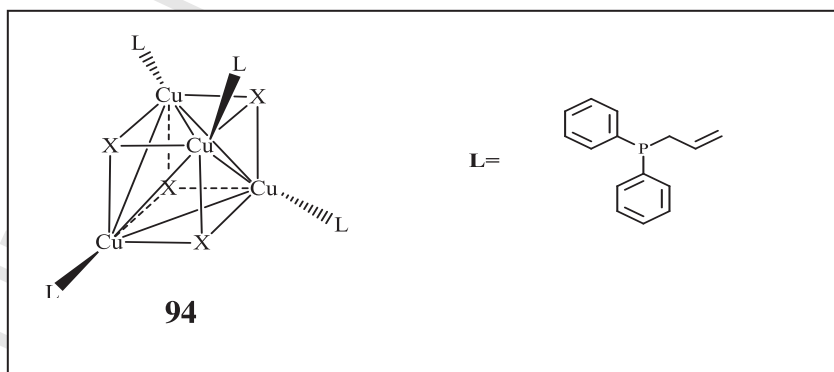
A multistimuli-responsive luminescent material showing independent thermo- and mechano-chromism associated with thermally affected frontier molecular orbital and mechanically affected packing modes, respectively was reported by Hong et al. [85].
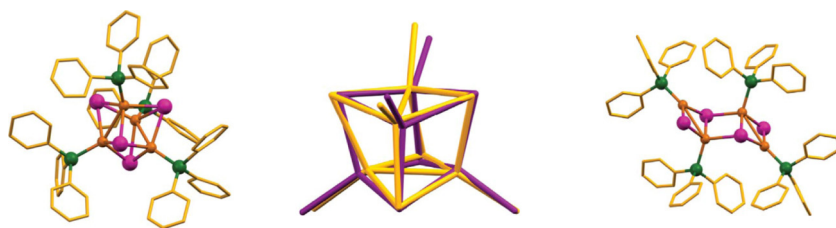
Fig. 18. The $[CuI(PPh_3)]_4$ cubane-like unit; hydrogen atoms have been removed for clarity and in shorter distances Cu atoms are bonded together (left); overlap between Cu_4I_4 clusters in **39** (yellow) and **42** (purple); phenyl rings have been removed for clarity (middle); the $[CuI(PPh_3)]_4$ form **98** unit; hydrogens have been removed for clarity (right). Reprinted with permission from Ref.[87]. Copyright 2011, Royal Society of Chemistry.

$[Cu_8I_8(4\text{-dpda})_6]_n$ (4-dpda = 4-(diphenylphosphino)-*N,N*-dimethylaniline), **95**, containing a discrete Cu_8I_8 cluster which can be seen as a double-cubane Cu_4I_4 cluster linked together through two Cu—I bonds, shows at room temperature in the solid state a green emission (λ_{em} = about 530 nm) attributed to a ^3CC excited state and a "classical" thermochromic behavior. The emission color of **95** can be also switched by mechanical forces. By grinding solid **95** in a mortar, an orange luminescence (associated with a red shift of about 100 nm) was observed. The original emission color was restored by treatment with drops of EtOH and drying. The dynamic recovery of the emission color between green and orange was attested with repeating cycles of grinding and treating the sample with solvent. The PXRD pattern of the ground and unground samples indicated that a crystal-to-amorphous phase conversion caused by grinding occurred. Upon treatment of the ground sample with EtOH, a reversion from the amorphous to the crystalline phase was accomplished. This observed mechanochromism is driven by stacking mode changes induced by pressure and the red shift observed after grinding was associated with stronger Cu···Cu interactions inside the Cu_8I_8 framework.

Ventura et al. synthesized and characterized two different crystalline forms (**96** and **97**) of the MOF of cluster $[Cu_4I_4(DABCO)_2]$ (DABCO = 1,4-diazabicyclo[2.2.2]octane) showing reversible solid-to-solid transformation, with **96** showing vapoluminescent behavior [86]. Form **96** was obtained by reaction of DABCO and CuI in aqueous solution or by solvothermal reaction, while form **97** was obtained by reacting DABCO and CuI in MeCN. When exposed to MeCN or MeOH vapor solid **96** transforms quantitatively into **97** in three days, whereas **97** reverts into **96** when heated up to 523 K in a closed pan. Both isomers show photoluminescence at room temperature in the solid state (at 580 and 556 nm respectively) associated with ^3CC excited state. At 77 K, isomer **96** displayed a bathochromic shift of 10 nm, while the more pronounced red-shift (22 nm) observed for **97** was explained with significantly reduced intermetallic distances on lowering the temperature.

Later, the same group, isolated six different coordination compounds from the solution and solid state reaction between CuI and PPh_3 [87]. In particular, three different already known tetrameric structures with $CuI:PPh_3$ 1:1 stoichiometry were prepared, namely the two closed cubane-type polymorphs $[CuI(PPh_3)]_4$ (**39**) and $[CuI(PPh_3)]_4$ (**42**) and an open step-like isomer $[CuI(PPh_3)]_4$ (**98**) (Fig. 18).

42 can be fully converted into **98** when exposed to saturated atmosphere of MeCN, as confirmed by XRPD measurements. Since solid **42** is characterized by a bright green emission (518 nm, of ^3CC character) while **98** shows only a very weak luminescence (527 nm, of ^3XLCT character), the conversion between the two isomeric forms produces a switch-on/switch-off signal. When **39**, which displays a bright green–yellow emission at 544 nm (of ^3CC character), was exposed to vapors of toluene it rapidly converted into **42**. The "classical" thermochromic behavior of the two polymorphs was here reinvestigated with results analogous to those previously observed [47].

Hong et al. have exploited cuprophilic interactions as a multi-responsive chromophore to prepare a simultaneously tri-stimuli-responsive luminescent material with reversible and independent thermo, mechano and vapochromism [88]. $[CuI(4\text{-dpda})]_4 \cdot CH_3CN$ (4-dpda = 4-(diphenylphosphino)-*N,N*-dimethylaniline), **99**, was prepared by reaction of CuI and 4-dpda in a ratio of 1:1 in CH_3CN. **99**·CH_3CN displays at room temperature in the solid state a single yellow-green LE emission (λ_{em} = 540 nm; ^3CC origin). The thermochromic properties of the compound, investigated by solid state temperature-dependent luminescence measurements and temperature-dependent single-crystal X-ray diffraction analysis, are based on a "classical" mechanism. The emission color of **99**·MeCN can also be switched from yellow-green to orange (λ_{em} = 590 nm) upon grinding in a mortar and the original emission color is restored by treatment with drops of MeCN and drying. XRPD studies revealed a crystal-to-amorphous phase conversion caused by grinding and the reversed phase change upon treatment with MeCN. The ground sample shows thermochromic luminescent characteristic of the Cu_4I_4 framework, demonstrating that the Cu_4I_4 monomers are not destroyed in the grinding process. It was concluded that the mechanical stimulus, altering the packing
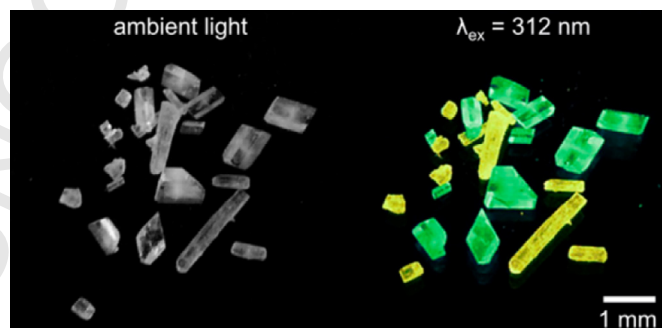

Fig. 19. Photos of the polymorphic crystals of **100** under ambient light and under UV irradiation at room temperature. Reprinted with permission from Ref.[89]. Copyright 2014, American Chemical Society.
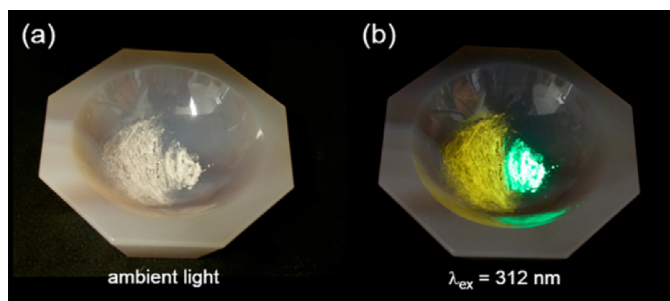
Fig. 20. Photos Fig. 4. Photos of the ground (left) and intact (right) crystalline powder of **100a** (a) under ambient light and (b) under UV irradiation at room temperature. Reprinted with permission from Ref. [89]. Copyright 2014, American Chemical Society.

modes, affects Cu···Cu interactions and, ultimately, the position of the ^{3}CC emission. Vapor-stimuli experiments showed that exposure of the yellow-green emitting crystals to the vapor of CH_2Cl_2 and $CHCl_3$, results in a color conversion to yellow and pale orange respectively. This color conversion processes are fully reversible upon re-exposure to MeCN vapor. X-ray diffraction studies revealed that the guest solvents, despite not having interaction with the host framework, do modulate the molecular packing and stacking in different ways that translates into the varied influences on Cu···Cu interactions through the outer organic ligand shell.

Perruchas et al. reported a cubane Cu(I) cluster showing mechano, thermo and vapochromic luminescent behavior [89]. $[Cu_4I_4(PPh_2(CH_2)_2(CH_3)_2SiOSi(CH_3)_2(CH_2)_2PPh_2)_2]$, **100**, presents two different crystalline polymorphs which exhibit distinct luminescence properties with one being green emissive **100a** ($\lambda_{em} = 522$ nm) and the other one being yellow emissive **100b** ($\lambda_{em} = 571$ nm) at room temperature (Fig. 19). Both emissions were assigned to a ^{3}CC excited state, and the higher energy band observed for the green cluster compared to its yellow polymorph well correlated with the longer Cu···Cu distances of the former.

100
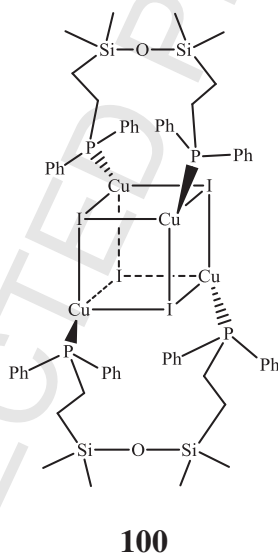
While the emission of **100b** is not affected by mechanical grinding, a 50 nm red shift is observed in the emission of **100a** ($\lambda_{em} = 578$ nm) (Fig. 20). Ground **100a** recovers its original crystalline phase and emission properties upon exposure of the partially amorphous crushed powders to EtOH vapor and the transformation can be repeated by successive grinding/vapor exposure cycles. An in-depth solid-state NMR study was performed to account for the origin of such mechanochromic properties which were associated to a grinding-induced contraction of the Cu···Cu distances in the $[Cu_4I_4]$ cluster core (without altering the cluster integrity) and eventually modification of the emissive state.

The "classical" thermochromic behavior of copper iodide phosphine cubane clusters was observed for pristine **100a** and the ground sample. For **100b**, a more complex trend was observed on lowering the temperature with three emission bands (at 419, 578, and 711 nm) simultaneously present at 75 K. Such observation of two low energy bands at low temperature was attributed to the two independent clusters in the asymmetric unit of the crystal structure having different $[Cu_4I_4]$ core geometries. The cluster with the shorter Cu···Cu bonds leading to the redder emission band (Table 5).

3. Light emitting devices

The use of easily processable organic materials for LEDs has received much interest since the pioneering work of Tang and Vanslyke [90], due to the enormous potential of OLEDs for smart phones, flat panel displays, and solid-light emitting applications. Challenges in the field of material science have arisen to find new materials, stable to air and moisture that can be operated at low voltages with high efficiencies. Another interesting class of light emitting devices, with a simpler architecture, is that of LECs, introduced in 1995 by Pei et

Table 5
Summary of emissive behavior of multi-stimuli Cu(I) complexes.

Compound	T (K)	Before grinding		After grinding	Mechanochromic proposed mechanism	Reference
		Cu···Cu (Å)	λ_{em} (nm)	λ_{em} (nm)		
94	275	3.3904–3.1792	530	580	Grinding induced local distortions with modification of Cu···Cu interactions	[84]
	8		440	470, 580		
95	300	2.99432–2.8733	530	620	Grinding induced amorphization with shortening of Cu···Cu distances	[85]
	10		447	460		
39	298	3.165–2.839	544			[87]
	90	3.081–2.743				
	77		410, 591			
42	298	3.174–2.945	518			[87]
	90	3.105–2.828				
	77		434, 516			
98	298	3.404–2.834	527			[87]
	77		515			
99	300		540	590	Grinding induced amorphization with alteration of Cu···Cu distances	[88]
	293	3.081–2.996				
	260	3.107–2.884	460, 540	434		
	230	3.098–2.869				
	200	3.090–2.850	447			
	170	3.084–2.835				
	160	3.079–2.829				
	10					
100a	290	3.104	522	578	Grinding induced amorphization with shortening of Cu···Cu distances	[89]
	100		419, 533	433, 578		
	8		404	420		
100b	290	2.953–2.816	572			[89]
	75		419, 578, 711			
	8		418, 582			

al. [91]. The main advantage of LECs is that they require less stringent packaging procedures not relying on air-sensitive charge-injection layers or metals for electron injection.

In OLEDs exciton formation under electrical excitation results in 25% singlet and 75% triplet excitons. However, in the organic fluorescent materials triplet excitons do not recombine radiatively, due to the spin selection rules. By the incorporation of heavy metals into the organic frameworks the increased spin–orbit interactions allow the phosphorescent $T_1 \rightarrow S_0$ transition, providing materials for OLEDs reaching the theoretical internal quantum efficiency of 100%. Nowadays almost 100% internal quantum efficiency has already been reported in red, green, and blue phosphorescent OLEDs by several research groups using vacuum thermal evaporation processes with Ir(III) and Pt(II) based complexes [92].

The high cost and the dependence on limited global resources of these noble metal based phosphorescent materials however impose several limitations to their use for the next generation of solid-state displays and light sources. Moreover devices based on phosphorescence often suffer from efficiency roll-off, caused by the long lifetimes of the triplet states, that might limit their practical use. In order to solve these problems, several strategies have been proposed to harvest triplet excitons for luminescence. Among them, Thermally Activated Delayed Fluorescence (TADF) was found to have the most rapid progress in recent investigations [see the recent review 93]. In OLEDs, TADF emission occurs through the following steps (Scheme 6): (1) triplet excitons T_1 are formed after electron/hole recombination in a triplet-to-singlet ratio of 3:1; (2) the accumulated T_1 triplet excitons are converted to S_1 via a Reverse Inter System Crossing (RISC) process with the aid of thermal energy; (3) the S_1 state recombine quickly after formation, giving Delayed Fluorescence (DF). DF has typical lifetimes of the order of μs, longer with respect to prompt fluorescence obtained by direct singlet generation but shorter than the typical lifetime of phosphorescence (100 μs-10ms), therefore reducing the efficiency roll-off in OLEDs devices. In order to facilitate the RISC process, small energy level difference between T_1 and S_1 (singlet–triplet energy splitting, ΔE_{ST}) is essential for efficient $T_1 \rightarrow S_1$ transition stimulated by thermal energy.

Cuprous complexes appear to be the ideal alternative to Ir and Pt heavy atom complexes both because they are relatively abundant, inexpensive, and non-toxic, and because their lowest triplet MLCT excited states have often a small singlet-triplet energy gap (ΔE_{ST}), providing an efficient pathway for RISC leading to TADF emission. In fact d^{10} metal complexes often have much weaker spin-orbit coupling than the d^6 and d^8 ones, but they generally have a small ΔE_{ST} and a stable T_1, which are two key features of the TADF phenomenon. For these reasons in the last few years a special interest in Cu(I) based complexes for light emitting devices have arisen and particular efforts have been devoted to the development of materials displaying TADF activity.

In this review, the literature reports on OLEDs and LECs devices employing Cu(I) complexes are summarized underlying the main progress obtained in the last years with different fabrication technologies of the OLED active layers. In the first section we report examples of OLEDs fabricated with vacuum deposition technologies (complex evaporation or in situ co-evaporation of metals and ligands) while in the second section those obtained by solution processing are reported.

In the third paragraph we summarize the results obtained for LEC devices.

Some typical architectures for OLEDs and LECs manufactured by different methods are reported in Fig. 21a–c. Charge regulating layers to favor charge injection, transport or exciton blocking are often inserted to enhance device performance.

In the discussion, we present the best device efficiencies independently on the emission color, and a summary of Cu(I) complex-based OLED performance, in terms of external quantum efficiency (EQE), current efficiency (CE), luminance (L), electroluminescence spectrum peak (λ_{EL}), voltage onset (V_{ON}), are reported in Table 6, together with device architectures, HOMO–LUMO energies and PLQY.

The performance of Cu(I) based OLEDs has improved dramatically since their first appearance in late 90s. Fig. 21d summarizes this progress for the different manufactured OLEDs in terms of power efficiency (PE) of the device and PLQY of the Cu(I) complex used as emitter. It can be seen that performance of vacuum and solution processed devices as well as LEC have already reached efficiencies exceeding 60 lm/W and 50 cd/A, hence fulfilling solid-state lighting and display commercial applications requirements [94].
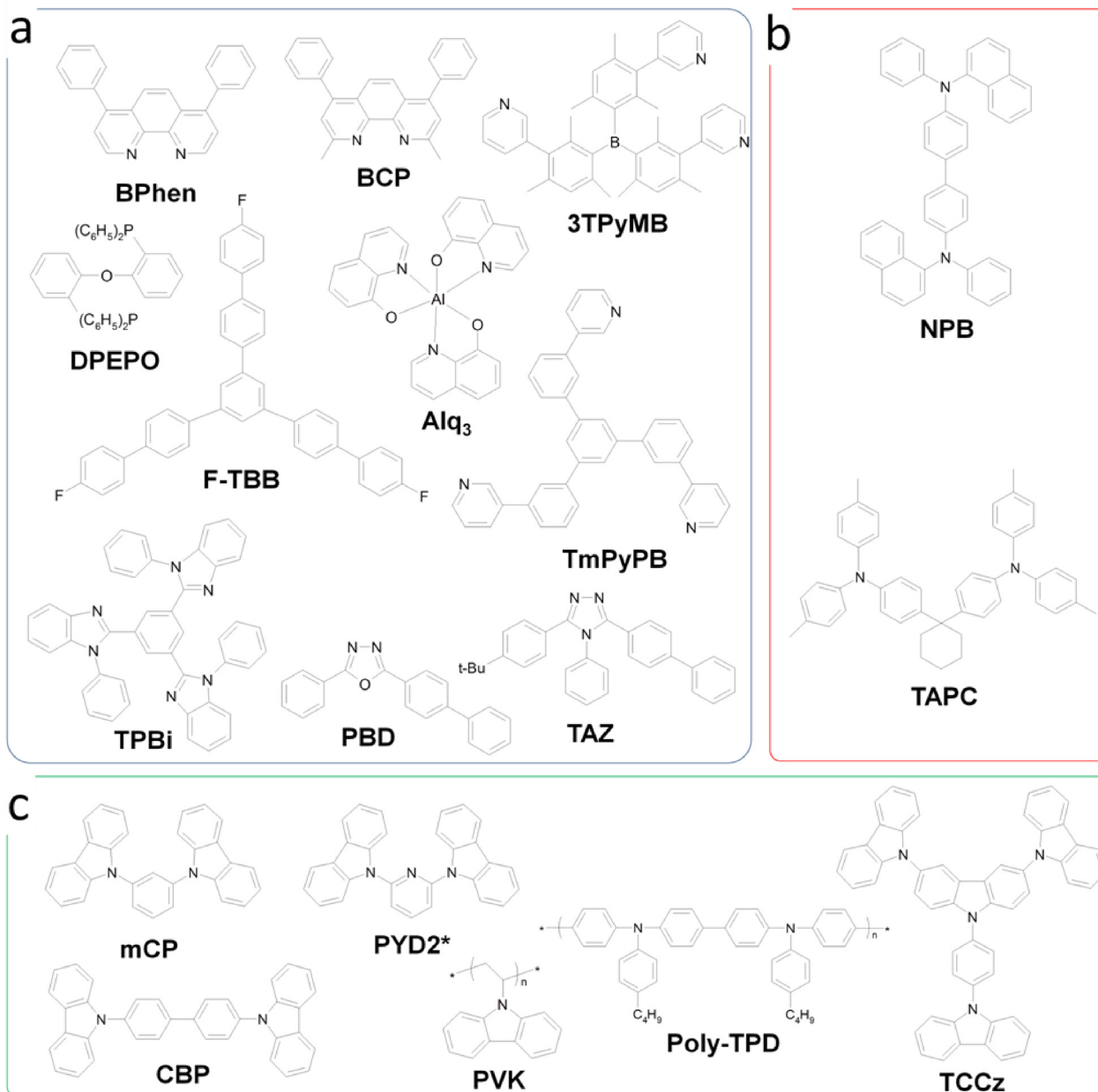
Chemical structure of ETLs (a), HTLs (b) and hosts (c) used in reviewed Cu(I)-based devices

3.1. OLEDs fabricated by evaporation techniques

There are only five reports on devices fabricated by vacuum deposition of Cu(I) complexes, mainly because of the thermal instability of such complexes. However, by a careful design of the molecular structure, few sublimable Cu(I) compounds were obtained and efficient

Table 6

Summary of Cu(I) complex-based OLED and LEC performances together with device architectures, HOMO-LUMO energies and PLQY.

Cu(I) complex	HOMO (eV)	LUMO (eV)	PLQY (%)	Device structure (Cu(I) complex doping ratio w/w %)	V_{ON} (V)	λ_{EL} (nm)	EQE_{MAX} (%)	CE_{MAX} (cd/A)	L_{MAX} (cd/m²) (@mA/cm²)	Reference
101	/	/	80	ITO/PF01/**101**:CPB/BPhen/KF/Al (10%)		565	4.8	10.4	1700@48	[95]
102	/	/	57	ITO/CFx/TAPC/CPB:CPB:TAPC/**102**:CPB:TAPC/CPB/ BAlq-13/LiF/Al (0.2%)		512	16.1	47.5	/	[96]
103	/	/	71	ITO/TAPC/**103**:mCP/3TPyMB/LiF/Al (10%)	2.7	517	21.3	65.3	/	[97]
104	/	/	/	ITO/TAPC/**104**:mCP/3TPyMB/TmPyPB/LiF/Al (8%)	3.5	≈530	6.6	20	598	[98]
105a	−5.13	−1.17	50	ITO/TAPC/**105**:mCP/3TPYMB/LiF/Al (10%)	3.4	552	11.9	34.6	/	[99]
105b	−5.61	−1.60	63		3.2	545	16.0	46.7		
105c	−5.87	−2.06	68		2.6	528	17.7	54.1		
106	/	/	64	ITO/NPD/**106**:mCPy/BCP/LiF/Al (20%)	3.6	530	4.4	13.8	9700	[101]
107	/	/	100	ITO/MoO₃/CBP/**107**:CPPyC/TPBi/LiF/Al (23%)		530	15.7	51.6	23,160	[102]
108	/	/	22	ITO/MoO₃/CPB/**108**:CpzPC/TPBi/LiF/Al (5%)	3.6	590	6.6	15.9	8619	[103]
109	−5.90	−2.60	19/28	ITO/MoO₃/CBP/**109**:TCIQ/TPBi/LiF/Al (5%)	3.2	580	4.1	10.4	7100	[104]
				ITO/MoO₃/CBP/**109**:TCIQ/TPBi/LiF/Al (0.2%)	3.5	White	0.8	1.4	3886	
110	/	/	42	ITO/**110**/PVK/TAZ/Al (10%)	12	516	0.1	/	50@20	[105] [106]
111	−5.50	−3.02	15	ITO/**111**/PVK/F-TBB/Alq3/LiF/Al (25%)	10	580	Low	0.25	35	[107]
112	−5.70	−2.90	69	ITO/**112**/PVK/BCP/Alq₃/LiF/Al (23%)	13	524	/	11	1484@27	[109]
112			59	ITO/PEDOT:PSS/**112**:PYD2/DPEPO/LiF/Al (10%)	5.6	507	15	49.5	3272@23	[110]
112	−5.70	−2.90	69	ITO/**112**:PMMA/Ag (25%)	4	/		1	90	[121]
112	/	/	71	ITO/**112**/Al	7	523	16	56	1650@25	[122]
112	/	/	9	ITO/PEDOT:PSS/**112**:ILᵃ/Al	3	574	/	4.55	60@5	[123]
113	−5.54	−3.22	43	ITO/PEDOT:PSS/**113**:TCCz/TPBI/LiF/Al (10%)	11	618	4.9	8	967	[111]
114	/	/	/	ITO/PEDOT:PSS/**114**/PVK/PBD/Alq₃/LiF/Al (0.2%)	7	576	/	1.85	178@15.5	[112]
115	−5.55	−2.88	16	ITO/PEDOT:PSS/**115**:TCCz/BCP/Alq₃/LiF/Al (10%)	7.7	555	/	8.87	465	[113]
117	−5.53	−2.49	75	ITO/PEDOT:PSS/**117**:26mCPy/DPEPO/LiF/Al (20%)	6.1	508	8.47	23.68	2033	[108]
118	/	/	25	ITO/PEDOT:PSS/**118**:PYD2/DPEPO/LiF/Al (5%)	/	548	7.4	/	/	[114]
121	−5.10	−2.50	59	ITO/PEDOT:PSS/Poly-TPD/**121**:mCPy/PVK:TPBI/LiF/Al (5%)	8	558	/	0.1	20@15	[116]
121	−5.20	−2.50	72	ITO/PEDOT:PSS/Poly-TPD/**121**:TPBI/PVK/TPBI/Ca/Al (45%)	4.1	551	/	9	1800@10	[117]
122	/	/	52	ITO/PEDOT:PSS/PVK/**122**:mCP:TAPC/3TPYMB/LiF/Al	5	521	7.8	21.3	/	[118]
123	/	/	/	ITO/**123**:PMMA/Al	/	590	/	0.16	/	[120]
124	−5.52	−2.64	39	ITO/PEDOT:PSS/**124**/Al	4	553	/	0.07	108	[124]

ᵃ IL = ionic liquid [EMIM][PF₆].
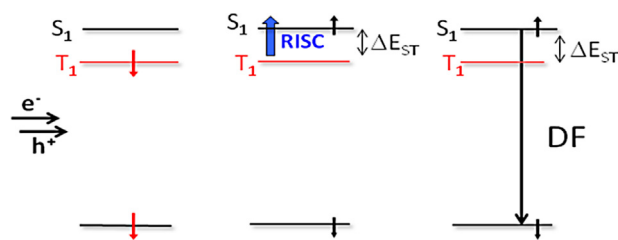
**Scheme 6.** Scheme of the main steps leading to TADF emission in OLEDs.
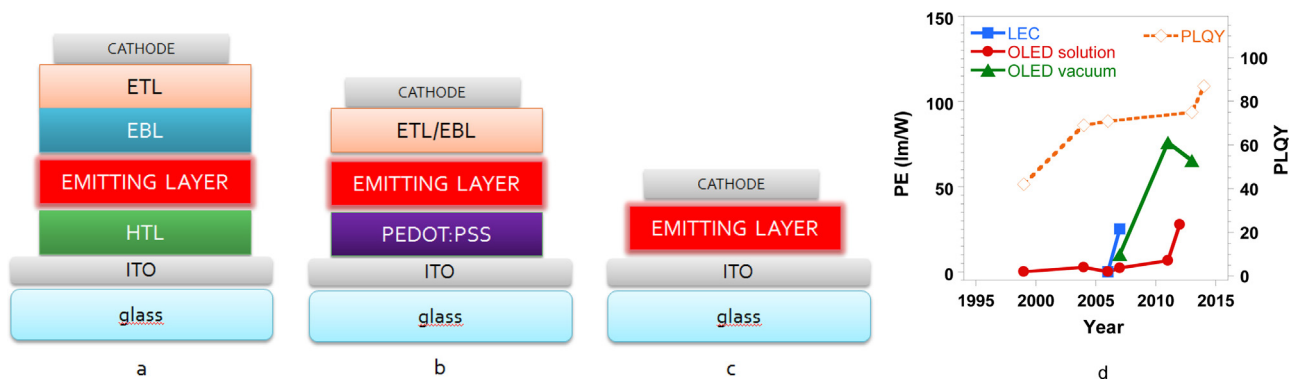
Fig. 21. Typical architecture for vacuum processed OLED (a), solution processed OLED (b) and solution processed LEC (c), the trends of devices efficiency as well as PLQY of the Cu(I) emitters are reported (d). ETL = electron transporting/injecting layer, EBL, exciton blocking layer; HTL, hole transporting/injecting layer.

green OLEDs with performance comparable to the iridium complex based ones were fabricated. For complexes neither soluble nor stable toward sublimation, hence not processable through traditional methods typically used to fabricate OLEDs, *in situ* co-deposition of Cu(I) with the ligands has been shown to provide an optimal alternative to the traditional methods. We report at first examples of OLEDs fabricated with the traditional sublimation method and then the more recent examples of *in situ* co-deposition.

### 3.1.1. Vacuum deposition of copper(I) complexes

Tsuboyama et al. in 2007 reported the first work on OLED devices based on an evaporated four coordinate binuclear complex of Cu(I) with the chelating ligand 1,2-bis[diphenylphosphino]benzene (dppb) [95]. [Cu(μ-I)(dppb)]$_2$, **101**, was co-evaporated with the *N,N*′-dicarbazolyl-4,4′-biphenyl (CBP) host to produce green electroluminescence (EL) with an EQE of 4.8% and PE of 4.2 lm/W at 93 cd/m^2. By studying the temperature dependence of the emission of 2-methyltetrahydrofuran solutions, the authors assigned the EL to a flattened structure of the ^{3}MLCT excited state, allowed by the microscopic viscosity of the amorphous host [95].
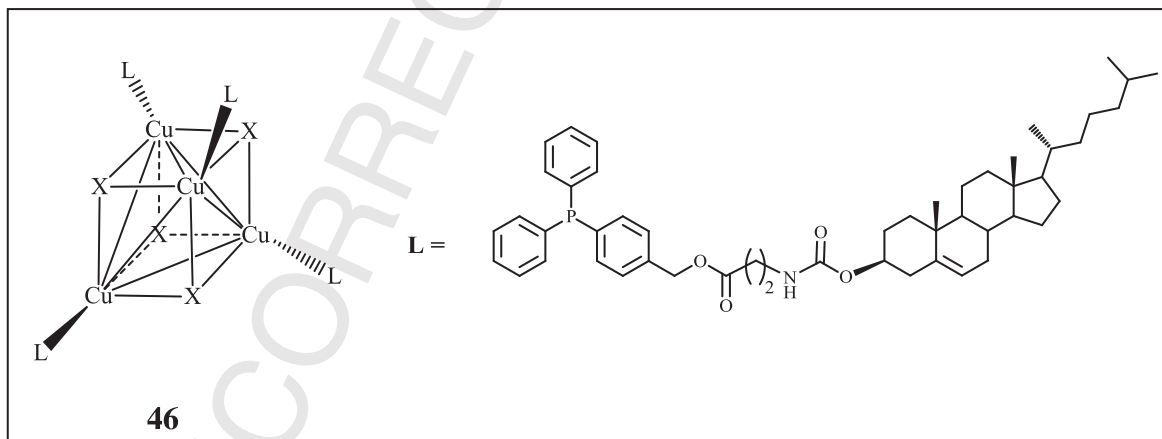

In 2010 Peters et al. [96] obtained a sublimable and highly emissive dinuclear Cu(I) complex (PLQY = 57%) with a tightly bound chelate ligand that can create a rigid environment around the copper center. [Cu(PNP-*t*Bu)]$_2$, **102**, (PNP-*t*Bu = bis(2-(ditertbutylphosphino)4-tertbutyl-phenylamide), was screened as an emissive layer dopant in different host materials, all having triplet energies high enough to avoid green phosphorescence quenching. The EQEs varied strongly with the host material. Green electroluminescence was obtained with CBP, 1,3-bis(carbazol-9-yl)benzene (mCP), and tris(4-carbazoyl-9-ylphenyl)amine (TCTA) that closely matched the PL spectrum of dopant **102** in 1,1-bis(4-(*N,N*-di-*p*-tolylamino)phenyl)cyclohexane (TAPC) films.

Vapor-deposited OLEDs doped with **102** in the emissive layer gave a maximum EQE of 16.1% (47.5 cd/A), demonstrating that triplet excitons can be harvested very efficiently through the delayed fluorescence channel. The maximum EQE was recorded at 0.01 mA/cm^2 and the efficiency decreased with increasing current reaching a value of 10.9% EQE (32 cd/A) at 1 mA/cm^2. The efficiency roll-off observed in

103
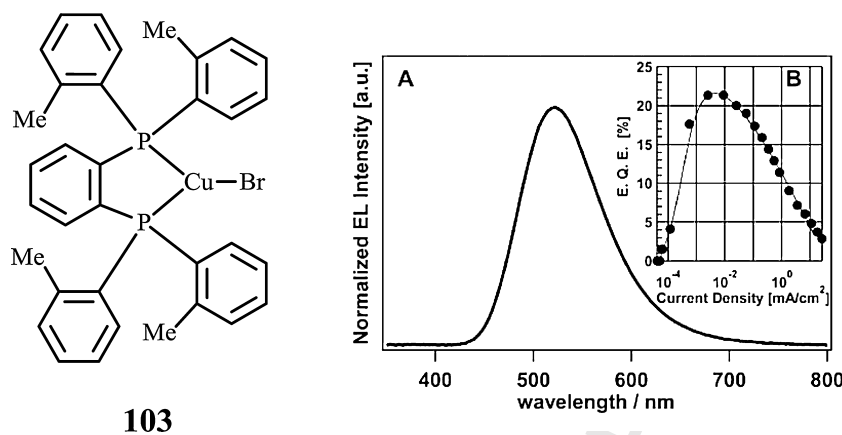
Fig. 22. (Left) Molecular structure of complex [CuBr(dtpb)] **103**. (Right) Properties of an OLED obtained by co-evaporation of complex **103** with mCP: (A) EL spectrum; (B) dependence of EQE on current density; Reprinted with permission from Ref. [97]. Copyright 2011, American Chemical Society.


104
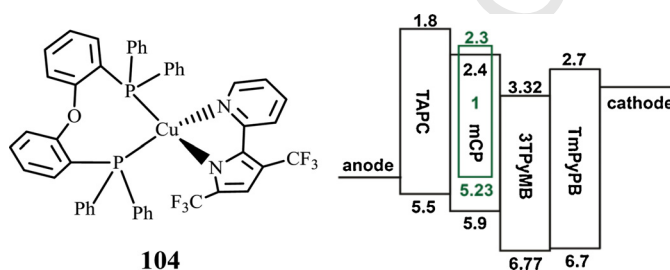
Fig. 23. (Left) Molecular structure of complex **104**. (Right) Schematic energy levels of the materials employed for OLED fabrication with **104**. Adapted with permission from Ref. [98] Copyright 2011, American Chemical Society. 3TPyMB = Tris[2,4,6-trimethyl-3-(pyridine-3-yl)phenyl]borane, TmPyPB = 1,3,5-tri[(3-pyridyl)phen-3-yl]benzene.

EL devices with increasing current was explained by quenching of the excited state by holes and/or dissociation of the excited state under the influence of the electric field.

In 2011 Osawa et al. [97] fabricated an even more efficient green OLED (Fig. 22) with a maximum EQE of 21.3%, by using a sublimable and simple three-coordinate Cu(I) complex: [CuBr(dtpb)] (dtpb = 1,2-bis(o-ditolylphosphino)benzene), **103**, as the emitter with the mCP host. The high efficiency of this complex was suggested to be due to the ability of the biphosphine ligand to prevent the Jahn-Teller excited state distortion [97]. This work therefore suggests that three coordinate Cu(I) complexes are promising EL materials in terms of efficiency and thermal stability.

Cu(I) complexes bearing functionalized 2-pyridyl pyrrolide anions together with phosphine ancillary ligands such as bis[2-(diphenylphosphino)phenyl]ether (DPEPhos)) or PPh$_3$ were reported by Chi, Chou and Chang [98]. [Cu(DPEPhos)(fpyro)] (fpyroH = 3,5-bis(trifluoromethyl)-2-(2′-pyridyl)pyrrole), **104**, exhibits intensive phosphorescence (PLQY = 0.35 in the solid state) and has been successfully utilized for fabricating OLEDs devices (Fig. 23) attaining peak EL efficiencies of 6.6%, 20.0 cd/A, and 14.9 lm/W for the forward directions.

In 2013 Osawa et al. synthesized and used as dopants in OLEDs sublimable tetrahedral Cu(I) complexes containing 1,2-bis(diphenylphosphino)benzene (dppb) derivatives as ligands and the anionic bidentate ligand diphenyl-bis(pyrazol-1-yl)borate (Ph$_2$Bpz$_2$).

Cz = Carbazolyl   **mCPy**

106
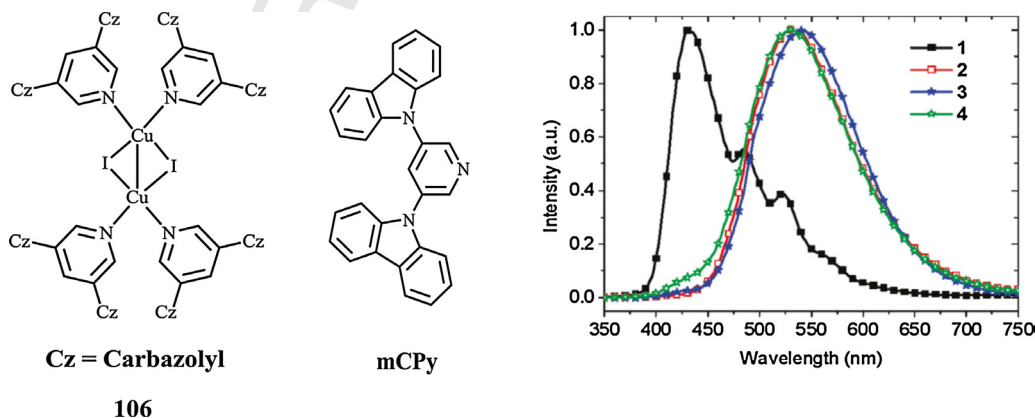
Fig. 24. Molecular structure of in situ co-deposited complex **106** and mCPy ligand. EL spectra of ITO/NPD/EML/BCP/LiF/Al devices at 8 V, where EML denotes neat mCPy (device 1), 1:4 CuI:mCPy (device 2), 1:6 CuI:mCPy (device 3), or 1:10 CuI:mCPy (device 4). NPD = 4,4′-bis[N-(1-naphthyl)-N-phenylamino]biphenyl, BCP = 2,9-Dimethyl-4,7-diphenyl-1,10-phenanthroline. Reprinted with permission from Ref. [101]. Copyright (2011) American Chemical Society.

Cu(dppb)(Ph$_2$Bpz$_2$) **105a**, Cu(dppb-F)(Ph$_2$Bpz$_2$) **105b**, and Cu(dppb-CF$_3$)(Ph$_2$Bpz$_2$) **105c** [99,100]. The PLQY increase with the number of fluorine atoms in the complex. Bottom-emitting devices with a three-layer structure and mCP host produced bright green emission with EQE reaching 17.7% for structure **105c**. EQE values for the three complexes follow the same trend as the PL-QYs.


105a-c
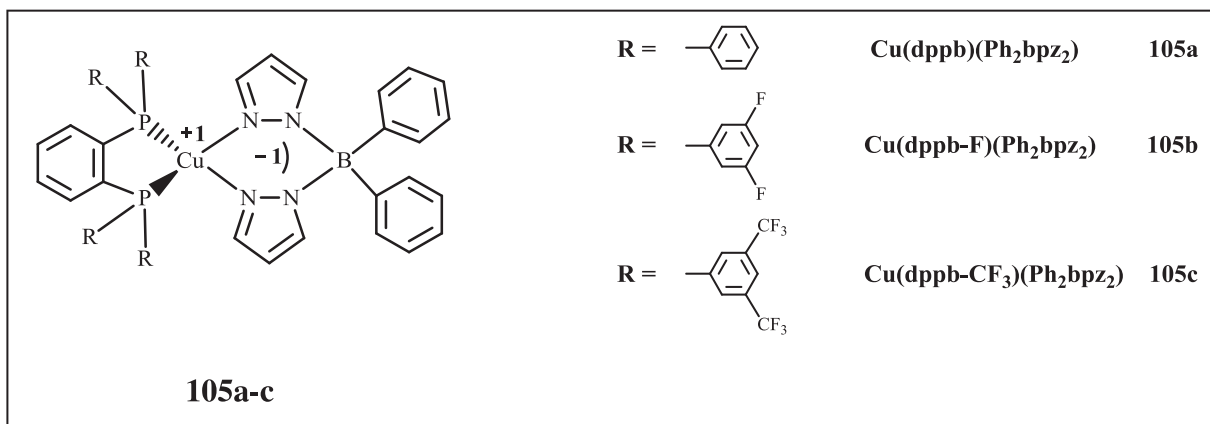
3.1.2. *Vacuum CuI-ligand* in situ *Co-evaporation*

When the complexes are not stable toward sublimation, *in situ* co-deposition of CuI with the ligands provides an optimal alternative to the traditional evaporation method. In this co-deposition approach a copper source and a ligand are co-deposited under vacuum to produce a Cu(I) complex in the resulting thin film. The organic compound often performs a double task: (i) it is the ligand necessary to form the emissive complex and (ii) it works as host necessary for the proper dispersion of the complex in the device active film. The challenge is to find an organic compound able to perform these two tasks. The ligand must react with CuI quickly to form a highly luminescent copper(I) complex and must have the optimal electronic properties (triplet and frontier orbital energies) to work as proper host material for the emissive layer of the OLED.

The method of *in situ* co-deposition of CuI with the ligand was first proposed by M.E. Thompson et al. in 2011 [101] using 3,5-bis(carbazol-9-yl)pyridine (mCPy) as ligand. With a simple three-layer device structure, pure green electroluminescence at 530 nm with maximum EQE of 4.4% and luminance of 9700 cd/m^2 was reported for the complex [CuI(mCPy)$_2$]$_2$, **106** (Fig. 24). Lifetime measurements on CuI:mCPy-based OLEDs showed encouraging results, with half-life of 21 h, corresponding to 440 h at 100 cd/m^2 for the device at a current density of 20 mA/cm^2 (L = 2100 cd/m^2) under vacuum (150 mTorr).

Later, Wang, Bian, Thompson et al. [102] proposed a novel ligand 3-(carbazol-9-yl)-5-((3-carbazol-9-yl)phenyl)pyridine (CPPyC) to be used in the *in situ* co-deposition procedure. CPPyC has a triplet energy level of 2.7 eV, promoting efficient energy transfer to the emissive Cu(I) complex formed by codeposition. PLQY approaching 100% was achieved when the CuI:CPPyC molar ratio approaches 1:10 (*i.e.* CuI doping concentration of 4 wt%). OLED devices showed green emission with a peak wavelength near 530 nm, indicating that emission originates entirely from the *in situ* formed [Cu$_2$I$_2$(CPPyC)$_4$] complex **107**. By comparing five devices with different complex concentrations in the CPPyC host, it was found that the device with 4 wt% CuI and 23 wt% complex concentration shows the best performance, with EQE reaching 15.7% (51.6 cd/A) at 100 cd/m^2 and 13.5% (44.4 cd/A) at 1000 cd/m^2. The PE was 38.9 lm/W at 100 cd/m^2 and 27.3 lm/W at 1000 cd/m^2, comparable to OLEDs with iridium based phosphors. Moreover, the device performance was found not to strongly depend on the doping level, this being an advantage for the manufacturing processes.

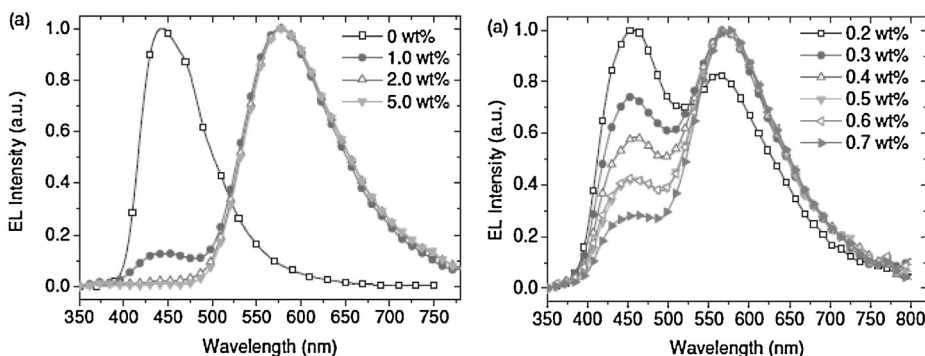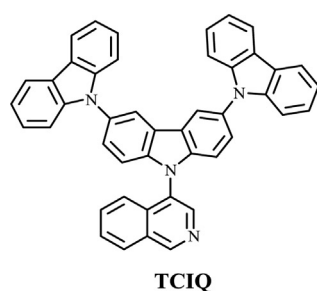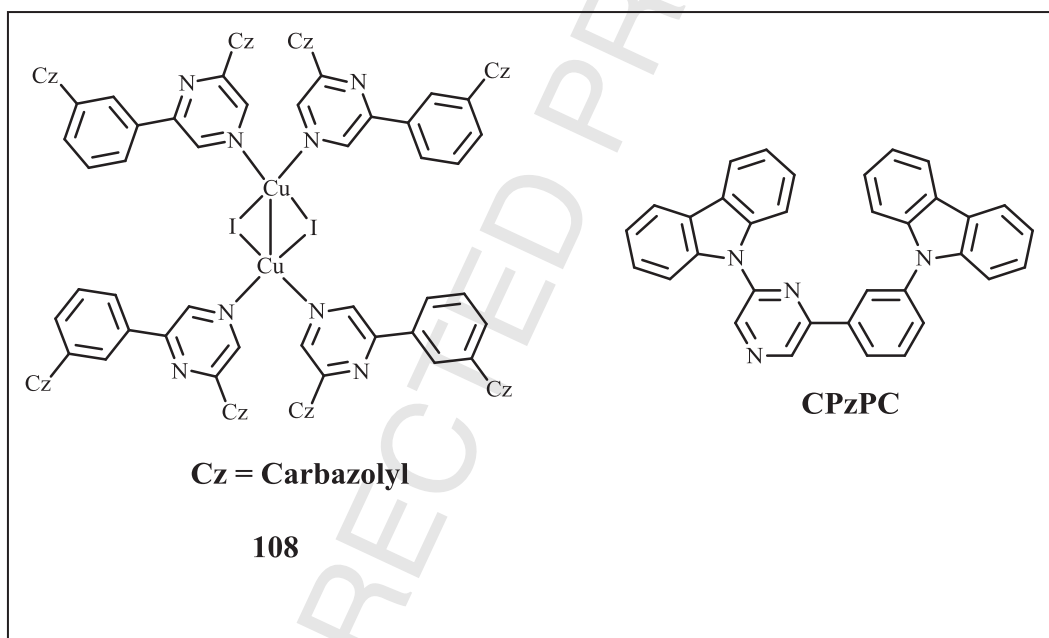**Cz = Carbazolyl**

107

CPPyC
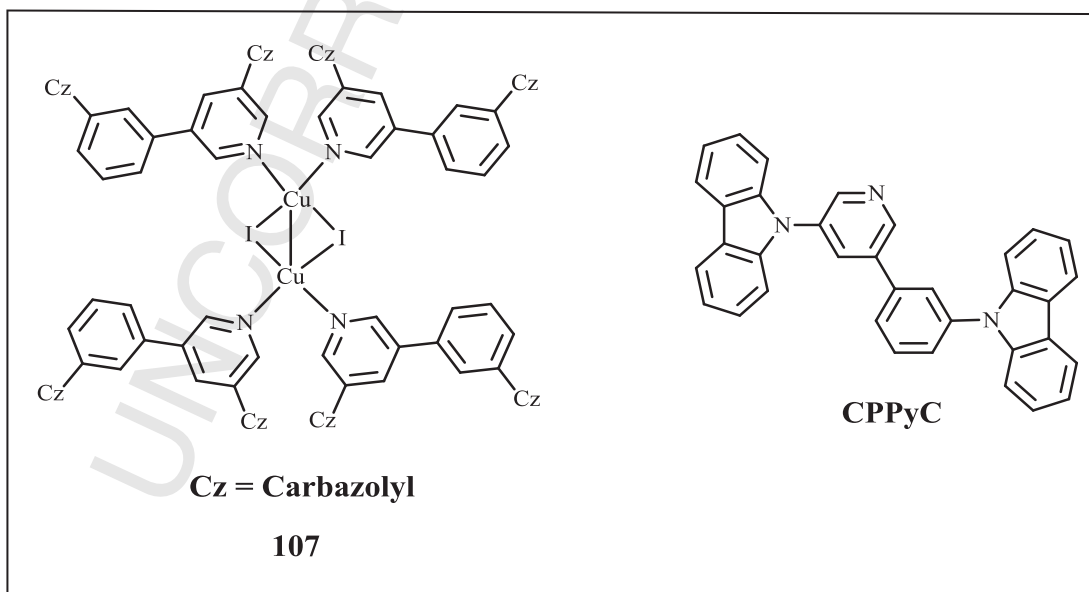
Fig. 25. EL spectra of devices with configuration of ITO/MoO$_3$ (1 nm)/CBP(35 nm)/CuI:TCIQ (x wt%, 20 nm)/TPBi (65 nm)/LiF (1 nm)/Al. Reprinted with permission from Ref. [104]. Copyright 2014, WILEY-VCH Verlag GmbH & Co. KGaA, Weinheim.

Wang, Liu, Lu et al. [103] proposed three pyrazinyl carbazole compounds for co-deposition with CuI. Among them 9-(3-(6-(carbazol-9-yl)pyrazin-2-yl)-phenyl)-carbazole (CPzPC) gave the best co-deposited CuI–CPzPC, **108**, films with a molar ratio of 1:7 (corresponding to a CuI doping concentration around 5 wt%). By using the film as the emissive layer and optimizing the device architecture and material selection, an orange-red emissive OLED was obtained with emission peaked at 590 nm, peak PE of 14.0 lm/W, current efficiency and EQE of 15.9 cd/A and 6.6%, respectively. At a brightness of 100 cd/m^2, a PE of 10.1 lm/W with an EQE of 6.3% (CE = 15.0 cd/A) was obtained at an applied voltage of 4.7 V.


Jiang, Liu, Bian et al. [104] reported four compounds containing pyridyl or isoquinolyl moieties for co-deposition with CuI to form luminescent Cu(I) complex doped films. Among them 4-[3,6-di(carbazol-9-yl)carbazol-9-yl]isoquinoline (TCIQ) was utilized and *in situ* co-deposited with CuI in different concentrations for the emissive layer in OLEDs. Since the complex Cu:TCIQ, **109**, emits yellow while the host TCIQ emits blue the authors obtained yellow and white OLEDs with a simple tri-layer structure, consisting of CBP and 1,3,5-tris(N-phenylbenzimidazole-2-yl)benzene (TPBI) as HTL and ETL respectively, by changing their ratio. Therefore compound TCIQ serves a dual role, as both a ligand for forming the emissive Cu(I) complex and as a blue emissive host matrix for the active film. As a result, pure yellow electroluminescence (EL) at around 580 nm was observed at a CuI doping concentration of 5 wt%, while a series of white light OLEDs with the best CIE color coordinates of (0.30, 0.32) and color rendering index (CRI) of 89 were obtained at CuI concentration below 1 wt% (Fig. 25).

3.2. OLEDs fabricated by solution method

Although vacuum thermal evaporation has been generally used as a fabrication process of OLEDs, several problems such as inefficient use of material, poor scalability and expensive equipment increase the fabrication costs of large devices. These issues can be solved by using solution processed technologies as spin coating, ink-jet printing or roll-to-roll. These technologies required the use of soluble complexes and the selection of high E_T small molecular or polymeric hosts for the Cu(I) complex emitters. A multilayer architecture is possible in solution processed devices thanks to the different solubility of HTL and active layer in orthogonal organic solvents. On the contrary, ETL consisting of small conjugated molecules is generally vacuum growth on top of the active layer. To date, no example is given of Cu(I) based OLED with active and ETL both fully processed by wet method.

The types of devices based on mononuclear and multinuclear, homo and heteroleptic, neutral and ionic Cu(I) complexes are reviewed.

The first reported solution-prepared Cu(I) based OLED dates back to 15 years ago. Ma et al. [105,106] reported the use of a highly luminescent tetranuclear Cu(I) compound [Cu$_4$(C≡CPh)$_4$(1,8-bis(diphenylphosphino)-3,6-dioxaoctane)$_2$], **110**, as dopant emitter in a well established solution-processed polyvinylcarbazole (PVK)-based device with triazole derivative (TAZ) as ETL and Al cathode. The 10 wt% doped device showed an EL spectrum peaked at 520 nm nearly identical to the PL spectrum of the complex in solution. The device reached a brightness of *ca.* 50 cd/m^2 at 20 mA/cm^2 and a maximum EQE of 0.1%.
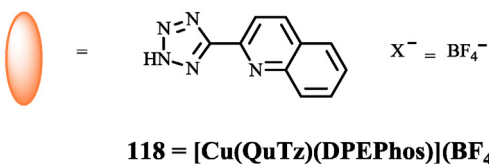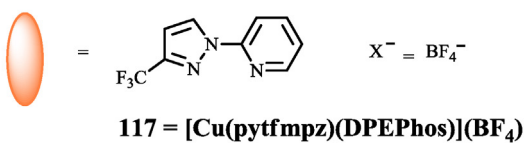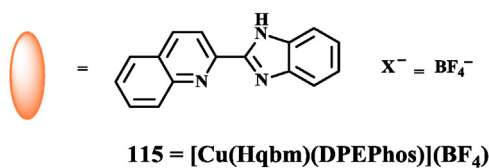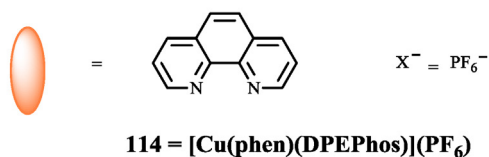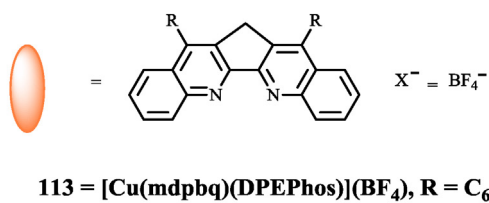

110

111
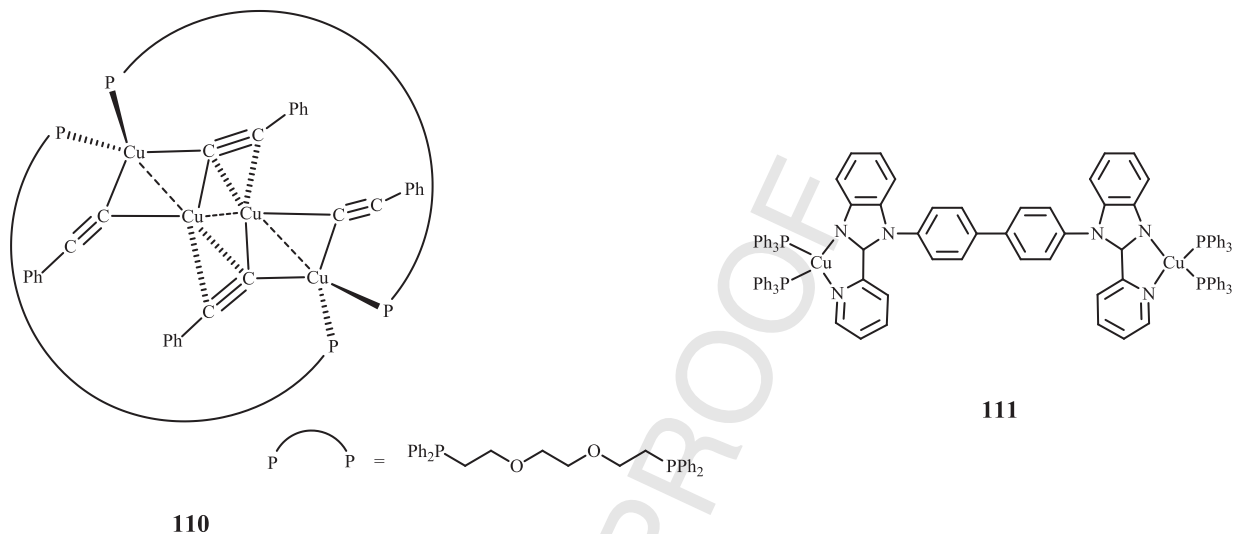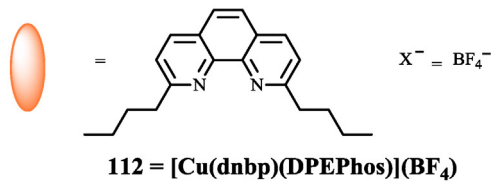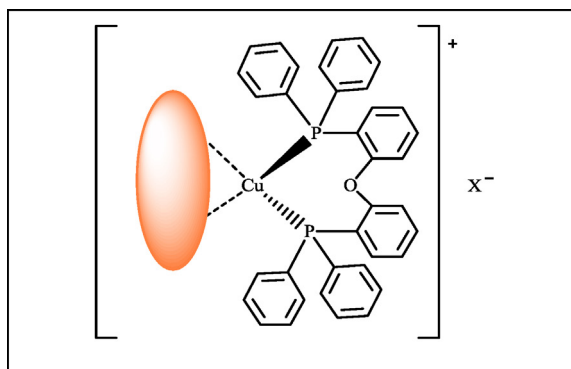
Jia et al. [107] reported dinuclear and trinuclear Cu(I) complexes with 2-(2′-pyridyl)benzimidazolyl derivatives showing good stability in solution and in the solid state. The most promising complex, [Cu$_2$(bmbp)(PPh$_3$)$_4$][BF$_4$]$_2$, **111**, (bmbp = 4,4′-bis[2-(2′-pyridyl)benzimidazolyl]biphenyl), was dispersed in PVK. Although its good PLQY (15%), the performance in a device architecture including fluorinated charge regulating/EBL 1,3,5-tris(4-fluoro-biphenyl-4′-yl)benzene (F-TBB), were poor with a brightness of 35 cd/m^2, CE of 0.25 cd/A and an EL peak at 580 nm. Most probably the exceptionally long decay lifetime hindered their use as emitter in EL devices.

Successively, research focused on mononuclear Cu(I) complexes with the bulky DPEPhos ligand to inhibit excited-state structural modification from distorted tetrahedrical geometry around the Cu(I) atom to flatten geometry, hence leading to enhanced emission intensity [5,93,108] by providing a firm framework around Cu(I). In this framework, a sharp improvement of the Cu(I) based OLED performance was achieved by Wang's group [109] with Cu(I) complexes containing DPEPhos, 2,9-di-n-butyl-1,10-phenanthroline (dnbp) as ancillary ligand and BF$_4$$^-$ as counterion (**112**). The devices based on the heteroleptic Cu(I) complex **112** showed performance comparable to that of Ir(III) in similar device architecture. Thanks to the incorporation of bulky alkyl groups in the 2 and 9 position of the phenanthroline ligand, a high PLQY (69%) and shorter PL decay time with respect to PPh$_3$-based complexes, were achieved. Thus device based on 23 wt% dispersion of the promising complex **112** in PVK matrix, showed a maximum CE of 11 cd/A with BCP/AlQ$_3$ double charge regulating layer [AlQ$_3$ = tris(8-hydroxyquinolinato)aluminum] and LiF/Al cathode.

112 = [Cu(dnbp)(DPEPhos)](BF₄)

113 = [Cu(mdpbq)(DPEPhos)](BF₄), R = C₆H₅

114 = [Cu(phen)(DPEPhos)](PF₆)

115 = [Cu(Hqbm)(DPEPhos)](BF₄)

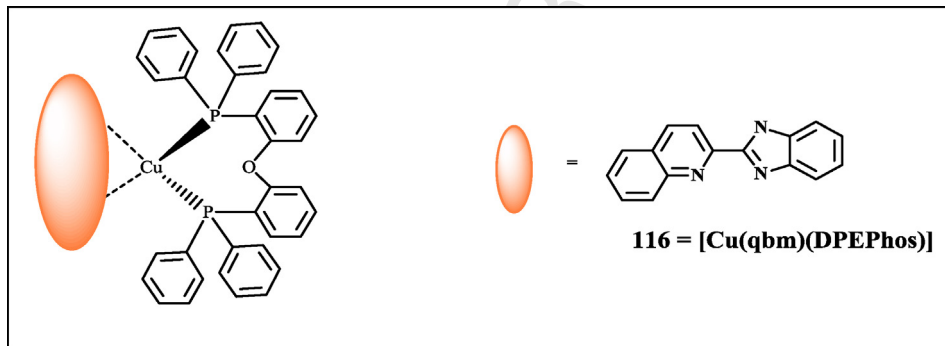**117 = [Cu(pytfmpz)(DPEPhos)](BF₄)**

118 = [Cu(QuTz)(DPEPhos)](BF₄)

Fig. 26. The EQE-current density curves of the ITO/PEDOT:PSS/**110**:host/ETL/LiF/Al OLEDs with different hosts (a) and ETLs (b). Reproduced with permission from Ref. [110]. Copyright 2012, WILEY-VCH Verlag GmbH & Co. KGaA, Weinheim.

More recently, Adachi and coworkers [110] carried out a deeper investigation of complex **112**, finding out that a long life green emission arises from two thermally equilibrated CT excited state and one non equilibrated triplet ligand centered excited state. OLEDs were fabricated with active layer consisting of high triplet energy charge transport materials as host for **112**. It was observed that, thanks to the efficient confinement of the triplet energy on the Cu(I) complex due to by the successful choice of the small molecular host 2,6-dicarbazolo-1,5-pyridine (PYD2) and of bis(2-(diphenylphosphino)phenyl)ether oxide] (DPEPO) as exciton blocking layer, it is possible to achieve high EQE of 15% and CE of 49.5 cd/A (Fig. 26) comparable to the Ir(III)-based devices performance.

A lot of work was devoted to the search of alternative ligands to substitute the dnbp one in mononuclear heteroleptic Cu(I) complexes.

The stimulating results achieved with mononuclear Cu(I) complexes, led to the synthesis of a series of orange-red emitting phosphorescent heteroleptic Cu(I) complexes by Wang and coworkers [111]. The effect of the rigid bulky biquinoline-type ligands over the emission intensity was evaluated. By dispersing the highly phosphorescent (PLQY = 43%) complex [Cu(mdpbq)(DPEphos)](BF$_4$), **113**, in the small molecule N-(4-(carbazol-9-yl)phenyl)-3,6-bis(carbazol-9-yl) carbazole (TCCz) instead of PVK as active layer, OLED were fabricated with various architectures. The device ITO/PEDOT/TCCz:**113** (10 wt%)/TPBI/LiF/Al showed a CE up to 8 cd/A, EQE of 4.9%, maximum brightness close to 1000 cd/m^2 and the CIE coordinates of (0.59, 0.41). By increasing the doping concentration to 15%, first efficient red EL with CIE (0.61, 0.39) and 4.5% and 6.4 cd/A value of EQE and CE respectively were registered from mononuclear Cu(I) complex (Fig. 27).

The effect of exchanging the mdpbq ligand with 1,10-phenanthroline (phen), **114**, or 2-(2′-quinolyl)benzimidazole (Hqbm), **115**, was studied by Ma's [112] Cheng's and Wang's groups [113] fabricating different device architectures. An orange EL with brightness of 1400 cd/m^2 was reported for complex **114**, but the modest CE of 1.8 cd/A is poorer than in OLED embedding mdpbq-based Cu(I) complexes. On the other hand, the device based on complex **115** showed slightly better performance with CE of 5.58 cd/A and very high brightness of 2820 cd/m^2 with EL peak at 555 nm. The corresponding neutral complex of **115** Cu(qbm)(DPEphos) **116** with identical skeleton showed further increase in OLED performance reaching CE of 8.87 cd/A thus approaching earlier reported best efficiency. A blue-shifted emission and longer lifetime were recorded for the neutral complex with respect to the ionic one due to the additional ligand-centered $\pi-\pi^*$ transition beside traditional MLCT.

Higher performance was achieved by replacing Hqbm with N-linked 2-pyridilpyrazolatediimine ligands in ionic Cu(I) complexes containing DPEphos ligands. The electron rich diimine ligand increased the HOMO-LUMO gap thus shifting the emission toward the blue region, and a fine tuning of the color as well as enhancement of the PLQY were achieved by functionalizing 2-pyridyl pyrazolate diimine ligand. Very recently, Yu, Lu and coworkers [108] obtained solution-processed OLEDs containing [Cu(pytfmpz)(DPEphos)](BF$_4$) **117** (pytfmpz = 3-trifluoromethyl-1-(2-pyridyl)pyrazole) in the emissive layer with excellent device performance by taking advantage of the singlet harvesting mechanism (ΔE_{ST} = 0.17–0.18 eV, Fig. 28). In the OLED based on **117** as dopant in PYD2, 2-(4-Biphenylyl)-5-phenyl-1,3,4-oxadiazole (PBD) as ETL, excellent EQE of 8.47%, CE of 23.68 cd/A, and a maximum L of 2033 cd/m^2 were observed.
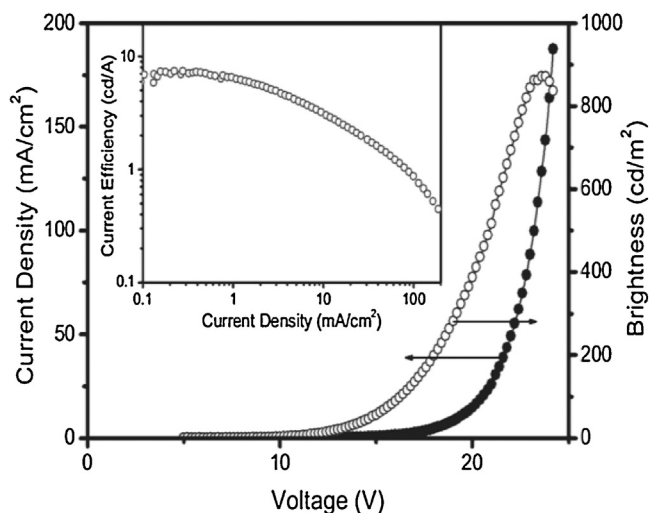
Fig. 27. I–L–V curves of the device with 15% of **113** in TCCz. Inset: the current density-efficiency plot of the device. Reproduced with permission from Ref. [111]. Copyright 2007, WILEY-VCH Verlag GmbH & Co. KGaA, Weinheim.

Fig. 28. Energy level diagram for the low-lying states of the complex **117**. Reprinted with permission from Ref. [108]. Copyright 2013, American Chemical Society.

Adachi and co-workers [114] rationally designed luminescent Cu(I) complexes with improved PLQY by suppressing not only the excited-state distortion but also C—H vibrational quenching. Heteroleptic complexes consist of DPEPhos bulky group and different aromatic N-heteroclyclic ligands (**118**). Higher PLQY was recorded for 2-(5-tetrazolyl)quinoline (QuTz) containing Cu(I) complex **118**, which exhibited lower frequency modes from N—N and N—H bonds compared with those from C—H bonds. Therefore, thanks to QuTz and DPEPhos, nonradiative decay caused by C—H vibrational quenching was suppressed as well as excited-state distortion. The 1,3-bis(carbazol-9-yl)benzene derivative PYD2 was selected as host matrix for its high (E_T) of 2.93 eV. A low doping level of **118** (5 wt%) in PYD2 gave Cu(I)-centered green (548 nm) emission with maximum EQE of 7.4%.

Fig. 29. Homoleptic complexes **119** (a) and heterloleptic **120** (b); (c) I–V–B characteristics of the device obtained from **119**. Inset: EL spectra of device based on **119** at a concentration of 12.5 wt% in a PVK matrix. Fig. reproduced with permission from Ref. [115]. Copyright 2007, Royal Society of Chemistry.

Armaroli, Destruel, Nierengarten and coworkers [115] compared devices based on homoleptic complexes [Cu(dppb)$_2$](BF$_4$) **119** and heteroleptic [Cu(P–P)$_2$](BF$_4$) **120** (Fig. 29a and b) in PVK, achieving a broad, almost white, EL band peaked at 580 nm (Fig. 29c) switched on at 15 V. A L of 490 cd/m^2 was recorded at 20 V.
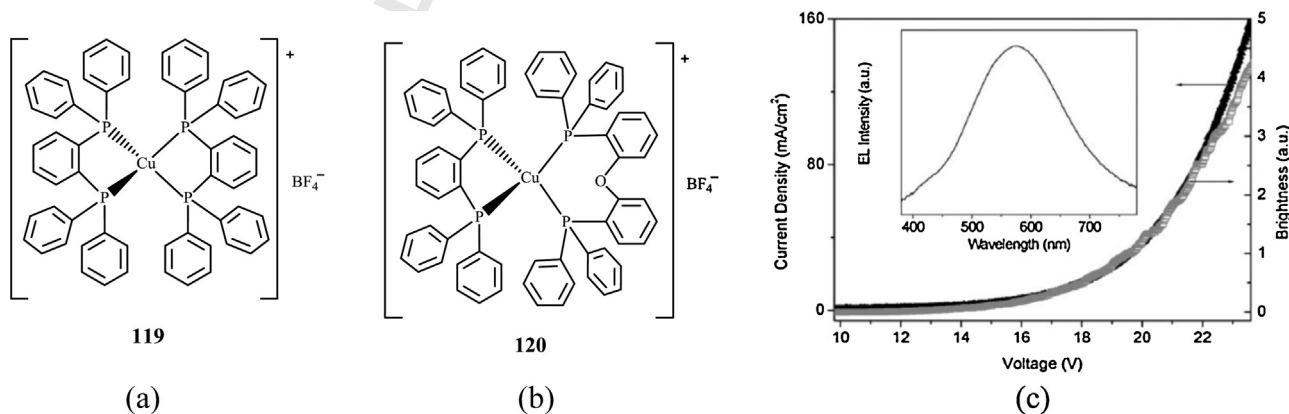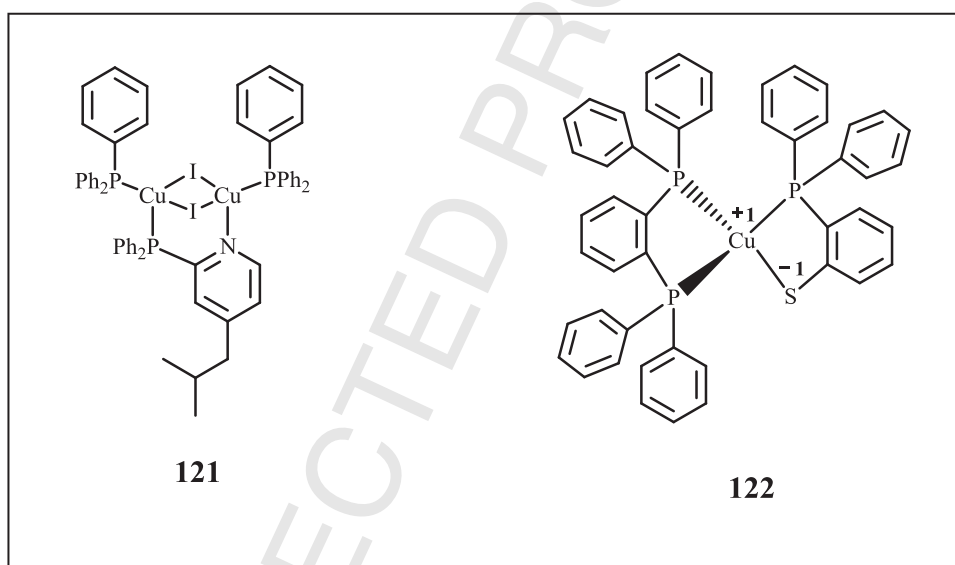
Besides Cu(I) diimide complexes, Cu(I) halide complexes are promising for their intriguing PL properties. Two recent successful studies on the employment of four coordinated binuclear Cu(I) complexes in OLEDs are discussed in the following.

Adachi and coworkers [110] measured an EQE of 9% and CE of 30.6 cd/A, the higher values reported so far for solution processed devices, by doping PYD2 matrix with 10% of green emitting four coordinate binuclear Cu(I) chelated with the ligand dppb [Cu(μ-I)(dppb)]$_2$, **101**, earlier successfully used in evaporated OLED [94]. Interestingly, they concluded that not only the host, but also a high triplet energy level of the exciton blocking layer is a key element for a successful triplet exciton confinement in the emitting layer. The use of DPEPO (E_T = 3 eV) almost doubled the performance (Fig. 27) with respect to the device employing 2-(diphenylphosphoryl)spirofluorene (SPP01, E_T = 2.9 eV).

A series of highly luminescent heteroleptic Cu(I) complexes, as promising candidate OLED emitters, was synthesized by Baumann and Bräse groups [116,117]. The butterfly shaped structure of the Cu(I) halide core is surrounded by one PÑ ligand, bridging the two metal centers, and two triphenylphosphine ligands, coordinating via their phosphorus atoms to the copper centers. A tuning of the emission maximum from yellow (581 nm) to deep-blue (451 nm) by changing the electronic characteristics of the bridging PÑ ligand, that affect the LUMO, was achieved. The complex bearing 2-(diphenylphosphino)-4-isobutylpyridine) along with the two triphenylphosphines as ancillary ligands, [Cu$_2$I$_2$(2-(diphenylphosphino)-4-isobutylpyridine))(PPh$_3$)$_2$], **121**, was used for a test device because of its photophysical properties (relatively short decay time of 2–2.8 μs), excellent quantum yields (91%), and high solubility in the organic solvents. OLED device was fabricated with the multilayer architecture glass/ITO/PEDOT:PSS/poly-TPD/**121**:TPBi:PVK (45:45:10)/TPBi/Ca/Ag (Poly-TPD = Poly[N,N′-bis(4-butylphenyl)-N,N′-bis(phenyl)-benzidine]) with a high doping ratio of the Cu(I) emitter in the mixed matrix. The HOMO and LUMO energies of the host and supporting layers fit well with the corresponding HOMO (−5.2 eV) and LUMO energies (−2.5 eV) of **121**. Strong luminance of 1800 cd/m^2 at 10 V and maximum CE of 9.0 cd/A were recorded.

121   **122**

Osawa et al. [118] synthesized the neutral [Cu(dppb)(PS)] complex **122** containing the anionic bidentate ligand 2-diphenylphosphinobenzenethiolate (PS). The thiolate ligand due to its strong electron donating character decreases the MLCT character of the excited state leading to TADF emission. Efficient green TADF in Cu(I) complex, with PL peak at 531 nm and PLQY of 52%, was verified by photophysical studies and TDDFT calculations and exploited to fabricate efficient OLEDs via wet process. A proper selection of components of the mixed host led to TADF-OLED with EQE = 7.8% and CE = 21.3 cd/A with CIE (0.40, 0.53).

3.3. LECs

LECs are single layer electroluminescent devices consisting of a luminescent compound in an ionic environment [119]. The mobile ions in the emitting layer drift toward the electrodes upon application of external electric field. As result, easy charge carrier injection can be achieved and thicker film can be prepared. Differently from OLEDs, they are insensitive to the work function of the electrodes, thus air stable metals such as gold, silver or aluminum, or even graphene can be employed. LEC devices based on ionic transition metal complexes as the only electronically active component have attracted considerable interest for their strong emitting properties, stability and color tunability as well as the low production costs associated with the spin-coating technique [119].

These type of devices were mainly based on cationic ruthenium(II) and iridium(III) complexes and in the last decade Cu(I) have emerged as a valuable alternative, but the results still remain modest.

The first Cu(I)-based LEC was reported by Wang et al. [120] involving a dinuclear orange emitting complex [Cu$_2$(tdpme)$_2$(4,4′-bpy)][BF$_4$]$_2$ (tdpme = 1,1,1-tris-diphenylphosphino-methyl-ethane and 4,4′-bpy = 4,4′-bipyridine) **123** to give a neat film or dispersed in inert host poly(methylmethacrylate) (PMMA) matrix. The best performance of 0.16 cd/A at 12 V with CIE chromaticity coordinates (0.568; 0.423) were recorded, but a red-shift of the EL with respect to PL was observed most likely due to polarization effect of molecular orbitals under high electric field. Interestingly the response time of the device is fast, being only 1 s, and switched on at 2 V.
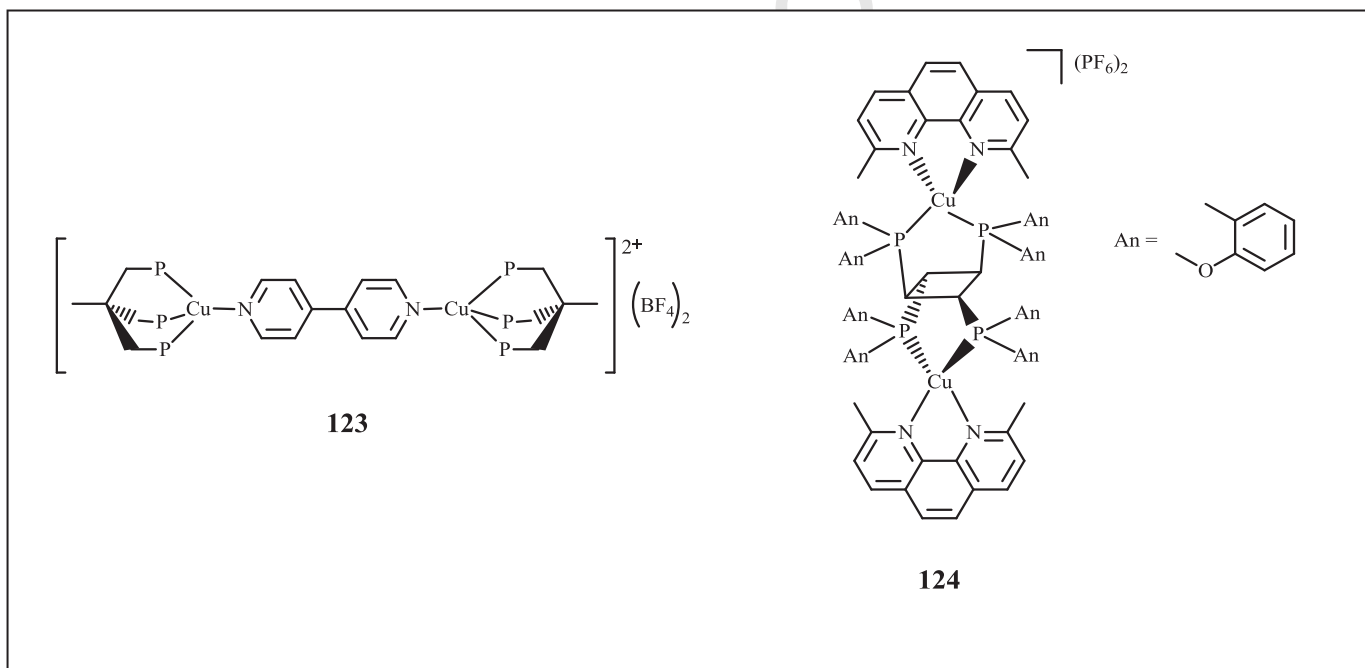
Armaroli, Nierengarten, Wegh and coworkers [121] simultaneously to Wang's group [122] fabricated the first LEC reported to date based on charged [Cu(NN̂)(PP̂)]$^+$ type complex [Cu(dnbp)(DPEphos)](BF$_4$), **112**, which has been previously used in an OLED device [109].

Armaroli found that, upon dispersion in PMMA matrix in 25/25 (w/w) ratio and by using a Ag cathode, a moderate CE of about 1 cd/A and approximately 90 cd/m^2 were recorded, comparable to the earlier fabricated multilayered OLED and in the same order of magnitude of that obtained for LEC devices with Ru(II) type compounds. The long response times were due to relatively low ion mobility.

Wang's group presented a device based on neat **112** film with green stable EL and the record CE of 56 cd/A corresponding to EQE of 16% comparable to the best reported Cu-based OLED [110]. By undertaking a pre-biasing at 25 V for 40 s such a treatment is beneficial also for reducing the response time. The insertion of a Ca layer between emitting layer an Al further increased device brightness up to 4100 cd/m^2. The effect of counterion structure was thoroughly investigated, but the BF$_4^-$ gave the best performance.

After few years, the yellow emitting complex **114** with [PF$_6^-$] as counterion, was used by Bolink, Constable and co-workers [123] in single layer device showing good performance by pre-biasing operation at high voltage, (that became a standard procedure). They added a ionic liquid (1-ethyl-3-methylimidazolium hexafluoridophosphate, [EMIM][PF$_6$]) to enhance ionic conductivity of the active layer, efficiency and to reduce turn on time. A CE enhancement, with respect to previous results, up to 4.55 cd/A, turn on time of 1.1 h at 3 V and CIE (0.47; 0.50) were registered with stability of the same order of magnitude as those obtained for most of the LECs based on Ru(II) and Ir(III) complexes exhibiting comparable efficiency.

The more recent result was achieved by De Cola's and Brüggeller's groups with dinuclear Cu(I) complex containing bis(bidentate)phosphine ligands [124]. Complex **124** possessing tetrakis(di(2-methoxyphenyl)phosphanyl)cyclobutane) (o-MeO-dppcb) and 2,9-dimethyl-1,10-phenanthroline as ancillary ligand was selected due to the promising PLQY of 49%. A not optimized device architecture showed brightness of 108 cd/m^2 at 5 V. The delayed fluorescence mechanism present in compound **124** is responsible for the good device performance.

4. Second order NLO

Non linear optics (NLO) deals with the interaction of electromagnetic fields (light) with matter to generate new electromagnetic fields, altered with respect to phase, frequency, amplitude or other propagation characteristics from the incident field [125]. Because of their great practical utility as molecular building blocks for optical communications, optical data processing and storage, electrooptical devices, parametric frequency converter (or mixing), electrooptic materials, the search for new compounds with large macroscopic second-order nonlinearities is ever growing [126–129].

One of the most intensively studied nonlinear optical phenomenon is second harmonic generation (SHG) or frequency doubling, which consists in the conversion of the incident laser radiation at frequency ω to radiation at the second harmonic frequency 2ω. By this process, for example the fundamental infrared radiation of a Nd:YAG laser can be converted by a nonlinear optical material to green light.

SH properties at molecular and bulk level are correlated with quadratic hyperpolarizability (β) and susceptibility ($\chi^{(2)}$) tensor, respectively. Geometrical symmetries may reduce the number of independent nonzero components of β and $\chi^{(2)}$ tensor. In particular they vanish in a centrosymmetric structural environment so that, to have a second-order NLO emission, the acentricity requirement must be fulfilled and this constitutes the major impediment when attempting to prepare massive compounds.

In the last few years, inorganic–organic hybrid compounds have emerged as interesting molecular chromophores for second-order non-linear optical applications, because they may offer a great diversity of tunable electronic properties by virtue of the metal center [10,130–137] and because they are capable to merge the advantages of the organic NLO chromophores (appreciable NLO response speed and intensity in a wide spectral range, straightforward synthetic approach) to those of an inorganic network (chemical, thermal and

Table 7
Summary of Cu(I) complexes for Second Harmonic Generation.

Compound	$I^{(2\omega)}$	β ($\times 10^{-30}$ esu)	β_0 ($\times 10^{-30}$ esu)	λ (μm)	Technique	Condensed phase/solution	Reference
125a		144	78	1.34	HLS	CHCl$_3$	[145]
125b		128	70	1.34	HLS	CHCl$_3$	[145]
125a		144		1.34	HLS	CH$_2$Cl$_2$	[146]
		113	86	1.91			
126a		268	203	1.91	HLS	CH$_2$Cl$_2$	[147]
126b		300	227	1.91	HLS	CH$_2$Cl$_2$	[147]
127a		266		1.91	HLS	CH$_2$Cl$_2$	[150]
127b		1672 (65%)		1.91	HLS	CH$_2$Cl$_2$	[150]
128a		164	40	1.064	HLS	DMF	[151]
128b		319	62	1.064	HLS	DMF	[151]
128c		198	46	1.064	HLS	DMF	[151]
128d		354	–	1.064	HLS	DMF	[151]
129	2/3[a]			1.907	Kurtz–Perry	Powder	[153,155]
130a	1[b]			1.907	Kurtz–Perry	Powder	[157]
130b	14[b]			1.907	Kurtz–Perry	Powder	[157]
130c	Negligible[d]			1.064	Kurtz–Perry	Powder	[157]
130d	2.3[d]			1.064	Kurtz–Perry	Powder	[157]
130e	Negligible[d]			1.064	Kurtz–Perry	Powder	[157]
130f	22.5[d]			1.064	Kurtz–Perry	Powder	[157]
130g	7.5[d]			1.064	Kurtz–Perry	Powder	[157]
130h	45[d]			1.064	Kurtz–Perry	Powder	[157]
131	22.5[d]			1.064	Kurtz–Perry	Powder	[160]
132	0.2[b]			1.064	Kurtz–Perry	Powder	[161]
133	Negligeble[b]			1.064	Kurtz–Perry	Powder	[162]
134	1[c]			1.064	Kurtz–Perry	Powder	[165]
135	Very weak[c]			1.064	Kurtz–Perry	Powder	[166]
136	1.5[b]			1.064	Kurtz–Perry	Powder	[167]
137	0.7[c]			1.064	Kurtz–Perry	Powder	[168]
138a	0.1[b]			1.064	Kurtz–Perry	Powder	[169]
138b	0.1[b]			1.064	Kurtz–Perry	Powder	[169]
138c	Negligible[b]			1.064	Kurtz–Perry	Powder	[169]
139	3–4[c]			1.064	Kurtz–Perry	Powder	[170]
140	0.8[b]			1.064	Kurtz–Perry	Powder	[171]
141	1[c]			1.064	Kurtz–Perry	Powder	[173]
142a	0.15[b]			1.064	Kurtz–Perry	Powder	[174]
142b	0.21[b]			1.064	Kurtz–Perry	Powder	[174]
142c	0.25[b]			1.064	Kurtz–Perry	Powder	[174]
142d	0.19[b]			1.064	Kurtz–Perry	Powder	[174]
142e	0.24[b]			1.064	Kurtz–Perry	Powder	[174]
142f	0.31[b]			1.064	Kurtz–Perry	Powder	[174]
143a	0.1[c]			1.064	SHG	Single crystal	[175]
143b	0.08[c]			1.064	SHG	Single crystal	[175]
129 film	3.5 pm/V			1.064	Poling and Maker Fringes	PMMA film	[181]
144	0.84[f]			1.064	Photoinduced	Single crystal	[182]

[a] [DAMS][PTS] = 1000 times urea; [b] urea; [c] potassium dihydrogen phosphate (KDP); [d] quartz; [e] d$_{33}$ (pm/V); [f] potassium titanyl phosphate (KTP).

993 mechanical stabilities). An organometallic fragment could act, when the ligand is covalently bonded and weakly coupled to the metal *via*
994 its π-system, as an inductive electron-acceptor species, depending on the electron configuration of the metal, on its oxidation state, and on
995 its ligand environment. However, in the excitation process the metal can act as an electron donor *via* a d → π* charge transfer [138]. These
996 factors influence the nature of the charge-transfer processes between the metal and the ligands or even inside the ligands themselves,
997 producing a significant effect on the quadratic hyperpolarizability of the ligands.

998   Different techniques can be employed to measure second order NLO parameters of compounds in solution and in the solid state, electric-
999 field-induced second harmonic generation (EFISH) and the harmonic light scattering (HLS) being the most frequently used for solutions,
1000 the Kurtz–Perry for powders and electric poling for host-guest thin films. In this review, studies on Cu(I) second order NLO active materials
1001 are summarized in different section according to the technique employed for the determination of the NLO parameters (see Table 7).

1002 *4.1. Harmonic light scattering*

1003   In HLS [139–143] experiment, the incoherently scattered frequency-doubled light arising from the SHG active molecules is detected.
1004 Although the material may be macroscopically isotropic, the correlation between local fluctuations induces a detectable second-harmonic
1005 light. The intensity of the second harmonic scattered light is proportional to the orientational average $\langle \beta_{ijk}(2\omega)\beta_{lmn}(2\omega)\rangle$, in accordance
1006 with:

1007
$$I^{2\omega} = GN \sum_{ijklmn} \langle \beta_{ijk}(2\omega)\beta_{lmn}(2\omega)\rangle I(\omega)^2 = GN\beta_{HLS}I(\omega)^2$$

1008   This expression provides the definition for β_{HLS}. It depends on the polarization of the fundamental and harmonic beams, providing a
means to determine different components of the β tensor. As compared to EFISH, the advantage of this technique is that it can be applied

to ionic and nonpolar molecules. However, two photon-induced fluorescence may significantly affect HLS measurements leading to an important overestimation of the hyperpolarizability values [144].

In 1999, H. Le Bozec reported the HLS efficiency of two D_{2d} tetrahedral octupoles based on Cu(I) with bipyridyl ligands [145]. Complexes **125a** and **125b** were prepared by reaction of the corresponding bipyridine with [Cu(MeCN)$_4$]PF$_6$ in CH$_2$Cl$_2$.
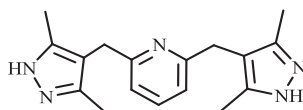

2,6-bis((3,5-dimethyl-1*H*-pyrazol-4-yl)methyl)pyridine

UV–vis spectra of the compounds in CH$_2$Cl$_2$ show intense intraligand charge-transfer bands (around 420 nm) red-shifted of about 30–40 nm with respect to the free ligands. The MLCT transition [Cu(I) → π*(bpy)] (at *ca.* 480 nm) can be distinguished as a shoulder of the more intense ILCT band. HLS measurements performed at 1340 nm on CHCl$_3$ solution gave β values equal to 144×10^{-30} and 128×10^{-30} esu for compound **125a** and **125b** respectively, indicating for both a good non linearity/transparency trade off. The HLS β value of **125a** was found to remain only slightly changed (113×10^{-30} esu) when, some years later, the same group performed new HLS measurements at 1910 nm in order to minimize the possible effect of the two photon-induced fluorescence [146].

Similarly, more recently, Akdas-Kilig et al. prepared compounds **126a** and **126b** with donor-substituted bipyridine ligands and their corresponding D$_{2d}$ (Cu(I), Ag(I), Zn(II)) octupolar metal complexes [147]. In particular, the electronic absorption spectra of the Cu(I) derivatives **126a** and **126b** exhibit red-shifted intense absorptions in the visible region (at *ca.* 427 nm) which were assigned to ILCT transition with the typical MLCT transition [Cu(I) → π*(bpy)] at *ca.* 440 nm appearing as a shoulder of the more intense ILCT band. HLS measurements were performed on both complexes in CH$_2$Cl$_2$ solution at 1910 nm giving for **126a** and **126b** β values of 268×10^{-30} and 300×10^{-30} esu, respectively. Such values are much larger than the one previously obtained for **125a** in agreement with an increase in the π-delocalization on the bipyridine ligands induced by the phenyl substituents. A similar observation was previously reported for iridium and ruthenium complexes featuring substituted phenanthroline ligands [148,149].

In 2012, Le Bozec et al. developed a Cu(I) complex **127** with a bipy ligand, namely 4,4′,6,6′-tetramethyl-2,2′-bipyridine, able to show reversible photochromic switching of NLO properties [150].
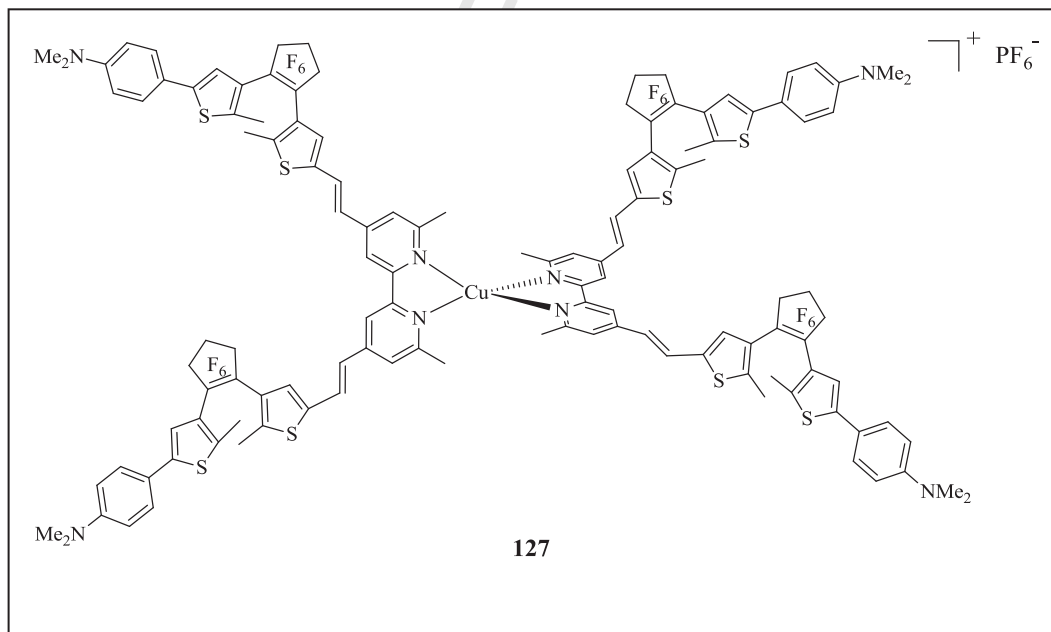
127

The Cu(I) compound, **127a**, was prepared by reaction of the ligand with [Cu(MeCN)$_4$]PF$_6$ in CH$_2$Cl$_2$-MeCN solution at room temperature. When measured at 1910 nm in CH$_2$Cl$_2$, **127a** showed a 266×10^{-30} esu β_{HLS} value, attributed to the low energy MLCT [Cu(I) → π*(bpy)] transition at 511 nm. Upon irradiation at 350 nm, the red solution of **127a** turned green, due to the formation of the fully closed form, **127b**, with a photostationary state >90%; upon irradiation at 650 nm, the quantitative regeneration of the fully open isomer was observed, indicating the fully reversible closed-to-open photoisomerization. A substantial enhancement of the second-order NLO activity was observed for **127b** associated with a ILCT red-shifted transition at 701 nm. At 65% ring-closing, as determined by ^{1}H NMR spectroscopy, a β_{HLS} of 1672×10^{-30} esu was measured.
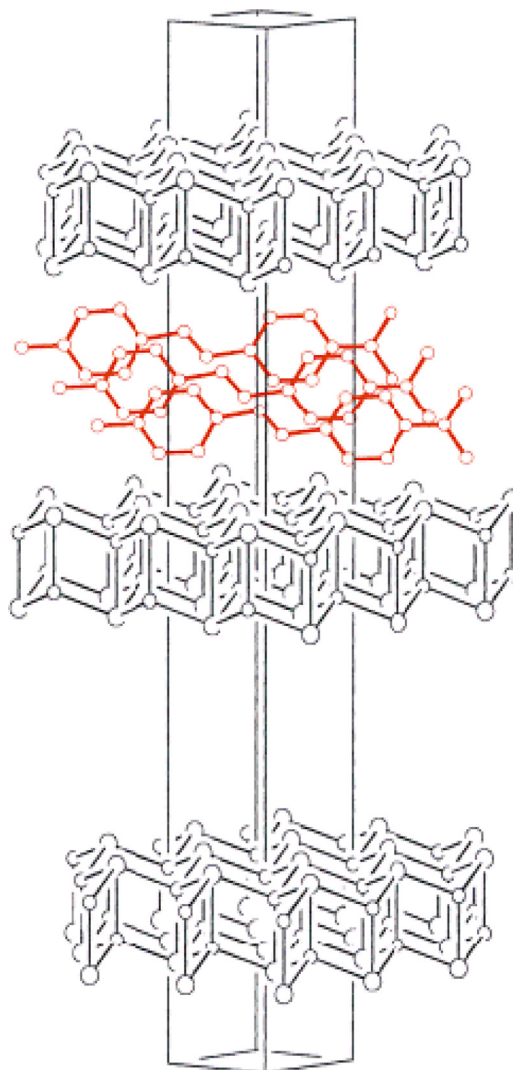
Fig. 30. Structure of **129**. Reprinted with permission from Ref. [153]. Copyright 2001 WILEY-VCH Verlag GmbH, Weinheim, Fed. Rep. of Germany.

Apart from bipy derivatives, in 2009, Wu et al. investigated a series of penta-nuclear clusters of formula [$MS_4Cu_4X_2Py_6$] (M = W, X = Br for **128a** and I for **128b**; M = Mo; X = Br for **128c** and I for **128d**) [151]. HLS measurements on bromide clusters resulted in β values equal to 164×10^{-30} and 198×10^{-30} esu for **128a**, having a Mo central atom, and **128c**, with a W atom, respectively. A similar trend, but higher values, were obtained for the two iodide clusters **128b** and **128d**, with β_{HLS} of 319×10^{-30} and 354×10^{-30} esu respectively, in agreement with the larger ionic radius of the iodine atom. By TDDFT analysis, it was concluded that, together with MLCT and LLCT processes, weak direct metal–metal interactions are also involved in the CT processes contributing to the quadratic hyperpolarizabilities of these poly-metal clusters. Such MMCT process may positively enhance the cluster's quadratic hyperpolarizability, as in **128c**, or can even contribute significantly, as in **128b**. In agreement, if inhibited by long metal–metal distances, a lower β_{HLS} is measured, as is the case for **128a**. Importantly, these results suggested that second-order NLO properties of poly-nuclear metal clusters can be tuned by adjusting direct metal–metal interactions, avoiding the use of more-extended conjugated ligands in an effort to enhance the molecular hyperpolarizability.

4.2. Kurtz–Perry

In a typical Kurtz–Perry set up [152], the powdered sample in a capillary tube, is irradiated with a pulsed laser. The second harmonic emitted light is collected by an elliptical mirror, filtered to select only the second order contribution and recollected with a photomultiplier tube and compared with that of a reference compound. Considering that the measured efficiency depends upon bulk susceptibility $\chi^{(2)}$, this method gives an indirect evaluation of the order of magnitude of $\chi^{(2)}$.

The first study on a powdered Cu(I) complex dates back to 2001 [153] when E. Cariati et al. reported a layered material of formula [DAMS][Cu_5I_6] ([DAMS$^+$] = trans-4-(4-dimethylaminostyryl)-1-methylpyridinium), **129**, showing at 1907 nm a SHG efficiency of the same order of magnitude of [DAMS][p-toluensulfonate] ([DAMS][PTS], reported to generate a second harmonic signal 1000 times that of standard urea [154]). The compound was prepared by either solution or solid mixing [155] of [DAMS]I and Cu(I), and, despite the impossibility to grow suitable single crystals for diffraction analysis, its structure was solved by means of XRPD. The structural pattern consists of polymeric CuI slabs stacked along the trigonal axis (Fig. 30), which are formed by two parallel, slightly corrugated sheets. [DAMS$^+$] cations fill the

empty space within the slabs and are organized in J-type (or Scheibe) aggregates [156] which were indicated as responsible of the high SHG signal observed.

The same group reported in 2002 an investigation on the solid-state emissive and second-order NLO responses of oligomeric and polymeric CuX/L adducts (where L is pseudoaromatic η^1-nitrogen donor) [157]. Two non-centrosymmetric 'chain' and 'stair' polymeric adducts between CuI and 4-acetylpyridine **130a–130b** were synthesized by reaction of the cubane [CuIpy]$_4$ with different amount of 4-acetylpyridine in CH$_2$Cl$_2$. In compound **130a**, with [Cu:I:acpy] = [1:1:1] stoichiometry, the [CuI(acpy)] asymmetric units arrange in polymeric [CuI(acpy)]$_n$ double-stranded 'stairs'; in **130b**, with [Cu:I:acpy] = [1:1:2] stoichiometry, copper and iodine atoms are arranged alternately along 'zig-zag single-stranded chains' originating a polymeric [CuI(acpy)$_2$]$_n$ motif.

The compounds' SHG properties, determined by the Kurtz–Perry method at 1907 nm, resulted in efficiency equal and 14 times that of standard urea respectively. To rationalize such a different second-order NLO behavior, a comparison of the experimental SHG's with the phase-matchable components of b_{eff} using Zyss' formulas [158,159] was carried out. It was concluded that the ^{3}MLCT* process alone is not enough to explain the electronic origin of the second-order NLO response for **130a** and **130b**. To get further insight, some structurally related non-centrosymmetric [CuX(L)]$_n$ 'chains' and 'stairs' adducts, namely [CuCl(quinoline)]$_n$ **130c** – 'stairs', [CuCl(2-methylquinoline)]n **130d** – 'chains', [CuBr(pyridine)]$_n$ **130e** – 'stairs', [CuBr(2,4,6-trimethylpyridine)]$_n$ **130f** – 'chains', [CuBr(2-methylquinoline)]$_n$ **130g** – 'chains' and [CuI(2,4,6-trimethylpyridine)]$_n$ **130h** – 'chains', were prepared and investigated. The emissive behavior of **130c–130h**, alone, did not allow to identify univocally the charge-transfer electronic transitions involved in the second-order NLO response, although a certain trend of the wavelength of the emission to the nature of the halide X suggested participation of the excited state ^{3}XLCT* to the charge-transfer process. This latter assumption was also confirmed by the SHG efficiencies of compounds having the same structural motifs and organic ligands but differing for the halides (e.g. compounds **130d** and **130g** with SHG of 2.3 and 7.5 times that of quartz, respectively). Moreover, inter-metal distances invariably greater than the sum of the van der Waals radii allowed to exclude a d → (s,p) contribution from Cu-delocalized orbitals. In addition, as was the case for **130a** and **130b**, 'chains' always showed larger second-order NLO efficiencies than 'stairs', suggesting that in the two structural motifs dipole–dipole interactions occur not only through space but also through bonds, in particular within the polymeric framework.

Pursuing the investigation on the second-order NLO behavior of CuI adducts Cariati et al. synthesized and studied the CuI adduct with trans-4′-(dimethylamino)-4-stilbazole **131** showing a polymeric helicoidal motif, in which each copper coordinates the nitrogen donor atom of one organic ligand, while the iodine atoms simply bridge two metal centers [160]. A SHG efficiency of 22.5 times that of standard quartz was measured at 1064 nm.

To ensures noncentrosymmetric solid-state organization, Anthony and Radhakrishnan [161,162] used a chiral push-pull ligand to prepare coordination polymers of Cu(I) and Ag(I). By reaction of N,N′-bis(4-cyanophenyl)-(1R,2R)-diaminocyclohexane (BCDC) with [Cu(CH$_3$CN)$_4$]PF$_6$ or AgClO$_4$, [Cu(BCDC)]PF$_6$·THF, **132**, with extended 2D network, [Cu(BCDC)$_2$]PF$_6$, **133**, with a three-dimensional architecture, and [Ag(BCDC)]ClO$_4$, with one-dimensional helical structure, were obtained. It was found that the coordination modes strongly influence the solid state SHG leading to a not measurable signal for **133**, a low signal, slight lower than that of the free ligand, for **132** and higher value, enhanced with respect to the free BCDC, for the Ag(I) compound.
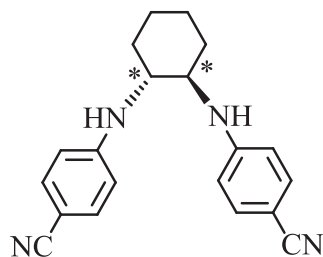

N,N′-bis(4-cyanophenyl)-(1R,2R)-diaminocyclohexane (BCDC).

Static hyperpolarizabilities calculated by the AM1/TDHF method showed a higher value for **133** than for **132** contrarily to what measured at bulk level [163,164]. Considering that the Ag(I) one-dimensional polymer showed the highest massive SHG value, the authors suggested a correlation between the dimensionality of the network topology and the NLO response, the lower dimensionality being more favorable to the SHG response.

In 2004 Yao et al. prepared a 3D polymer with trimeric Cu(I) unit, namely [Cu$_3$(CN)(IN)$_2$]$_n$ (IN = isonicotinate), **134**, by reaction of Cu(NO$_3$)$_2$·3H$_2$O with isonicotinic and terephthalic acids under hydrothermal conditions [165]. Single-crystal X-ray diffraction analysis revealed a 3-D open frameworks consisting of three copper(I) atoms, two IN ions and one cyanic ion. Kurtz–Perry measurements at 1064 nm indicated a SHG intensity similar to that of standard KDP. According to its transparency in the visible range, its insolubility in common organic solvents and its high thermal stability (up to 543 K) the compound was suggested as potential candidate for practical applications.

Hong et al., in 2004, prepared, through solvothermal redox reaction a new polymeric metal organosulfide, namely $[Cu_3(pymt)_3]_n$ (pymt = pyrimidine-2-thiolate), **135** [166].
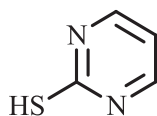
Pyrimidine-2-thiol (Hpymt).

At room temperature, in the solid state, the compound produces an intense red emission (λ_{em} = 752 nm) which was assigned a triplet excited state of LMCT and/or MLCT character, mixed with metal-centered (ds/dp) states. Despite its noncentrosymmetric solid-state organization, the compound showed a very weak SHG efficiency respect to KDP as standard, when tested by the Kurtz–Perry method at 1064 nm.

Xiong et al. prepared the one-dimensional chain coordination polymer $\{[Cu(PPh_3)-(N,N-(2\text{-pyridyl})(4\text{-pyridylmethyl})amine)](ClO4)\}_n$, **136**, by reaction of N,N-(2-pyridyl)(4-pyridylmethyl)amine with $[Cu(MeCN)_2(PPh_3)_2]ClO_4$ under solvothermal conditions [167]. According to X-ray diffraction analysis, the compound crystallizes in a noncentrosymmetric space group (Cc). The presence of strong hydrogen bonds among perchlorate anions and amines resulted in the formation of a three-dimensional network. SHG Kurtz–Perry measurements at 1064 nm showed a signal 1.5 times that of standard urea and this was explained by hydrogen bonds constituting a donor–acceptor system which can significantly enhance the SHG response or a useful way of linking donor and acceptor.
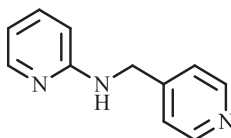

N,N-(2-pyridyl)(4-pyridylmethyl)amine

Du et al., in 2006, isolated two noncentrosymmetric 2D coordination polymers of formula $[MOS_3Cu_3\{S_2P(OMe)_2\}_2]$ (**137**, M = W; **137a**, M = Mo) [168]. Of the two, only **137** was tested by the Kurtz–Perry method giving a SHG signal about 0.7 times that of standard KDP.

In 2008, Zhang et al., prepared by reaction of copper halides with pyridine-4-thiol (pytH) under hydrosolvothermal conditions, three noncentrosymmetric coordination polymers, namely, $[Cu_2(pyt)Cl]$, **138a**, $[Cu_2(pyt)Br]$, **138b**, and $[Cu_5(pytH)_3Cl_5]$, **138c**, as revealed by X-ray single-crystal diffraction analysis [169]. At room temperature, the three solid compounds show strong yellow or red emission (at 565, 544 and 624 nm respectively). Such emissions were assigned to LMCT and/or MLCT transitions. Kurtz–Perry measurements resulted in a SHG signal equal to 0.1 *vs.* urea for isostructural for **138a** and **138b** and a very low signal for **138c**.

Lu et al., in 2010, reported an acentric three-dimensional polar material, $[Cu_2(L)Br]_n$ (L = 5-(4-pyridyl)tetrazole), **139**, obtained by reaction of CuBr with HL under solvothermal conditions [170]. SHG Kurtz–Perry measurement resulted in a signal 3–4 times higher than standard KDP.
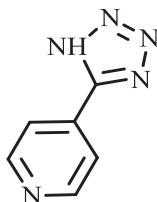

5-(4-pyridyl)tetrazole

Sun et al. in 2010, prepared and characterized the noncentrosymmetric complex $[Cu_3(L)_2(CH_3CN)_3(ClO_4)_3]$, **140** [where L = 1,3,5-tris(2-oxazolinyl)benzene] showing a SHG activity 0.8 times that of standard urea [171]. A value higher than the similar Ag(I) complex previously reported [172].

1,3,5-tris(2-oxazolinyl)benzene
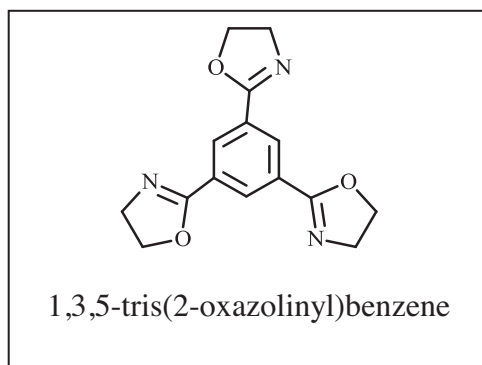
Sheng et al. in 2012 synthesized the noncentrosymmetric dinuclear molecule-bridged Cu(I) complex of formula [(μ-bpym)(CuL)$_2$](ClO$_4$)$_2$·(CH$_3$CN)$_2$(H$_2$O) (bpym = 2,20-bipyrimidine, L = (R)-(+)-2,2′-bis(diphenylphospho)-1,10-dinaphthalene), **141** [173]. The solid compound, while not luminescent at room temperature, at 10 K displayed a red emission (λ_{max} at 706 nm), suggesting an important role of thermal vibration on its luminescent properties. In agreement with previous studies, the emission was attributed a MLCT excited state. An efficiency equal to KDP standard was measured by the Kurtz–Perry method.

141
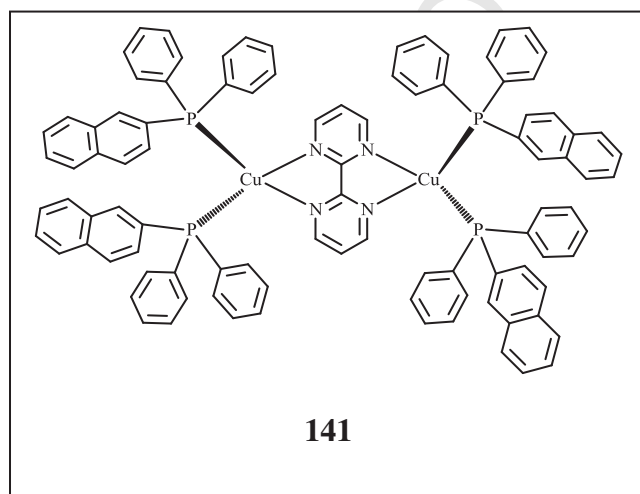
Chavan et al. synthesized a series of heterobimetallic complexes of the type [Cu(L$_{1-3}$)(NC$_5$H$_4$C≡CRu(dppe)$_2$Cl)I], **142a–142c**, and [Cu(L$_{1-3}$)(NC$_5$H$_4$C≡CC$_6$H$_4$C≡CRu(dppe)$_2$Cl)I], **142d–142f**, by reaction of trans-[RuCl(dppe)$_2$(C≡C-py-3)] and trans-[RuCl(dppe)$_2$(C≡CC$_6$H$_4$C≡C-py-3)] with CuI in the presence of Schiff base ligands L$_{1-3}$ (where L$_1$ = N-(2-pyridylmethylene)phenylamine, L$_2$ = 4-bromo-N-(pyridylmethylene) phenylamine and L$_3$ = 4-nitro-N-(2-pyridylmethylene)phenylamine) [174].

142a: R=H	**142d**: R=H
142b: R=Br	**142e**: R=Br
142c: R=NO$_2$	**142f**: R=NO$_2$
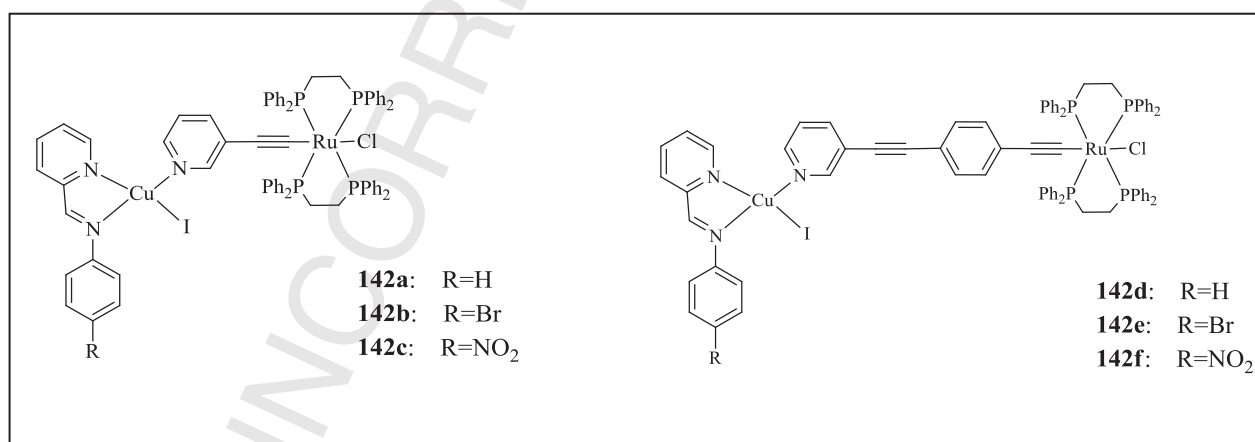
In CH$_2$Cl$_2$ solution the compounds exhibited photoluminescence at about 460 nm correlated with ILCT mixed with MLCT transitions. All complexes resulted to be second harmonic generators with efficiency ranging from 0.15 to 0.31 that of standard urea, the highest value was obtained for compound **142f** bearing a NO$_2$ group in the coordinated Schiff base ligands.

Ye et al. prepared two noncentrosymmetric Cu(I) clusters, namely H$_3$TTB[Cu$_4$Cl$_3$], **143a**, and H$_3$TTB[Cu$_8$Br$_{11}$], **143b**, (TTB = 1,3,5-tris(diallylaminomethyl)-2,4,6-trimethylbenzene) by reaction, under solvothermal conditions, of CuX (X = Cl, Br) and TTB in the presence

of HCl and HClO$_4$ respectively [175]. Differently from the above reported studies, the SHG efficiency of the two compounds was measured on single crystals. When compared to KDP, the SHG signal resulted in a not null but modest value.

1,3,5-tris(diallylaminomethyl)-2,4,6- trimethylbenzene (TTB).
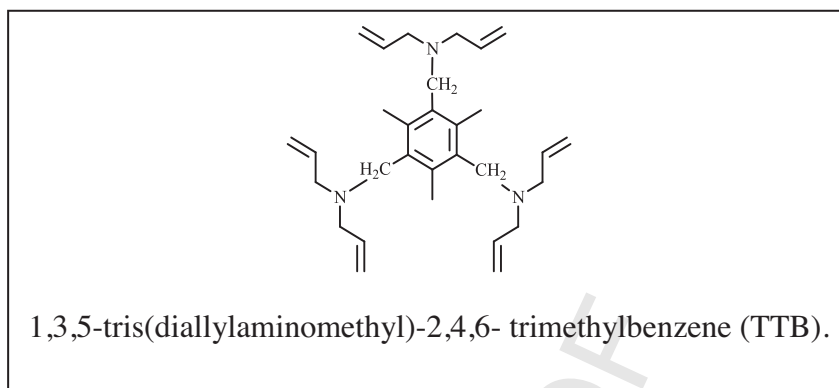
4.3. SHG from oriented films

Large $\chi^{(2)}$ values can be obtained starting from molecular second order NLO chromophores as building blocks by engineering their organization in a non centrosymmetric way. To reach this goal various strategies have been proposed such as stepwise construction of multilayers, Langmuir–Blodgett films, self-assembly in layered crystalline structures or in films, chirality to induce acentric crystalline structures, ordered inclusion in 1D or 2D host structures and electrical poling the latter being an intensively investigated field [176,177]. In the poling process, the initial random dispersion of the polar chromophores is broken to generate asymmetry by aligning their dipole moments under a strong directional electric field at a temperature, near the T_g, where the chromophores' dipoles can be readily oriented. Cooling at room temperature acentric polymeric thin films are obtained. However, poling process suffers the outcome of an easy decay of the electrooptical properties due to orientational relaxation of the aligned NLO chromophores and, often, of scattering losses originated by the inhomogeneity of the film. In particular, the electric field poling process is usually applied to polymers mixed with neutral second order NLO chromophores since ionic chromophores may produce, under the effect of the directional strong electric field, an opposite diffusion of cations and anions toward the surface of the film. Measurements of the nonlinear optic coefficients d_{ij} are based on the method of the Maker fringes, in which the sample is rotated around an axis perpendicular to the incidence plane of the fundamental beam and the SHG intensity is determined as a function of the rotation angle [178–180].

In 2011 Cariati et al. reported a direct procedure, different from the above described bottom-up approach, based on a successful two step (electric poling and thermal annealing) process to produce in situ oriented nanocrystals of [DAMS][Cu$_5$I$_6$], **129**, dispersed in PMMA on a glass substrate **129 film** [181].

An electric poling pretreatment (8.5 kV at 358 K) of a dispersion of **129** in a PMMA film is followed by solely controlled thermal annealing at 413 K, a temperature higher than the T_g of PMMA (353 K). The oriented NLO active and polar nanocrystals obtained are sufficiently small to guarantee a good optical quality of the film, but large enough to be characterized by a very low mobility in the PMMA matrix thus producing a high stability of their orientation and consequently a long lasting SHG. By Maker Fringes measurements, the macroscopic nonlinear optical coefficients d$_{33}$ of the poled and annealed film resulted in values up to 3.5 pm/V. A rigorous control of the heating ramp was required since a fast temperature increase produces a very low dependence of the SHG from the angle of the incident radiation, which is the typical behavior of a disordered system.

We comment here, on a very peculiar study performed on a single crystal in which asymmetry was generated by photoinduction produced by applying an external laser field. Krishnakumar et al. [182] reported the synthesis and the NLO properties of single crystal of Cu(SC(NH$_2$)$_2$)$_3$(ClO$_4$), **144**, prepared by reaction of Cu(ClO$_4$)$_2$ with thiourea, belonging to monoclinic centrosymmetric space group. To observe SHG, a polarized UV laser (337 nm) was applied to generate a charge density noncentrosymmetry due to polarization of the medium.

The SHG signal was detected only immediately after photoinduction and effective SHG achieved its maximum (about 0.84 pm/V) at photoinducing power density of about 1430 kW/cm^2, at an angle of about 35° between the pumping and fundamental power beam's polarizations. Such maximum was the result of a competition between the anharmonic photothermal expansions and the thermal destruction due to crystal surfaces heating (about 281–285 K).

5. Summary

The interest in luminescent metal complexes has increased tremendously in the last ten years along with the expansion of their field of application. They are used as emitters for OLEDs, LECs, chemical sensors, resonators for organic lasers, photocatalysts and in biological and biomedical applications The criteria of high (photoluminescence/electroluminescence) quantum efficiencies, abundance, low cost and low toxicity point obviously to the use of Cu(I) derivatives. Moreover, Cu(I) compounds display a very rich photophysical behavior associated not only to the numerous different structural formats but also to the effect induced by external stimuli. Subtle changes in the crystal packing lead to important Cu—Cu bond variations and great luminescence modifications that can be exploited for the fabrication of extremely efficient sensors. In addition, the possibility of obtaining complexes with fluorescent emission by triplet states harvesting through TADF processes has motivated the search of new Cu(I) based systems with TADF activity for OLED applications.

One of the major drawback of Cu(I) complexes for light emission applications is their susceptibility to structural changes in the excited state that, activating non-radiative decay pathways, strongly reduces their emission efficiency. The design and synthesis of new complexes, with steric properties able to inhibit flattening of the complex structure in the excited state, is an important challenge for chemists for the development of a next generation of emissive materials.

Despite the low stability of most Cu(I) complexes toward solution processing and vacuum sublimation, the excellent results so far obtained in studies concerning OLED devices based on some highly stable complexes have proved the great potentiality of these materials in low cost flat panel displays and solid state lighting technologies. In the next years, further efforts in material development and device engineering are expected to improve both the color tuning, in particular in the blue and red emission ranges, and the device performance in order to reach commercial standards. Moreover, the long exciton lifetime of the TADF materials have particular interest in other emerging applications, such as solar cells, since they may offer long diffusion lengths of excitons prior to their dissociation, as well as for oxygen and temperature sensors.

In conclusion, in most of the traditional as well as in many new emerging technological fields, the role that Cu(I) based complexes may play is expected to be more and more relevant in the next years.

Acknowledgments

References

[1] R. Peng, M. Li, D. Li, Coord. Chem. Rev. 254 (2010) 1–18.
[2] O.S. Wenger, Chem. Rev. 113 (2013) 3686–3733.
[3] Z. Hu, B.J. Deibert, J. Li, Chem. Soc. Rev. 43 (2014) 5815–5840.
[4] X. Zhang, B. Li, Z.H. Chen, Z.N. Chen, J. Mater. Chem. 22 (2012) 11427–11441.
[5] A. Barbieri, G. Accorsi, N. Armaroli, Chem. Commun. (2008) 2185–2193.
[6] C.M. Che, C.C. Kwok, C.F. Kui, S.L. Lai, K.H. Low, Reference Module in Chemistry, Molecular Sciences and Chemical Engineering, Comprehensive Inorganic Chemistry II (Second Edition), From Elements to Applications, in: Coordination and Organometallic Chemistry, vol. 8, 2013, pp. 607–655.
[7] M. Wallesch, D. Volz, D.M. Zink, U. Schepers, M. Nieger, T. Baumann, S. Bräse, Chem. Eur. J. 20 (2014) 6578–6590.
[8] H. Xu, R. Chen, Q. Sun, W. Lai, Q. Su, W. Huang, X. Liu, Chem. Soc. Rev. 43 (2014) 3259–3302.
[9] O. Maury, H. Le Bozec, Acc. Chem. Res. 38 (2005) 691–704.
[10] S. Di Bella, Chem. Soc. Rev. 30 (2001) 355–366.
[11] A. Bondi, J. Phys. Chem. 68 (1964) 441–451.
[12] S.S. Batsanov, Inorg. Mater. 37 (2001) 871–885.
[13] S. Nag, K. Banerjee, D. Datta, New J. Chem. 31 (2007) 832–834.
[14] F.A. Cotton, X. Feng, M. Matusz, R. Poli, J. Am. Chem. Soc. 110 (1988) 7077–7083.
[15] F.A. Cotton, X. Feng, D.J. Timmons, Inorg. Chem. 37 (1998) 4066–4069.
[16] R. Clerac, F.A. Cotton, L.M. Daniels, J. Gu, C.A. Murillo, H.C. Zhou, Inorg. Chem. 39 (2000) 4488–4493.
[17] P.C. Ford, E. Cariati, J.L. Bourassa, Chem. Rev. 99 (1999) 3625–3647, and references therein.
[18] H.D. Hardt, A. Pierre, Inorg. Chim. Acta 25 (1977) L59–L60, and references therein.
[19] A. Vogler, H. Kunkely, J. Am. Chem. Soc. 108 (1986) 7211–7212.
[20] D. Tran, J.L. Bourassa, P.C. Ford, Inorg. Chem. 36 (1997) 439–442.
[21] E. Cariati, J.L. Bourassa, P.C. Ford, Chem. Commun. (1998) 1623–1624.
[22] E. Cariati, B. Xianhui, P.C. Ford, Chem. Mater. 12 (2000) 3385–3391.
[23] F. De Angelis, S. Fantacci, A. Sgamellotti, E. Cariati, R. Ugo, P.C. Ford, Inorg. Chem. 45 (2006) 10576–10584.
[24] F. Parmeggiani, A. Sacchetti, J. Chem. Educ. 89 (2012) 946–949.
[25] K.R. Kyle, C.K. Ryu, J.A. DiBenedetto, P.C. Ford, J. Am. Chem. Soc. 113 (1991) 2954–2965.
[26] A. Dossing, C.K. Ryu, S. Kudo, P.C. Ford, J. Am. Chem. Soc. 115 (1993) 5132–5137.
[27] H.V. Rasika Dias, H.V.K. Diyabalanage, M.A. Rawashdeh-Omary, M.A. Franzman, M.A. Omary, J. Am. Chem. Soc. 125 (2003) 12072–12073.
[28] H.V. Rasika Dias, H.V.K. Diyabalanage, M.G. Eldabaja, O. Elbjeirami, M.A. Rawashdeh-Omary, M.A. Omary, J. Am. Chem. Soc. 127 (2005) 7489–7501.
[29] M.A. Omary, M.A. Rawashdeh-Omary, M.W. Alexander Gonser, O. Elbjeirami, T. Grimes, T.R. Cundari, H.V.K. Diyabalanage, C.S. Palehepitiya Gamage, H.V. Rasika Dias, Inorg. Chem. 44 (2005) 8200–8210.
[30] I.I. Vorontsov, A.Y. Kovalevsky, Y.S. Chen, T. Graber, M. Gembicky, I.V. Novozhilova, M.A. Omary, P. Coppens, Phys. Rev. Lett. 94 (2005), 193003-1–193003-4.
[31] J.X. Zhang, J. He, Y.G. Yin, M.H. Hu, D. Li, X.C. Huang, Inorg. Chem. 47 (2008) 3471–3473.
[32] J. He, J.X. Zhang, C.K. Tsang, Z. Xu, Y.G. Yin, D. Li, S.W. Ng, Inorg. Chem. 47 (2008) 7948–7950.
[33] T. Jozak, Y. Sun, Y. Schmitt, S. Lebedkin, M. Kappes, M. Gerhards, W.R. Thiel, Chem. Eur. J. 17 (2011) 3384–3389.
[34] S.Z. Zhan, M. Li, X.P. Zhou, J.H. Wang, J.R. Yang, D. Li, Chem. Commun. 47 (2011) 12441–12443.
[35] S.Z. Zhan, M. Li, S.W. Ng, D. Li, Chem. Eur. J. 19 (2013) 10217–10225.
[36] J.H. Wang, M. Li, J. Zheng, X.C. Huang, D. Li, Chem. Commun. 50 (2014) 9115–9118.
[37] D. Cauzzi, R. Pattacini, M. Delferro, F. Dini, C. Di Natale, R. Paolesse, S. Bonacchi, M. Montalti, N. Zaccheroni, M. Calvaresi, F. Zerbetto, L. Prodi, Angew. Chem. Int. Ed. 51 (2012) 9662–9665.
[38] A. Kishimura, T. Yamashita, K. Yamaguchi, T. Aida, Nat. Mater. 4 (2005) 546–549.
[39] W. Ouellette, A.V. Prosvirin, V. Chieffo, K.R. Dunbar, B. Hudson, J. Zubieta, Inorg. Chem. 45 (2006) 9346–9366.
[40] I. Jeß, P. Taborsky, J. Pospíšil, C. Näther, Dalton Trans. (2007) 2263–2270.
[41] M.J. Lim, C.A. Murray, T.A. Tronic, K.E. deKrafft, A.N. Ley, J.C. deButts, R.D. Pike, H. Lu, H.H. Patterson, Inorg. Chem. 47 (2008) 6931–6947.
[42] S. Yuan, S. Wang, D.X. Wang, H.F. Lu, S.Y. Feng, D. Sun, CrystEngComm 15 (2013) 7792–7802.
[43] D. Sun, S. Yuan, H. Wang, H.F. Lu, S.Y. Feng, D.F. Sun, Chem. Commun. 49 (2013) 6152–6154.
[44] S. Yuan, S.S. Liu, D. Sun, CrystEngComm 16 (2014) 1927–1933.
[45] A. Yadav, A.K. Srivastava, A. Balamurugan, R. Boomishankar, Dalton Trans. 43 (2014) 8166–8169.
[46] C. Tard, S. Perruchas, S. Maron, X.F. Le Goff, F. Guillen, A. Garcia, J. Vigneron, A. Etcheberry, T. Gacoin, J.P. Boilot, Chem. Mater. 20 (2008) 7010–7016.
[47] S. Perruchas, C. Tard, X.F. Le Goff, A. Fargues, A. Garcia, S. Kahlal, J.Y. Saillard, T. Gacoin, J.P. Boilot, Inorg. Chem. 50 (2011) 10682–10692.
[48] H. Kitagawa, Y. Ozawa, K. Toriumi, Chem. Commun. 46 (2010) 6302–6304.
[49] S. Perruchas, N. Desboeufs, S. Maron, X.F. Le Goff, A. Fargues, A. Garcia, T. Gacoin, J.P. Boilot, Inorg. Chem. 51 (2012) 794–798.
[50] I. Roppolo, E. Celasco, A. Fargues, A. Garcia, A. Revaux, G. Dantelle, F. Maroun, T. Gacoin, J.P. Boilot, M. Sangermano, S. Perruchas, J. Mater. Chem. 21 (2011) 19106–19113.
[51] I. Roppolo, E. Celasco, M. Sangermano, A. Garcia, T. Gacoin, J.P. Boilot, S. Perruchas, J. Mater. Chem. C 1 (2013) 5725–5732.
[52] Q. Benito, A. Fargues, A. Garcia, S. Maron, T. Gacoin, J.P. Boilot, S. Perruchas, F. Camerel, Chem. Eur. J. 19 (2013) 15831–15835.
[53] Z. Liu, P.I. Djurovich, M.T. Whited, M.E. Thompson, Inorg. Chem. 51 (2012) 230–236.
[54] W.F. Fu, X. Gan, C.M. Che, Q.Y. Cao, Z.Y. Zhou, N. Nian-Yong Zhu, Chem. Eur. J. 10 (2004) 2228–2236.
[55] T.H. Kim, K.Y. Lee, Y.W. Shin, S.T. Moon, K.M. Park, J.S. Kim, Y. Kang, S.S. Lee, J. Kim, Inorg. Chem. Commun. 8 (2005) 27–30.

[56] T.H. Kim, Y.W. Shin, J.H. Jung, J.S. Kim, J. Kim, Angew. Chem. Int. Ed. 47 (2008) 685–688.
[57] P.D. Harvey, M. Knorr, Macromol. Rapid Commun. 31 (2010) 808–826.
[58] M. Knorr, A. Pam, A. Khatyr, C. Strohmann, M.M. Kubicki, Y. Rousselin, S.M. Aly, D. Fortin, P.D. Harvey, Inorg. Chem. 49 (2010) 5834–5844.
[59] M. Knorr, F. Guyon, A. Khatyr, C. Däschlein, C. Strohmann, S.M. Aly, A.S. Abd-El-Aziz, D. Fortin, P.D. Harvey, Dalton Trans. (2009) 948–955.
[60] H. Xie, I. Kinoshita, T. Karasawa, K. Kimura, T. Nishioka, I. Akai, K. Kanemoto, J. Phys. Chem. B 109 (2005) 9339–9345.
[61] X.C. Shan, F.L. Jiang, D.Q. Yuan, M.Y. Wu, S.Q. Zhanga, M.C. Hong, Dalton Trans. 41 (2012) 9411–9416.
[62] X.C. Shan, F.L. Jiang, D.Q. Yuan, H.B. Zhang, M.Y. Wu, L. Chen, J. Wei, S.Q. Zhang, J. Pan, M.C. Hong, Chem. Sci. 4 (2013) 1484–1489.
[63] A.N. Ley, L.E. Dunaway, T.P. Brewster, M.D. Dembo, T.D. Harris, F. Baril-Robert, X. Li, H.H. Patterson, R.D. Pike, Chem. Commun. 46 (2010) 4565–4567.
[64] J.P. Killarney, M. McKinnon, C. Murphy, K.M. Henline, C. Wang, R.D. Pike, H.H. Patterson, Inorg. Chem. Commun. 40 (2014) 18–21.
[65] K.M. Henline, C. Wang, R.D. Pike, J.C. Ahern, B. Sousa, H.H. Patterson, A.T. Kerr, C.L. Cahill, Cryst. Growth Des. 14 (2014) 1449–1458.
[66] Y.J. Li, Z.Y. Deng, X.F. Xu, H.B. Wu, Z.X. Cao, Q.M. Wang, Chem. Commun. 47 (2011) 9179–9181.
[67] J.P. Safko, J.E. Kuperstock, S.M. McCullough, A.M. Noviello, X. Li, J.P. Killarney, C. Murphy, H.H. Patterson, C.A. Baysec, R.D. Pike, Dalton Trans. 41 (2012) 11663–11674.
[68] A. Kobayashi, K. Komatsu, H. Ohara, W. Kamada, Y. Chishina, K. Tsuge, H.C. Chang, M. Kato, Inorg. Chem. 52 (2013) 13188–13198.
[69] J.H. Wang, M. Li, D. Li, Chem. Sci. 4 (2013) 1793–1801.
[70] D.E. Royzman, A.M. Noviello, K.M. Henline, R.D. Pike, J.P. Killarney, H.H. Patterson, C. Crawford, Z. Assefa, J. Inorg. Organomet. Polym. 24 (2014) 66–77.
[71] A. Chakraborty, K.K. Ramachandran, S.S. Yamijala, S.K. Pati, T.K. Maji, RSC Adv. 4 (2014) 35167–35170.
[72] Y. Yu, X.M. Zhang, J.P. Ma, Q.K. Liu, P. Wang, Y.B. Dong, Chem. Commun. 50 (2014) 1444–1446.
[73] C.E. Strasser, V.J. Catalano, J. Am. Chem. Soc. 132 (2010) 10009–10011.
[74] I.O. Koshevoy, Y.C. Chang, A.J. Karttunen, M. Haukka, T. Pakkanen, P.T. Chou, J. Am. Chem. Soc. 134 (2012) 6564–6567.
[75] J.R. Shakirova, E.V. Grachova, A.S. Melnikov, V.V. Gurzhiy, S.P. Tunik, M. Haukka, T.A. Pakkanen, I.O. Koshevoy, Organometallics 32 (2013) 4061–4069.
[76] X. Zhang, C. Zhenguo, Y. Zhang, S. Liu, J. Xu, J. Mater. Chem. C 1 (2013) 3376–3390.
[77] Z. Chi, X. Zhang, B. Xu, X. Zhou, C. Ma, Y. Zhang, S. Liu, J. Xu, Chem. Soc. Rev. 41 (2012) 3878–3896.
[78] F. Gong, Q. Wang, J. Chen, Z. Yang, M. Liu, S. Li, G. Yang, Inorg. Chem. 49 (2010) 1658–1666.
[79] Q. Xiao, J. Zheng, M. Li, S.Z. Zhan, J.H. Wang, D. Li, Inorg. Chem. 53 (2014) 11604–11615.
[80] X.C. Shan, F.L. Jiang, H.B. Zhang, X.Y. Qian, L. Chen, M.Y. Wu, S.A. AL-Thabaiti, M.C. Hong, Chem. Commun. 49 (2013) 10227–10229.
[81] T. Wen, D.X. Zhang, J. Liu, R. Lin, J. Zhang, Chem. Commun. 49 (2013) 5660–5662.
[82] T. Wen, D.X. Zhang, H.X. Zhang, H.B. Zhang, J. Zhang, D.S. Li, Chem. Commun. 50 (2014) 8754–8756.
[83] T. Wen, X.P. Zhou, D.X. Zhang, D. Li, Chem. Eur. J. 20 (2014) 644–648.
[84] S. Perruchas, X.F. Le Goff, S. Maron, I. Maurin, F. Guillen, A. Garcia, T. Gacoin, J.P. Boilot, J. Am. Chem. Soc. 132 (2010) 10967–10969.
[85] X.C. Shan, H.B. Zhang, L. Chen, M.Y. Wu, F.L. Jiang, M.C. Hong, Cryst. Growth Des. 13 (2013) 1377–1381.
[86] D. Braga, L. Maini, P.P. Mazzeo, B. Ventura, Chem. Eur. J. 16 (2010) 1553–1559.
[87] L. Maini, D. Braga, P.P. Mazzeo, B. Ventura, Dalton Trans. 41 (2012) 531–539.
[88] X.C. Shan, F.L. Jiang, L. Chen, M.Y. Wu, J. Pan, X.Y. Wan, M.C. Hong, J. Mater. Chem. C 1 (2013) 4339–4349.
[89] Q. Benito, X.F. Le Goff, S. Maron, A. Fargues, A. Garcia, C. Martineau, F. Taulelle, S. Kahlal, T. Gacoin, J.P. Boilot, S. Perruchas, J. Am. Chem. Soc. 136 (2014) 11311–11320.
[90] C.W. Tang, S.A. Vanslyke, Appl. Phys. Lett. 51 (1987) 913–915.
[91] Q. Pei, G. Yu, C. Zhang, Y. Yang, A.J. Heeger, Science 269 (1995) 1086–1088.
[92] S.Y. Kim, W.I. Jeong, C. Mayr, Y.S. Park, K.H. Kim, J.H. Lee, C.K. Moon, W. Brütting, J.J. Kim, Adv. Funct. Mater. 23 (2013) 3896–3900.
[93] Y. Tao, K. Yuan, T. Chen, P. Xu, H. Li, R. Chen, C. Zheng, L. Zhang, W. Huang, Adv. Mater. 26 (2014) 7931–7958.
[94] For general lighting application, the light source typically requires a brightness of 3000–5000 cd/m², and exceeding standard fuorescent tubes efficiency (60–70 lm/W).
[95] A. Tsuboyama, K. Kuge, M. Furugori, S. Okada, M. Hoshino, K. Ueno, Inorg. Chem. 46 (2007) 1992–2001.
[96] J.C. Deaton, S.C. Switalski, D.Y. Kondakov, R.H. Young, T.D. Pawlik, D.J. Giesen, S.B. Harkins, A.J.M. Miller, S.F. Mickenberg, J.C. Peters, J. Am. Chem. Soc. 132 (2010) 9499–9508.
[97] M. Hashimoto, S. Igawa, M. Yashima, I. Kawata, M. Hoshino, M. Osawa, J. Am. Chem. Soc. 133 (2011) 10348–10351.
[98] C.W. Hsu, C.C. Lin, M.W. Chung, Yu. Chi, G.H. Lee, P.T. Chou, C.H. Chang, P.Y. Chen, J. Am. Chem. Soc. 133 (2011) 12085–12099.
[99] S. Igawa, M. Hashimoto, I. Kawata, M. Yashima, M. Hoshino, M. Osawa, J. Mater. Chem. C 1 (2013) 542–551.
[100] S. Igawa, M. Hashimoto, A. Tsuboyama, M. Osawa, M. Hoshino, Patent JP2011213643A (2010).
[101] Z. Liu, M.F. Qayyum, C. Wu, M.T. Whited, P.I. Djurovich, K.O. Hodgson, B. Hedman, E.I. Solomon, M.E. Thompson, J. Am. Chem. Soc. 133 (2011) 3700–3703.
[102] Z. Liu, J. Qiu, F. Wei, J. Wang, X. Liu, M.G. Helander, S. Rodney, Z. Wang, Z. Bian, Z. Lu, M.E. Thompson, C. Huang, Chem. Mater. 26 (2014) 2368–2373.
[103] F. Wei, J. Qiu, X. Liu, J. Wang, H. Wei, Z. Wang, Z. Liu, Z. Bian, Z. Lu, Y. Zhao, C. Huang, J. Mater. Chem. C 2 (2014) 6333–6341.
[104] X. Liu, T. Zhang, T. Ni, N. Jiang, Z. Liu, Z. Bian, Z. Lu, C. Huang, Adv. Funct. Mater. 24 (2014) 5385–5392.
[105] Y. Ma, C.M. Che, H.Y. Chao, X. Zhou, W.H. Chan, J. Shen, Adv. Mater. 11 (1999) 852–857.
[106] Y. Ma, W.H. Chan, X.M. Zhou, C.M. Che, New J. Chem. (1999) 263–265.
[107] W.L. Jia, T. McCormick, Y. Tao, J.P. Lu, S. Wang, Inorg. Chem. 44 (2005) 5706–5712.
[108] X.L. Chen, R. Yu, Q.K. Zhang, L.J. Zhou, X.Y. Wu, Q. Zhang, C.Z. Lu, Chem. Mater. 25 (2013) 3910–3920.
[109] Q.S. Zhang, Q.G. Zhou, Y.X. Cheng, L.X. Wang, D.G. Ma, X.B. Jing, F.S. Wang, Adv. Mater. 16 (2004) 432–463.
[110] Q. Zhang, T. Komino, S. Huang, S. Matsunami, K. Goushi, C. Adachi, Adv. Funct. Mater. 22 (2012) 2327–2336.
[111] Q. Zhang, J. Ding, Y. Cheng, L. Wang, Z. Xie, X. Jing, F. Wang, Adv. Funct. Mater. 17 (2007) 2983–2990.
[112] H. Xia, L. He, M. Zhang, M. Zeng, X. Wang, D. Lu, Y. Ma, Opt. Mater. 29 (2007) 667–671.
[113] J. Min, Q. Zhang, W. Sun, Y. Cheng, L. Wang, Dalton Trans. 40 (2011) 686–693.
[114] A. Wada, Q. Zhang, T. Yasuda, I. Takasu, S. Enomoto, C. Adachi, Chem. Commun. 48 (2012) 5340–5342.
[115] O. Moudam, A. Kaeser, B. Delavaux-Nicot, C. Duhayon, M. Holler, G. Accorsi, N. Armaroli, I. Séguy, J. Navarro, P. Destruel, J.F. Nierengarten, Chem. Commun. (2007) 3077–3079.
[116] D. Voltz, D.M. Zink, T. Bocksrocker, J. Friedrich, M. Nieger, T. Baumann, U. Lemmer, S. Bräse, Chem. Mater. 25 (2013) 3414–3426.
[117] D.M. Zink, D. Voltz, T. Baumann, M. Mydlak, H. Flügge, J. Friedrich, M. Nieger, S. Bräse, Chem. Mater. 25 (2013) 4471–4486.
[118] M. Osawa, I. Kawata, R. Ishii, S. Igawa, M. Hashimoto, M. Hoshino, J. Mater. Chem. C 1 (2013) 4375–4383.
[119] R.D. Costa, E. Ort, H.J. Bolink, F. Monti, G. Accorsi, N. Armaroli, Angew. Chem. Int. Ed. 51 (2012) 8178–8821.
[120] Y.M. Wang, F. Teng, Y.B. Hou, Z. Xu, Y.S. Wang, W.F. Fu, Appl. Phys. Lett 87 (2005), 233512-1–233512-3.
[121] N. Armaroli, G. Accorsi, M. Holler, O. Moudam, J.F. Nierengarten, Z. Zhou, R.T. Wegh, R. Welter, Adv. Mater. 18 (2006) 1313–1316.
[122] Q. Zhang, Q. Zhou, Y. Cheng, L. Wang, D. Ma, X. Jing, F. Wang, Adv. Funct. Mater. 16 (2006) 1203–1208.
[123] R.D. Costa, D. Tordera, E. Ortí, H.J. Bolink, J. Schönle, S. Graber, C.E. Housecroft, E.C. Constable, J.A. Zampese, J. Mater. Chem. 21 (2011) 16108–16118.
[124] C. Bizzarri, C. Strabler, J. Prock, B. Trettenbrein, M. Ruggenthaler, C.H. Yang, F. Polo, A. Iordache, P. Brüggeller, L. De Cola, Inorg. Chem. (2014), http://dx.doi.org/10.1021/ic5012204.
[125] R.W. Boyd, Nonlinear Optics, second ed., Academic Press, San Diego, 2003.
[126] T. Verbiest, S. Houbrechts, M. Kauranen, K. Clays, A. Persoons, J. Mater. Chem. 7 (1997) 2175–2189.
[127] B.J. Coe, Chem. Eur. J. 5 (1999) 2464–2471;
       R. Dagani, Chem. Eng. 74 (1996) 22–27.
[128] J. Zyss, Molecular Nonlinear Optics, Academic Press, New York, 1994.
[129] Y. Shi, W. Wang, J.H. Bechtel, A. Chen, S. Garner, S. Kalluri, W.H. Steier, D. Chen, H.R. Fetterman, L.R. Dalton, I.E.E.E Luping Yu, J. Sel, Top. Quant. Electron. 2 (1996) 289–299.
[130] H.S. Nalwa, Appl. Organomet. Chem. 5 (1991) 349–377.
[131] N.J. Long, Angew. Chem. Int. Ed. Engl. 34 (1995) 21–38.
[132] J. Heck, S. Dabek, T. Meyer-Friedrichsen, H. Wong, Coord. Chem. Rev. 190–192 (1999) 1217–1254.
[133] D.M. Roundhill, J.P. Fackler, Optoelectronic Properties of Inorganic Compounds, Plenum Press, New York, 1999.
[134] H. Le Bozec, T. Renouard, Eur. J. Inorg. Chem. (2000) 229–239.
[135] P.G. Lacroix, Eur. J. Inorg. Chem. 2 (2001) 339–348.
[136] B.J. Coe, in: J.A. McCleverty, T.J. Meyer (Eds.), Comprehensive Coordination Chemistry II, vol. 9, Elsevier Pergamon, Oxford, UK, 2004, pp. 621–687.

[137] B.J. Coe, N.R.M. Curati, Comments Inorg. Chem. 25 (2004) 147–184.
[138] D.R. Kanis, P.G. Lacroix, M.A. Ratner, T.J. Marks, J. Am. Chem. Soc. 116 (1994) 10089–10102.
[139] R.W. Therune, P.D. Maker, C.D. Savage, Phys. Rev. Lett. 14 (1965) 681–684.
[140] K. Clays, A. Persoons, Phys. Rev. Lett. 66 (1991) 2980–2983.
[141] K. Clays, K. Wostyn, A. Persoons, Adv. Funct. Mater. 12 (2002) 557–563.
[142] M.J. French, Hyper Rayleigh and Hyper Raman Spectroscopy in Chemical Applications of Raman Spectroscopy, Academic Press, New York, 1981.
[143] R.L. Sutherland, Handbook of Nonlinear Optics, Marcel Dekker Inc., New York, 1996.
[144] I.D. Morrison, R.G. Denning, W.M. Laidlaw, M.A. Stammers, Rev. Sci. Instrum. 67 (1996) 1445–1453.
[145] T. Renouard, H. Le Bozec, S. Brasselet, I. Ledoux, J. Zyss, Chem. Commun. (1999) 871–872.
[146] O. Maury, L. Viau, K. Sénéchal, B. Corre, J.P. Guégan, T. Renouard, I. Ledoux, J. Zyss, H. Le Bozec, Chem. Eur. J. 10 (2004) 4454–4466.
[147] H. Akdas-Kilig, J.P. Malval, F. Morlet-Savary, A. Singh, L. Toupet, I. Ledoux, J. Zyss, H. Le Bozec, Dyes Pigments 92 (2011) 681–688.
[148] A. Valore, M. Balordi, A. Colombo, C. Dragonetti, S. Righetto, D. Roberto, R. Ugo, T. Benincori, G. Rampinini, F. Sannicolò, F. Demartin, Dalton Trans. 39 (2010) 10314–10318.
[149] A. Valore, E. Cariati, C. Dragonetti, S. Righetto, D. Roberto, R. Ugo, F. De Angelis, S. Fantacci, A. Sgamellotti, A. Macchioni, D. Zuccaccia, Chem. Eur. J. 16 (2010) 4814–4825.
[150] H. Nitadori, L. Ordronneau, J. Boixel, D. Jacquemin, A. Boucekkine, A. Singh, M. Akita, I. Ledoux, V. Guerchais, H. Le Bozec, Chem. Commun. 48 (2012) 10395–10397.
[151] Q. Li, K. Wu, Y. Wei, R. Sa, Y. Cui, C. Lu, J. Zhu, J. He, Phys. Chem. Chem. Phys. 11 (2009) 4490–4497.
[152] S.K. Kurtz, T.T. Perry, J. Appl. Phys. 39 (1968) 3798–3813.
[153] E. Cariati, R. Ugo, F. Cariati, D. Roberto, N. Masciocchi, S. Galli, A. Sironi, Adv. Mater. 13 (2001) 1665–1668.
[154] S.R. Marder, J.W. Perry, C.P. Yakymyshyn, Chem. Mater. 6 (1994) 1137–1147.
[155] E. Cariati, R. Macchi, D. Roberto, R. Ugo, S. Galli, N. Masciocchi, A. Sironi, Chem. Mater. 19 (2007) 3704–3711.
[156] D. Mobius, Adv. Mater. 7 (1995) 437–444.
[157] E. Cariati, D. Roberto, R. Ugo, P.C. Ford, S. Galli, A. Sironi, Chem. Mater. 14 (2002) 5116–5123.
[158] J. Zyss, J.L. Oudar, Phys. Rev. A 26 (1982) 2028–2048.
[159] J. Zyss, D.S. Chemla, in: D.S. Chemla, J. Zyss (Eds.), Nonlinear Optical Properties of Organic Molecules and Crystals, vol. 1, Academic Press Inc., Orlando, FL, 1987, pp. 23–187.
[160] E. Cariati, D. Roberto, R. Ugo, P.C. Ford, S. Galli, A. Sironi, Inorg. Chem. 44 (2005) 4077–4085.
[161] S.P. Anthony, T.P. Radhakrishnan, Chem. Commun. (2004) 1058–1059.
[162] S.P. Anthony, T.P. Radhakrishnan, Cryst. Growth Des. 4 (2004) 1123–1127.
[163] M.J.S. Dewar, E.G. Zoebisch, E.F. Healy, J.J.P. Stewart, J. Am. Chem. Soc. 107 (1985) 3902–3909.
[164] S.P. Karna, M. Dupuis, J. Comput. Chem. 12 (1991) 487–504.
[165] Y. Kang, Y.G. Yao, Y.Y. Qin, J. Zhang, Y.B. Chen, Z.J. Li, Y.H. Wen, J.K. Cheng, R.F. Hu, Chem. Commun. (2004) 1046–1047.
[166] L. Han, M. Hong, R. Wang, B. Wu, Y. Xu, B. Lou, Z. Lin, Chem. Commun. (2004) 2578–2579.
[167] X.F. Huang, Y.H. Li, Q. Wu, Q. Ye, R.G. Xiong, Inorg. Chim. Acta 358 (2004) 2097–2100.
[168] Z. Li, S. Du, X. Wu, Inorg. Chem. Commun. 9 (2006) 79–81.
[169] Z.M. Hao, X.M. Zhang, Cryst. Growth Des. 8 (2008) 2359–2363.
[170] F. Wang, J. Zhang, R. Yu, S.M. Chen, X.Y. Wu, S.C. Chen, Y.M. Xie, W.W. Zhou, C.Z. Lu, Cryst. Eng. Commun. 12 (2010) 671–673.
[171] Y.Q. Huang, Z.L. Shen, X.Y. Zhou, T.A. Okamura, Z. Su, J. Fan, W.Y. Sun, J.Q. Yu, N. Ueyama, Cryst. Eng. Commun. 12 (2010) 4328–4338.
[172] Y.Q. Huang, Z.L. Shen, T. Okamura, Y. Wang, X.F. Wang, W.Y. Sun, J.Q. Yu, N. Ueyama, Dalton Trans. (2008) 204–213.
[173] C.H. Tan, X. Ma, Q.L. Zhu, Y.H. Huang, R.B. Fu, S.M. Hu, T.L. Sheng, X.T. Wu, J. mol. Struct. 1007 (2012) 26–30.
[174] B.G. Bharate, A.N. Jadhav, S.S. Chavan, Polyhedron 33 (2012) 179–184.
[175] Q. Ye, M.L. Liu, Z.Q. Chen, S.W. Sun, R.G. Xiong, Organometallics 31 (2012) 7862–7869.
[176] R. Macchi, E. Cariati, D. Marinotto, D. Roberto, E. Tordin, R. Ugo, R. Bozio, M. Cozzuol, D. Pedron, G. Mattei, J. Mater. Chem. 20 (2010) 1885–1890, and references therein.
[177] D.M. Burland, R.D. Miller, C.A. Walsh, Chem. Rev. 94 (1994) 31–75.
[178] P.D. Maker, R.W. Terhune, M. Nisenoff, C.M. Savage, Phys. Rev. Lett. 8 (1962) 21–23.
[179] J. Jerphagnon, S.K. Kurtz, Phys. Rev. B 1 (1970) 1739–1744.
[180] W.N. Herman, L.M. Hayden, J. Opt. Soc. Am. B 12 (1995) 416–427.
[181] R. Macchi, E. Cariati, D. Marinotto, E. Tordin, R. Ugo, G. Santoro, M.C. Ubaldi, S.M. Pietralunga, G. Mattei, J. Mater. Chem. 21 (2011) 9778–9783.
[182] V. Krishnakumar, S. Kalyanaraman, M. Piasecki, I.V. Kityk, P. Bragiel, J. Raman Spectrosc. 39 (2008) 1450–1454.